



Investigation toward the role of the surface texturing of the compression ring in the lubricated piston-cylinder contact

Master Thesis

Yu Yan

ID No 242827

Under the supervision of:

Prof. Dieter Fauconnier (Ugent)

Prof. Federico Colombo (Polito)

Klara Bartha (Ugent)

A thesis presented for the degree of Msc. Automotive engineering in Politecnico Di Torino

Dipartimento Di Ingegneria Meccanica E Aerospaziale
(DIMEAS)

Italy

10/12/2018

Acknowledgements

This work has been carried out at laboratory Soete In University of Gent. I would like to thank my supervisor Klara Bartha for her patience and time and helping me with the modeling and writing. I also want to thank my Professor Dieter Fauconnier for valuable discussions and guiding during the project and giving me this chance to explore my curiosity and knowledge. I want to thank Professor Federico Colombo for his kindly help.

I also like to express my gratitude to my friends and colleagues in this laboratory for providing an enjoyable and developing work place.

I would like to thank my best friend and my parents' support during these months to let me finish this thesis.

Yu Yan
2018

Contents

1	Introduction	1
1.1	Friction reduction in the engine compartment	1
1.2	The lubricant oil	1
1.3	The profile of the compression ring	2
1.4	Surface texturing on the compression ring and the cylinder liner system .	3
1.4.1	Numerical studies	4
1.4.2	Experimental studies	5
2	Physical Description And Governing Equations	7
2.1	Physical Description	7
2.1.1	Engine Piston Rings	7
2.1.2	Engine Model	8
2.2	Governing Equations And The Algorithm	12
2.2.1	The Reynolds Equation	12
2.2.2	Temperature Equation	13
2.2.3	Cavitation Model	14
2.2.4	Forces	15
2.2.5	Film Thickness Equation	17
2.2.6	Algorithm	20
3	Result	22
3.1	Stribeck Curve	22
3.2	A Comparison Study	28
3.3	Texture Profile Analysis	36
3.3.1	Analysis At The Cold Engine Operating Temperature	36
3.3.2	Analysis At The Warm Engine Operating Temperature	50
3.3.3	Discussion	65
3.4	Ring Profile Study	67
4	Conclusion and future work	70
4.1	Conclusion	70
4.2	Future Work	71

List of Figures

1.1	The figure of different texture profiles on one side of textured ring[24] . . .	3
1.2	Schematic view of the pocked piston ring surface[20].	3
2.1	Diagram of piston with piston rings[7]	7
2.2	The kinematics of the piston motion (left) and thermo-dynamic diesel cycle(right)[7]	8
2.3	Piston speed, radial load and chamber pressure at each crank angle for a smooth compression ring, under the warm engine operating conditions. . .	9
2.4	Piston Ring Geometry[7]	12
2.5	Transverse grooves on one side of ring[24]	18
2.6	A 2D graph of transverse groove texture considering $S_p = 0.5$ and $\varepsilon \approx 0.11$ [24]	19
2.7	The 2D and 3D plot of the textured ring [24], considering transverse grooves: $S_p = 0.5$ and $\varepsilon \approx 0.11$	20
2.8	A computational flow chart for outer loop	21
3.1	The Stribeck curve of the Hersey number at x axis, COF at y axis	23
3.3	The curves of the Hersey number at x axis, the dimensionless film thickness (Λ)	25
3.5	The curves of the dimensionless film thickness (Λ) at x axis, COF at y axis	26
3.6	The figure of the asperity friction force and the normal load at each crank angle	27
3.7	The figure of viscous friction force at each crank angle	28
3.8	The figure of dimensionless film thickness at each crank angle under an isothermal warm condition. A comparison of a smooth ring and a textured ring is considered. Two texture parameters for the texture are assumed as: $S_p=0.5$, $\varepsilon=0.11$	29
3.9	The figure of coefficient of friction (COF) at each crank angle under an isothermal warm condition. A comparison of a smooth ring and a textured ring is considered. Two texture parameters for the texture are assumed as: $S_p=0.5$, $\varepsilon=0.11$	29
3.10	The figure of dimensionless film thickness value at each crank angle for the textured rings and smooth rings. A half intake process is concerned . . .	30
3.11	The figure of coefficient of friction (COF) at each crank angle for the textured rings and smooth rings. A half intake process is regarded	31
3.12	The figure of $\Delta\Lambda$ at each crank angle for the condition K and Q. A half intake process is concerned	32

3.13	The figure of ΔCOF at each crank angle for condition K and Q. A half intake process is concerned	32
3.14	The figure of Λ value at each crank angle for the verification of the effect of engine configuration. A half intake process is concerned	33
3.15	The figure of COF at each crank angle for the verification of the effect of engine configuration. A half intake process is concerned	33
3.16	The figure of Λ value at each crank angle for the verification of the effect of operating conditions and surface roughness. A half intake process is concerned	34
3.17	The figure of COF at each crank angle for the verification of the effect of operating conditions and surface roughness. A half intake process is concerned	34
3.18	The figure of viscosity along the ring profile (x direction). Isothermal engine condition is considered for the warm and cold engines. The plot is taken at the crank angle ($\Psi=70$) when the piston reaches its maximum speed	35
3.19	The figure of vapour volume fraction's behavior along the smooth ring profile (x direction) for two cases with respect to different temperatures. The crank angle ($\Psi=70$) is considered.	35
3.20	The figure of $\Delta\Lambda$ at entire engine cycle for three textures with the same area density ($0.75S_p$). An isothermal cold engine operating condition is considered	37
3.21	The figure of $\Delta\Lambda$ at entire engine cycle for three textures with the same area density (S_p). An isothermal cold engine operating condition is considered	37
3.22	The figure of $\Delta\Lambda$ at entire engine cycle for three textures with the same area density ($1.25S_p$). An isothermal cold engine operating temperature is considered	38
3.23	The figure of pressure comparison between a textured ring ($1.25S_p - 0.5\varepsilon$) and the smooth ring. $\Psi = 70^\circ$ is considered.	39
3.24	The figure of film thickness (h) along the ring profile for the textured ring ($1.25S_p - 0.5\varepsilon$) and the smooth ring	40
3.25	The figure of vapour volume fraction along x direction of the smooth ring and a textured ring ($1.25S_p - 0.5\varepsilon$). A cold engine operating temperature is considered ,and $\Psi = 70^\circ$	40
3.26	The figure of ΔCOF at entire engine cycle. The textured rings have the same area density ($0.75 S_p$). The negative value region is shown inside the rectangle	41
3.27	The figure of ΔCOF at entire engine cycle. The textured rings have the same area density (S_p). The negative value region is shown inside the rectangle.	41
3.28	The figure of ΔCOF at entire engine cycle. The textured rings have the same area density ($1.25S_p$). The negative value region is shown inside the rectangle.	42
3.29	The figure of coefficient of friction (COF) and the dimensionless film thickness at the region of top dead center (the mixed lubrication regime), different texture profiles are considered as well as a smooth ring	43

3.30	The figure of viscous shear stress along the ring profile (x-direction) of a textured ring ($1.25S_p - 2\varepsilon$) and the smooth ring at mid-stroke	44
3.31	The figure of α and pressure distribution along the ring profile for the textured ring($1.25S_p - 2\varepsilon$) and the smooth ring at mid-stroke. The cold engine operating temperature is considered.	44
3.32	The figure of the energy loss E at entire engine cycle. Textured ring ($1.25S_p - \varepsilon$) and smooth ring are considered as well as an isothermal cold engine operating temperature	46
3.33	The figure of $\bar{\alpha}$, different texture profiles are considered as well as a smooth ring considering an isothermal cold engine operating condition	47
3.34	The figure of α value along the ring profile for the textured ring($1.25S_p - 2\varepsilon$) and the smooth ring at mid-stroke $\Psi = 70^\circ$. The cold engine operating temperature is considered.	47
3.35	The figure of \bar{a} and \bar{b} at entire engine cycle. An isothermal cold engine operating condition is concerned	48
3.36	The figure of dimensionless film thickness with respect to crank angle at entire cycle. The smooth one is considered as well as the isothermal cold engine operating temperature	49
3.37	The figure of the sum of the effects coming from \bar{a} and \bar{b} at entire engine cycle. The smooth one is considered, as well as the cold engine operating temperature	49
3.38	The figure of $\Delta\Lambda$ at entire engine cycle for three textured rings with the same area density ($0.75S_p$). A non-isothermal warm engine condition is investigated	50
3.39	The figure of $\Delta\Lambda$ at entire engine cycle for three textured rings with the same area density (S_p). A non-isothermal warm engine condition is investigated	51
3.40	The figure of $\Delta\Lambda$ at entire engine cycle for three textured rings with the same area density ($1.25S_p$). A non-isothermal warm engine condition is investigated	51
3.41	The figure of pressure distribution and vapour volume fraction along the ring profile (x-direction) between a smooth and textured ring. A non-isothermal warm engine operating condition is considered.	52
3.42	The figure of ΔCOF at entire engine cycle for three textured rings with the same area density ($0.75S_p$). An non-isothermal warm engine condition is investigated. The negative value region is represented inside the rectangle.	53
3.43	The figure of ΔCOF at entire engine cycle for three textured rings with the same area density (S_p). An non-isothermal warm engine condition is investigated. The negative value region is represented inside the rectangle	53
3.44	The figure of ΔCOF at entire engine cycle for three textured rings with the same area density ($1.25S_p$). An non-isothermal warm engine condition is investigated. The negative value region is represented inside the rectangle	54
3.45	The figure of the viscous shear stress along the ring profile (x-direction) for the textured rings and the smooth ring. A non-isothermal warm engine operating temperature is considered	55

3.46	The figure of the film thickness along the ring profile (x-direction) for the textured rings and the smooth ring. A non-isothermal warm engine operating temperature is considered	56
3.47	The figure of the energetic loss (E) at entire engine cycle. Textured rings ($0.75S_p - 2\varepsilon$ and $1.25S_p - 2\varepsilon$) are considered as well as a smooth ring under a non-isothermal warm engine condition	57
3.48	The figure of the COF and the dimensionless film thickness at combustion and expansion processes. Different texture profiles are considered as well as a smooth ring under an non-isothermal warm engine operating condition	57
3.49	The figure of vapour volume fraction value at entire engine cycle. Different texture profiles are considered as well as a smooth ring under a non-isothermal warm engine operating condition	58
3.50	The figure of the vapour volume fraction along the ring profile (x-direction) between a smooth and the textured rings. A non-isothermal warm engine operating condition is considered.	59
3.51	The figure of the dimensionless film thickness at entire engine cycle between the smooth ring and the textured rings. A non-isothermal warm engine operating condition is considered	60
3.52	The figure of $\Delta\Lambda$ at entire engine cycle for three textured rings with the same area density ($0.75S_p$). An isothermal engine condition is investigated	61
3.53	The figure of $\Delta\Lambda$ at entire engine cycle for three textured rings with the same area density (S_p). An isothermal engine condition is investigated	61
3.54	The figure of $\Delta\Lambda$ at entire engine cycle for three textured rings with the same area density ($1.25S_p$). An isothermal engine condition is investigated	62
3.55	The figure of ΔCOF at entire engine cycle for three textured rings with the same area density ($0.75S_p$). An isothermal engine temperature is investigated. The negative value region is represented inside the rectangle.	63
3.56	The figure of ΔCOF at entire engine cycle for three textured rings with the same area density (S_p). An isothermal engine temperature is investigated. The negative value region is represented inside the rectangle.	63
3.57	The figure of ΔCOF at entire engine cycle for three textured rings with the same area density ($1.25S_p$). An isothermal warm engine temperature is investigated. The negative value region is represented inside the rectangle	64
3.58	The figure of $\bar{\alpha}$ value at each each crank angle. Different textures are considered as well as a smooth ring under an isothermal warm engine	65
3.59	The figure of $\Delta\Lambda$ at each crank angle. Different ring profiles are considered under a non-isothermal warm engine operating condition	67
3.60	The figure of ΔCOF at each crank angle. Different ring profiles are considered under a non-isothermal warm engine operating condition	68
3.61	The figure of the energy loss E[w] at entire engine cycle. Different ring profiles are considered under a non-isothermal warm engine operating condition	69

List of Tables

2.1	SAE 5W-30 oil is comparable with ISOVG 100 at 95° Celcius[7]	10
2.2	Engine general data[7]	11
3.1	A texture geometry matrix	36
3.2	A matrix of $\Delta\Lambda\%$ at the cold engine operating condition	38
3.3	A matrix of $\Delta\text{COF}\%$ at the cold engine operating condition	42
3.4	A matrix of $\Delta E_{\text{total}}\%$ at the cold engine operating temperature	45
3.5	A matrix of $\Delta\Lambda\%$ at the non-isothermal warm engine condition	52
3.6	A matrix of $\Delta\text{COF}\%$ at the non-isothermal warm engine condition	54
3.7	A matrix of $\Delta E_{\text{total}}\%$ at the non-isothermal warm engine condition	56
3.8	A matrix of $\Delta\Lambda\%$ at the isothermal engine condition	62
3.9	A matrix of $\Delta\text{COF}\%$ at the isothermal engine condition	64
3.10	A matrix of $\Delta E_{\text{total}}\%$ at the isothermal engine condition	65
3.11	A matrix of E_{total} under a non-isothermal warm engine operating condition	69

‘Engineering is the art of modelling materials we do not wholly understand, into shapes we cannot precisely analyze so as to withstand forces we cannot properly assess, in such a way that the public has no reason to suspect the extent of our ignorance.’

- Dr. A.R. Dykes, Address to the Institute of Structural Engineers (1978)

Abstract

The major part of energy loss within the internal combustion engines originates from the friction between piston rings and the cylinder liner. There are typically three rings fit into a groove on the piston-head mantle, i.e. the compression ring, the scraper ring and the oil control ring. In this work, we focus on the compression ring. As the piston head reciprocates on the cylinder liner, the compression ring is pushed radially against the cylinder liner with variable forces, i.e. the pretension of the ring and the pressure generated from the combustion chamber. At the top and bottom dead centre, the velocity of the piston head changes sign, which leads to short breakdown of the lubricant film. Thus, the surface-to-surface contact occurs and friction losses increase. However, Various sources in literature claim that surface texturing of the piston ring and the cylinder liner system can reduce the friction loss and even maintain the lubricant film at the top and bottom dead centres. In this work, a numerical study is concerned to analyze the effects of surface texturing of the barrel-shaped compression ring of a four-stroke diesel engine, and it is supplied with the lubricant ISO VG 100. The mixed-lubrication model includes the Reynolds equation and temperature equation is used for the lubricant flow. Meanwhile, the Greenwood-Tripp contact model plays an important role in the mechanical contact between surface asperities. The groove-shaped texture at two sides of compression ring is implemented. To better predict the best shape of grooves, two texture parameters are taken into account to minimize friction force and energy losses at entire cycle. They are the area density and depth-to-width ratio. A detailed analysis of the pressure distribution along ring profile and total gases released from the lubricant at entire cycle are included to identify the physical phenomena that makes the texture successful.

Chapter 1

Introduction

1.1 Friction reduction in the engine compartment

In the automotive industry, the piston and the cylinder liner system is recognized as the essential joint for transmitting forces generated through the combustion processes. Due to concerns about the energy crisis, increasing fuel price and climate change, fuel consumption, and energy loss are regarded as important factors for machine design. Specifically, remarkable attention has been paid to the friction reduction of the piston ring-cylinder line system. Recently, a lot of researches have been carried out to identify ways to reduce energy losses and improve the efficiency of the internal combustion engines (ICEs). The friction loss and mechanical wear contribute significantly to the power loss of ICEs. There are three different rings on the piston-head mantle. i.e. the compression ring, the scraper ring, and the oil control ring. Whilst, most of the friction come from the compression ring (top ring), which take around 35% to 40% of the total engine friction[26].

1.2 The lubricant oil

The properties of the lubricant oil are important, because they can influence the tribological parameters. They are the film thickness, the friction force between the compression ring and the cylinder liner. Thus, lubricant oil becomes an indispensable component inside engine compartment for providing a good sealing to avoid chamber gases flow into the crank case and a free motion between the piston and the cylinder liner. However, when the piston moves to dead centers, the surface contact between two sliding surfaces occurs and generates a great asperity friction forces, which can reduce the engine efficiency. Furthermore, a continuous development of a better lubrication in the piston ring-cylinder liner system is carried out. A dynamic analysis of pistons rings' tribological effect on a four-stroke diesel engine was estimated by Ahmed et al.[1]. A mixed lubrication model, as well as a temperature-related viscosity model were devised to evaluate the friction force and power loss with different lubricant oils (i.e. SAE 10W40 and SAE 20W40). They found that one lubricant with a larger value of viscosity causes a thicker film, which reduces asperity friction force but increases the hydrodynamic friction force. Therefore a suitable oil has to be chosen to optimize the film thickness and resulting in

the friction reduction in the piston ring and the cylinder liner system. In addition, Zavos et al.[29] showed that the use of multi-grade oil SAE 5W-30 reduces 50% friction force than the mono-grade oil SAE 30 at the same temperature range. Also, those low-viscous lubricants increase the load-carrying capacity by the pseudoplastic effect. At the high operating temperature around 120°C, the minimum film thickness declines from 0.7% to 6% for the multi-grade oils compared with the mono-grade oil SAE 30.

1.3 The profile of the compression ring

The profile of the compression ring becomes an essential feature to investigate and develop, because the profile of the compression ring determines the hydrodynamic load-carrying capacity and friction losses[30]. Checo et al.[3] developed a numerical model to simulate the compression ring and the cylinder liner contact at the hydrodynamic lubrication condition. A dimple-shaped texture was implemented on the cylinder liner, in which a mass-conservative Elrod-Adam model was used. They found that different profiles of the ring can change tribological behaviors and the more conformal the ring profile is created, more friction reduction will get. It has been found that an asymmetrical profile has more benefits because its asperity contact force is significantly reduced with respect to a barrel-shaped profile, especially when the piston moves to the TDC or BDC[11]. On the other hand, a smaller width of compression ring is harder to manufacture an asymmetrical profile. Bilboulet et al. [2] did the comparison between a parabolic ring and a flat ring. Their study has shown that the texture on a parabolic ring reduces the load carrying capacity. But it is improved for a textured flat ring. At the same time, Zhang et al [30] proposed a numerical method to determine the ring profile. A polynomial function is used to obtain the ring shape, the sequential quadratic programming algorithm to optimize the profile under the specific engine processes as well. Friction force and the oil film thickness are taken into account through the usage of the Reynolds equation with some flow factors and the temperature equation. They found that by considering the ring profile of the degree of polynomial between 2 and 5 obtains the minimum friction force and the maximum load-carrying capacity in both the hydrodynamic and mixed lubrication regimes. Instead of changing the shape of ring, different crown heights are also modified. Sonthalia et al.[21] used a numerical model, in which the Reynolds equation was applied to the piston ring and the cylinder liner contact in the hydrodynamic lubrication regime. They predicted that the ring profile with a higher crown height had generated a lower friction force. meanwhile, an experimental study of an optimum piston profile manufactured in a low-speed spark ignition (SI) engine was done by Zhang et al[30]. They also proved the same result. On the other hand, Liu et al [16] indicated that a smaller crown height or a wider ring improves the average friction force and has fewer impacts on the power loss. In their study, a micro-dimple texture on the cylinder liner was evaluated. The Reynolds equation and the mass conservative Jakobsson-Floberg-Olsson (JFO) boundary condition are adopted, as well as the Greenwood asperity contact model.

1.4 Surface texturing on the compression ring and the cylinder liner system

Surface texturing has been treated as an option to improve the friction force reduction and load-carrying capacity in the last decade. For instance, each micro-dimple can be served as a micro-hydrodynamic bearing for the full and the mixed lubrication[6]. Furthermore, different texture profiles are investigated in the piston ring and the cylinder liner contact. Those texture profiles are the dimple [14], cylindrical[5], pore-shaped [17], pocket-shape[20] and groove-shaped[24]. Some of those profiles are represented as below:

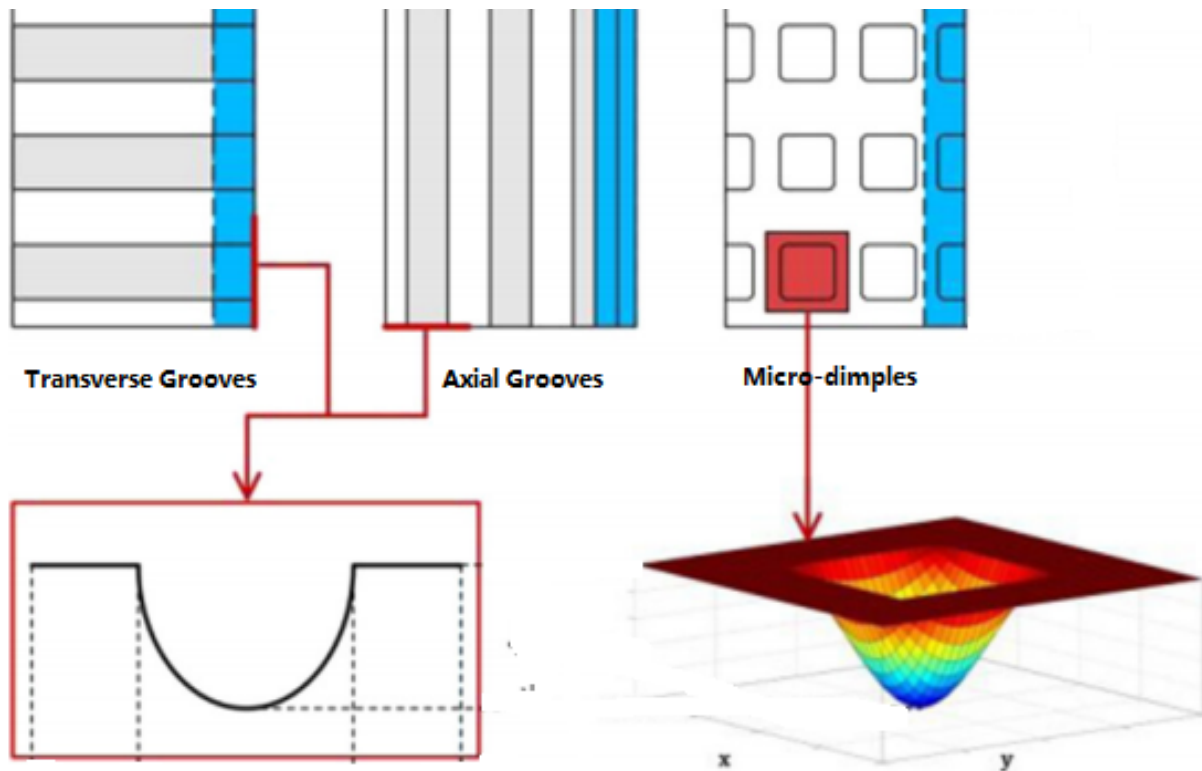


Figure 1.1: The figure of different texture profiles on one side of textured ring[24]

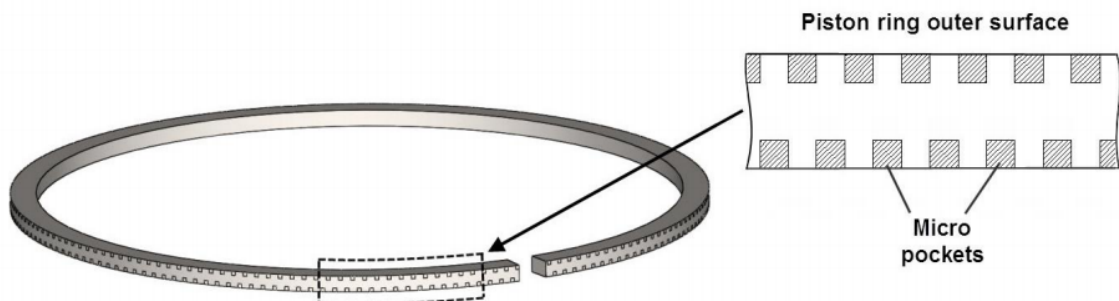


Figure 1.2: Schematic view of the pocked piston ring surface[20].

1.4.1 Numerical studies

The texture on the compression ring

Numerical simulation becomes dispensable method to devise the surface texturing, because it is flexible and cost-effective. A numerical study to predict the effect of surface texturing on reciprocating automotive components was carried out by Ronen et al.[17]. The Reynolds equation and was taken into account inside a simplified piston/cylinder system (two parallel surfaces). The spherical pore-shaped texture locates at two side of the compression ring. Also, some non-dimensional parameters are evaluated, i.e. the area density, depth-to-width ratio and the number of pore along the axial direction of the piston ring. Their influences on the minimum film thickness (clearance) and the average friction force at each crank angle are taken into account. They concluded that the pressure distribution generated from two adjacent pores should not be ignored. The tribological parameters improves because of surface texturing. Whilst, this textured ring reduces 30% friction force or even more. Meanwhile, an analytical model to study the potential effect of partial surface texturing on two parallel surfaces was done by Kligerman et al[14]. The dimensionless friction force and some texture parameters were considered in their model for a comparison study between the partially textured ring and fully textured one. They found that the partial textured ring with the optimum texture has lower average friction force than the corresponding optimum fully textured ring and this improvement is even more effective for a wide ring. On the other hand, the location of texture does not have much effect on friction reduction. Different texture profiles on two side of compression ring are designed and taken into account by Usman et al.[24]. Those textures are micro-dimple, transverse grooves and axial grooves. They used a modified Reynolds equation and considered an isothermal oil temperature, which is related to the piston location on the cylinder liner. Also, an optimized geometry parameters (area density and depth-to-width ratio) for each texture pattern were evaluated to improve the minimum film thickness and the reduction of friction. They concluded that transverse grooves which is perpendicular to the sliding direction has better tribological performance than other type of textures in 90% of the engine cycle. Shallow surface textures decreases friction force, especially the transverse grooves who relevantly reduces friction force at mid-stroke. In addition, the micro-dimple texture more decreases the asperity friction force compared with the smooth ring[24]. Furthermore, to reduce the friction force generated from the piston ring and the cylinder liner system (PRCL), it has been investigated by an numerical model, which is developed by Shen et al.[20]. The mass-conservative form of the Reynolds equation as well as the Elrod and Adams cavitation model were considered. They found that the texture parameters of the pocket-shaped texture has better improvement compared to the shape of the texture.

The texture on the cylinder liner

The numerical analysis of surface texturing on the compression ring reciprocating on the engine cylinder liner is also regarded as a promising way to improve the minimum film thickness and friction reduction. Since, implementing the texture on the cylinder liner, the minimum film thickness is time-varying and depends on the location of the piston on the cylinder liner, different simulation method should be developed. Gu et al.[9] used a

numerical model to investigate the effect of surface texturing on both the compression ring and the cylinder liner under the cold and warm engine conditions. They considered a mixed lubrication model implemented by the Reynolds equation as well as The Vogal and Roeland equations. The friction mean effective pressure (FMEP) and thermal analysis were used to evaluate the texture's influences on tribological behaviors. It has been shown that the textures on ring/liner conjunction reduces the friction loss on both engine conditions. On the other hand, the textured liner reduces more friction than the textured ring. In addition, spherical dimples on the cylinder liner was investigated by Liu et al.[16]. In order to study the surface contact at dead centers, a numerical model includes the Reynolds equation and the mass conservative JFO boundary condition, as well as a Greenwood asperity contact model. They found that the area density of spherical dimples has more impact on the average friction force and the minimum film thickness than the radius of dimple. Also, the spherical dimple on the cylinder liner can reduced more the friction force at the mixed lubrication regime than at the hydrodynamic lubrication regime. At the same time, Yin et al.[28] developed an theoretical model, in which the surface roughness of the PRCL system was considered. The average Reynolds equation with Greenwood asperity contact model as well as a JFO cavitation boundary condition were adopted. They also found that the area density of the spherical dimple has more effect on the oil minimum film thickness and average friction force than the radius of this dimple. The textured ring has better lubricant performance in the mixed lubrication regime than the hydrodynamic lubrication regime.

1.4.2 Experimental studies

The texture on the compression ring

According to the results from the numerical simulation, some experimental investigations were done to investigate the surface texturing's tribological effects on the compression ring and cylinder liner system. Ryk et al [18] designed a text rig to provide a linear reciprocating motion between two rough surfaces to simulate the system of PRCL (piston ring and cylinder liner). The laser surface texturing (LST) method was used to generate the partial textured ring and the fully textured one. Under the limit of speed and variable loads, they found that the friction reduction is up to 25% less at the partial textured ring compared to the fully textured one. Another experimental study of the surface texturing on three different kinds of piston rings of a naturally aspirated CI (combustion ignition) engine is carried out[5]. A partial LST using a eddy-current dynamo-meter text bench was applied as well as a constant load and different engine speeds. A comparison analysis of a barrel-shaped Cr-coated textured ring, a cylindrically shaped ring with a Cr coating with respect to the smooth one was done for the analysis of the fuel consumption and exhaust gas composition. They said that textured ring does not have great effect on the exhaust gas composition. However, be considering a optimum partial texture located at two end of ring, there is a significant reduction of the fuel consumption up to 4%. Furthermore, another partially textured ring is carried out by Shen et al.[20], a pocket shaped texture on two side of the piston ring was designed. The centre-symmetrical pocket was created on specimens which was placed inside a lubricant container. A tribometer with reciprocation drive was used to simulate the PRCL contact, and two sensors to measure the displacement and friction force. In their study, an optimum texture shape was found

to reduce the friction loss.

The texture on the cylinder liner

The experimental investigation of surface texturing on the cylinder liner was done by Spencer et al [22]. Two parts of surface topology were included in their study, i.e. the surface roughness and texture. they measured the surface roughness in white light interferometry (WLI) and atomic force microscopy (AFM) way and it seems much better for them to use AFM from the accuracy point of view. An artificial honing cross grooves was generated and distributed on the cylinder liner and was measured by WLI technique. After that, a numerical simulation considering the full film Reynolds equation including a periodic boundary condition was done. A mixed lubrication model of a surface contact model was applied as well as the Jakobsen-Floberg-Olson (JFO) cavitation model. In the time-dependent full cycle engine, they said that it is more accurate to include the texture in the globe scale instant of implementing some flow factors. A solution subjected to a better geometry parameters was developed as well.

In this study, in order to investigate the surface texturing's tribological effect on the PRCL contact, a numerical simulation of a textured compression ring with a barrel-shaped profile moving on an ideal circular cylinder liner in the VW Golf Mk6 diesel engine was concerned. The mixed lubrication model which combines the Reynolds equation and the temperature equation for the lubricant, whereas the Greenwood-Tripp model is used to take into account the condition when there is the surface contact. Due to the reciprocating motion between the piston and the cylinder liner, the hydrodynamic lubrication regime and the mixed lubrication regime are considered respectively at different engine processes. During this study, the capability to construct the texture on the compression ring were obtained, and to investigate the effect of tribological parameters at each crank angle. i.e. the dimensionless film thickness and the coefficient of friction. Also, this work comprises a detailed analysis of the pressure and vapour volume fraction at some typical engine operating condition. Furthermore, a comparison study between textured rings with different texture profiles and the smooth ring is made to identify the physical phenomena that predicts a better texture.

Chapter 2

Physical Description And Governing Equations

2.1 Physical Description

2.1.1 Engine Piston Rings

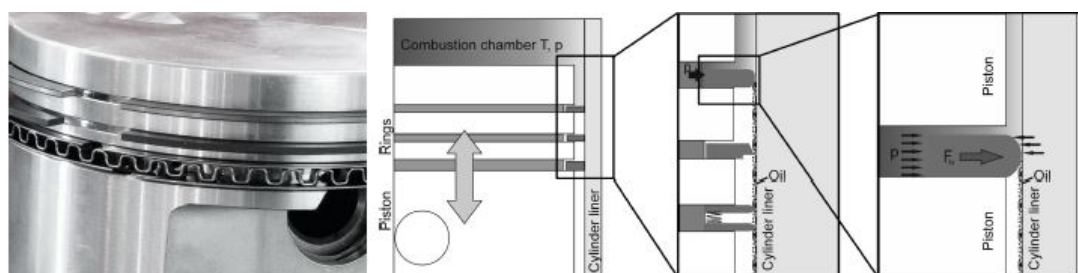


Figure 2.1: Diagram of piston with piston rings[7]

An image of the piston rings is displayed on the Figure 2.1. On the piston-head mantle, three metal split rings can be found, which are fastened into their grooves. The rings play an crucial role in preventing combustion gas leaking to the crancase, guiding the piston's reciprocating motion and controlling lubricant and engine oil consumption under normal engine operations. Whilst, each one serves different purposes. 1) The compression ring, the focus of this study, which has an excellent sealing effect, maximizes power output and prevents blow-out gases leaking to the carter. 2) The scraper ring has a tapered profile, which scraps unnecessary oil back into the crank case and prevents lubricant from getting inside the combustion chamber. 3) The oil control ring, which is a component consisting of an expansion ring and two rails, controls the supply of lubricant oil from the crank case to the cylinder liner through a small slot. During the reciprocating motion of the piston inside the lubricated cylinder liner, the compression ring is exposed to a higher pressure and temperature from the engine chamber than other rings. The load generated at the surface of the compression ring depends on each crank angle (Ψ). The pressure from the combustion chamber and the pretension of the ring should be balanced by the lubricant's hydrodynamic force at mid-stroke. Furthermore, at the top and bottom dead centre where the piston's motion reverses, asperities interaction occurs and starts to play

an major role in carrying the load. Hence, boundary friction is generated and increases the fuel consumption and the energy loss. In addition, the motion of the piston is not stable inside the chamber, the slamming occurs between the piston and the cylinder liner. In order to prevent it, the profile of the ring has to be chosen carefully. In this work, a barrel profile compression ring is considered as well as the texture on it.

2.1.2 Engine Model

In this study, a model of the compression ring-cylinder liner system is considered for the Volkswagen Golf Mk6 Diesel Engine: VW 2.0 R4 16v TDI CR with the maximum power of 105kW-141bhp at 4200 rpm, 320 newton metres at 1750-2500 rpm. Details related to the geometric parameters of the cylinder liner and the compression ring, as well as the operating conditions are listed in Table 2.2. While, Table 2.1 contains the properties of the multi-grade oil SAE 5w-30. As we consider a nominal oil temperature of 95°C, this lubricant's viscosity is comparable to that of the sing-grade ISO VG 100, which will be further used in this work. In this study, a nominal oil temperature of 95° at the crankcase side of the ring is considered and the temperature variation at this side corresponding to each crank angle is neglected. The thermo-mechanical properties of the compression ring and cylinder liner system are dependent on the lubricant's pressure and temperature. The data is obtained from the UGent simulation code of Prof.Fauconier[7].

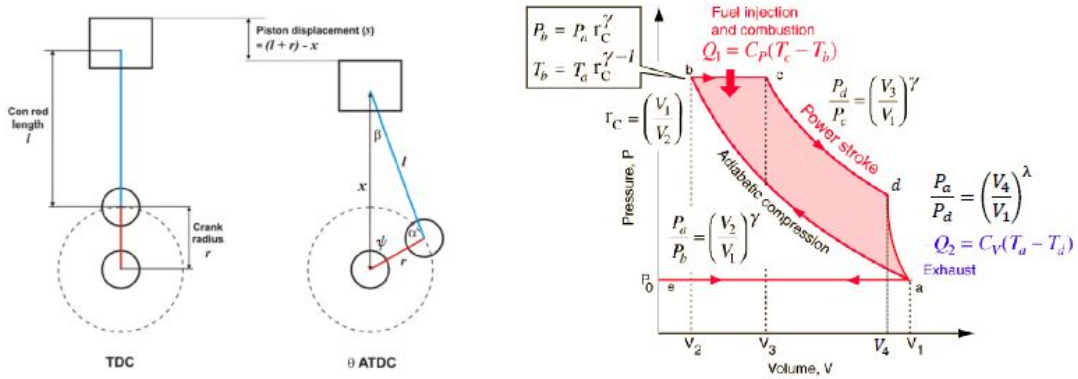


Figure 2.2: The kinematics of the piston motion (left) and thermo-dynamic diesel cycle(right)[7]

The kinematics of the piston motion and the thermo-dynamic diesel cycle are shown on Figure 2.2. For the compression and expansion processes adiabatic conditions are considered, and an isobaric ignition process is assumed. The pressure and temperature values at each crank angle are calculated by the equations in the figure of thermo-dynamic diesel cycle. Those pressure and temperature alternate at each crank angle and are correlated with the compression ratio ($\frac{V_1}{V_2}$) and the adiabatic coefficient (γ). Furthermore, for the normal engine speed a constant value is used. Before making a thermo-mechanical analysis, the piston's speed, acceleration and displacement at the chamber should be known. The velocity of the piston (U) is a function of the crank angle and given by following data:

$$U = -nR_c (\sin(\Psi) + \tan(\beta) \cos(\Psi)) \quad (2.1)$$

$$\beta = \arcsin\left(\frac{r}{l} \sin(\Psi)\right) \quad (2.2)$$

Where Ψ is the crank angle, β is the angle between the connecting rod and vertical line (x) in the graph of kinematics of piston motion, r and l is the crank length and the length of connecting rod respectively. n is the engine speed and R_c is the crank radius. Figure

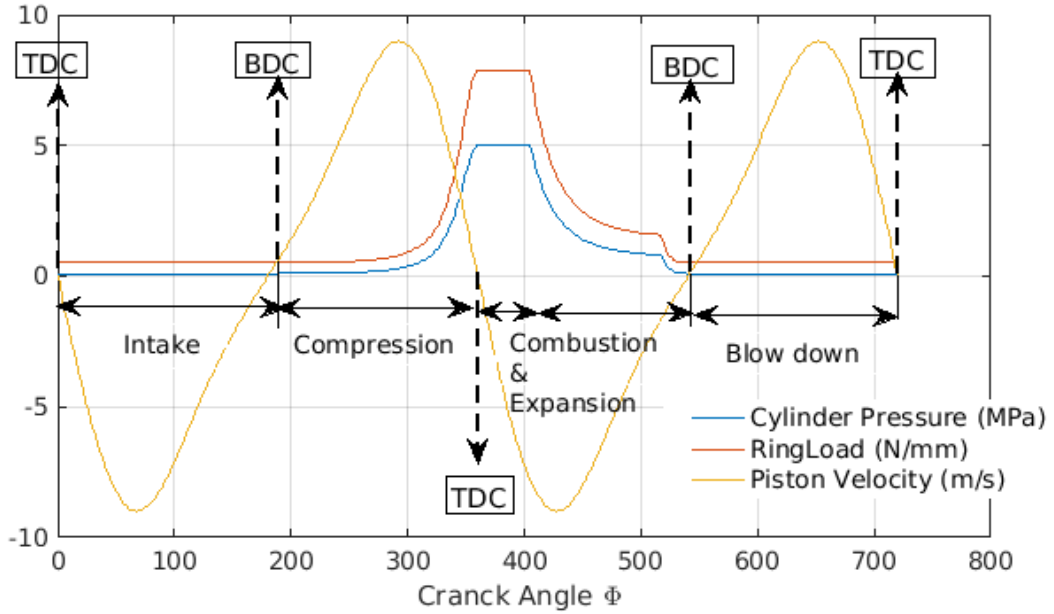


Figure 2.3: Piston speed, radial load and chamber pressure at each crank angle for a smooth compression ring, under the warm engine operating conditions.

2.3 shows how the piston velocity, the cylinder pressure and the radial load vary with respect to the crank angle. The maximum piston speed occurs at the mid-stroke of each process and the direction of piston changes at the dead centres. Regarding the pressure, the highest value occurs at the combustion stroke due to the ignition process. Meanwhile, the radial load per unit length in the circumferential direction on the compression ring is related to the pressure induced in the engine chamber.

Table 2.1: SAE 5W-30 oil is comparable with ISOVG 100 at 95° Celcius[7]

Lubricant Properties		
Liquid Thermal Expansion β_t	0.00065	1/K
Liquid Specific Heat Capacity $C_{p,l}$	1670	J/KgK
Liquid Thermal Conductivity K_l	0.15	w/mK
Liquid Speed of Sound c_l	1461	m/s
Liquid Limiting Shear Stress τ_o	2	MPa
Vapour Dynamic Viscosity μ_v	$0.359e - 3(@T_{oil})$	Pas
Vapour Density ρ_v	$\frac{P_{vap}}{RT}, R = 57.75$	kg/m ³
Vapour Specific Heat Capacity $C_{p,v}$	1983	J/KgK
Vapour Thermal Conductivity K_v	0.15	W/mK
Saturation Pressure P_{sat}	9628	Pa
Vapour Volume Fraction $\alpha@P_{sat}$	0.01	
Vapour Volume Fraction $\alpha@P_{vap}$	0.99	

Table 2.2: Engine general data[7]

Cylinder and Piston		
Symbols	Number	Unit
Bore D	81	mm
Stroke s	95.5	mm
Compression Ratio CR	18	
liner Youngs Modulus E_c	95	GPa
Liner Poisson Ratio ν_c	0.2	
Liner RMS roughness σ_c	0.2	μm
Connecting Rod length/Crank length	2	
Minimum Volume V_{min}	$\frac{\pi D^2}{4} s \frac{1}{CR-1}$	m^3
Maximum Volume V_{max}	$V_{min} * CR$	m^3
Compression Ring		
Height b	1.5	mm
width w	3.5	mm
Crown Height δ	10	μm
Profile	$f_r = 4 \frac{\mu x^2}{b^2}$	
Free Gap Size $l_{gap,f}$	12	mm
Gap Size l_{gap}	0.5	mm
Youngs modulus E_r	201	Gpa
Poisson Ratio ν_r	0.3	
Moment of Inertia I	$\frac{bw^3}{12}$	m^4
Elastic Ring Preload Pressure P_e	$\frac{16l_{gap,f}E_r I}{3\pi b D^4}$	Pa
RMS roughness δ_r	0.05	μm
Boundary coefficient of friction f_b	0.15	
Operation Conditions		
Atmospheric Inlet Pressure P_{atm}	101325	Pa
Engine RPM n	2400	rad/s
IVC(Intake valve closing)	180	Degree Crank Angle
SOC(Start of combustion)	360	Degree Crank Angle
EOC(End of combustion)	405	Degree Crank Angle
EVO(Exhaust valve open)	517.5	Degree Crank Angle
Adiabatic Expansion Coefficient γ	1.35	
Combustion Pressure P_c	$P_{atm} * CR^\gamma$	Pa
Nominal Oil Temperature T_{oil}	95	$^\circ C$
Nominal Liner Temperature T_{wall}	95	$^\circ C$

2.2 Governing Equations And The Algorithm

2.2.1 The Reynolds Equation

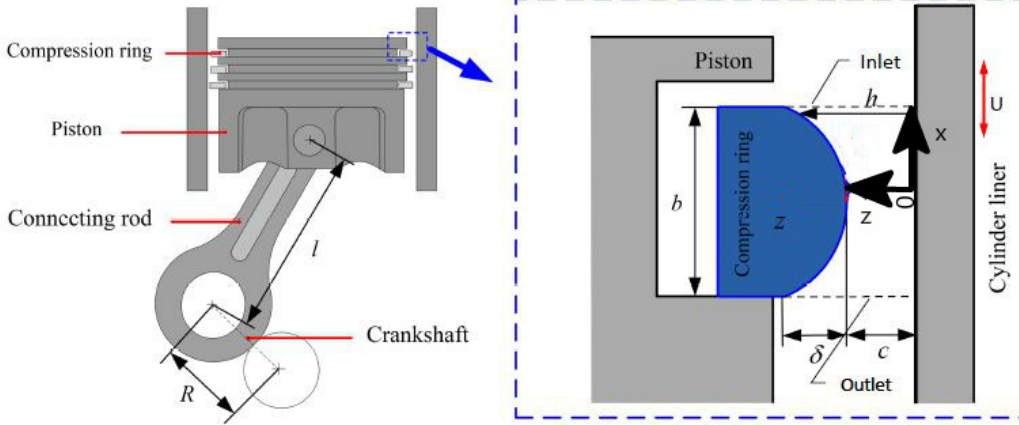


Figure 2.4: Piston Ring Geometry[7]

In this work, the pressure distribution at the fluid-lubricated interface is calculated from the Reynolds equation. A partial differential equation derived from the Navier-Stokes equations. Because of the reciprocating motion of the piston ring along the cylinder liner, the transient 2D Reynolds equation is implemented. Due to the reason that the compression ring's diameter is larger than the axial width of the ring, this compression ring and liner system can be regarded as an infinitely long sliding bearing[12]. By assuming that the ring has perfectly symmetric conformity and ignoring the influence of the lubricant film's change on radial direction, the ring-liner system can be treated as a one-dimensional situation. The layout of the Piston ring and the cylinder liner (PRCL) system is shown on Figure 2.4. For the simulations, a circumferential coordinate system is chosen with dimensions $x \in [-\frac{b}{2}, \frac{b}{2}]$, the circumferential direction $\theta \in [0, 2\pi]$. In order to accurately represent the textured profile in the simulations, a small grid size is needed. Since simulating the full engine cycle is time consuming, in the circumferential direction only one degree is considered and a periodic boundary condition is used. Then, the 2D Reynolds equation can be formulated as[7]:

$$\left[\phi \frac{\partial^2 p}{\partial x^2} + \frac{\partial \phi}{\partial x} \frac{\partial p}{\partial x} \right] + \frac{1}{R_{cyl}^2} \left[\phi \frac{\partial^2 p}{\partial \theta^2} + \frac{\partial \phi}{\partial \theta} \frac{\partial p}{\partial \theta} \right] = \frac{U}{2} \frac{\partial \rho h}{\partial x} + \frac{1}{R_{cyl}} \frac{V}{2} \frac{\partial \rho h}{\partial \theta} + \frac{\partial \rho h}{\partial t} \quad (2.3)$$

With :

$$\phi = \frac{\rho h^3}{12\mu} \quad (2.4)$$

Where U is the fluid velocity along x direction and V is the fluid velocity along circumferential direction. As a cavitation model is considered in this study, p , ρ are the pressure and density of the homogeneous mixture. R_{cyl} is the cylinder bore's radius and h represents the fluid thickness. This equation contains four major terms, the variation of film thickness in time, the Poiseuille and the Couette contribution of fluid velocity, which

comes from the Stokes equation and the translational squeeze effect. For the boundary condition, the Dirichlet boundary condition is applied and shown as follows:

$$\text{Inlet: } p\left(\frac{b}{2}, \theta\right) = p_{\text{carter}} = p_{\text{comb}}(\psi) - p_a \quad (2.5)$$

$$\text{Outlet: } p\left(-\frac{b}{2}, \theta\right) = p_{\text{carter}} = 0; \quad (2.6)$$

In order to accurately represent the textured profile in the simulations, a small grid size is needed. Since simulating the full engine cycle time consuming, in the circumferential direction only one degree is considered and a periodic boundary condition is used. Spencer et al.[22] used this periodic boundary condition in their study of surface topology and they reported it to be a good model to consider when the film thickness and the pressure behave periodically. Hence, the boundary condition for pressure in θ direction will be the following:

$$\text{Side: } p(x, 0) = p(x, 2\pi) \quad (2.7)$$

Meanwhile, the derivatives of the Reynolds equation can be calculated by a 2^{nd} -order central finite difference operator.

2.2.2 Temperature Equation

The compression ring is exposed to the combustion chamber. Hence, a large amount of heat has to be transferred from the piston to the cylinder liner through the lubricant film. At the PRCL interface, the temperature variation in the lubricant has to be regarded. In this work, the convective heat transfer in the lubricant film is taken into account and the thermal conduction across the film thickness is neglected. This is justified by the value of Péclet number Pe , which is large enough for the sliding velocity between the piston ring and the cylinder liner. However, at the two dead centers, the piston's velocity decreases and approaches zero, the thermal conduction might take place. In the case the shear heating is also negligible due to the low velocity, we can assume a constant oil temperature. So, when $Pe > 1$, the temperature equation for a thin lubricant film will be as follows[7]:

$$\rho c_p u \frac{\partial T}{\partial x} + \rho c_p v \frac{1}{R_{cyl}} \frac{\partial T}{\partial \theta} = \mu \left\{ \left(\frac{\partial u}{\partial z} \right)^2 + \left(\frac{\partial v}{\partial z} \right)^2 \right\} \quad (2.8)$$

Here c_p is the heat capacity, T represents the temperature, u and v are the three dimensional fluid velocity profiles determined as [10]:

$$u(x, \theta, z) = \frac{1}{\mu} \frac{\partial p}{\partial x} \left(\frac{z^2 - h(x, \theta)z}{2} \right) - \frac{U}{h(x, \theta)} z + U \quad (2.9)$$

$$v(x, \theta, z) = \frac{1}{\mu} \frac{1}{R_{cyl}} \frac{\partial p}{\partial \theta} \left(\frac{z^2 - h(x, \theta)z}{2} \right) - \frac{V}{h(x, \theta)} z + V \quad (2.10)$$

Where U is the piston velocity. The above equations indicate that the velocity of a fluid film between two surfaces in relative motion is the sum of the velocities of the Poiseuille

and Couette flow. As we are only interested in the 2D density field $\rho(x, \theta)$ and 2D viscosity field $\mu(x, \theta)$, we take representative average values across the film, rather than using a full 3D field. The temperature equation is supplemented by Neumann boundary conditions in the x direction (at the inlet and the outlet), and periodic boundary condition in the θ direction (side) as:

$$\text{Inlet: } \begin{cases} T(\frac{b}{2}, \theta) = T_{oil} & U \leq 0 \\ \frac{\partial T}{\partial x}(\frac{b}{2}, \theta) = 0 & U > 0 \end{cases} \quad (2.11)$$

$$\text{Outlet: } \begin{cases} T(-\frac{b}{2}, \theta) = T_{oil} & U > 0 \\ \frac{\partial T}{\partial x}(-\frac{b}{2}, \theta) = 0 & U \leq 0 \end{cases} \quad (2.12)$$

$$\text{Side: } \frac{\partial T}{\partial \theta}(x, 0) = \frac{\partial T}{\partial \theta}(x, \frac{2\pi}{360}) = 0 \quad (2.13)$$

As mentioned above, when the Péclet number is less than 1, the temperature equation is not solved, but a constant temperature value is used for the oil temperature.

2.2.3 Cavitation Model

Cavitation is the phenomenon that takes place when the lubricant oil pressure decreases below to the saturation pressure or vapour pressure. There are two kinds of cavitation in fluid-film lubrication[20], i.e. gaseous cavitation and vapour cavitation. Gaseous cavitation forms when the pressure goes below the atmospheric saturation pressure and the dissolved gas comes out of the solution. For the vapour cavitation, if the pressure is further reduced to that vapour pressure and the lubricant starts to evaporate[20]. The piston ring reciprocates along the liner and the hydrodynamic pressure is built up. At the trailing part of the barrel-shaped ring the oil pressure drops below saturation pressure, and cavitation occurs. In our case, a cavitation model is used to represent the phenomenon that the formation of gas bubbles. Furthermore, a homogeneous mixture model is used to account for the effects of cavitation. The vapour volume fraction α , which is the ratio of the generated gases and the fluid volume, is defined as a function of the mixture's pressure and temperature. Those equations are showed as[7]:

$$\alpha(P, T) = \frac{1}{2}[1 + \tanh(A(T)(P - (T)))] \quad [27] \quad (2.14)$$

Where A and B are determined from imposing two points:

$$\begin{aligned} \rho = 0.01 &\leftrightarrow P_{\text{absolute}} = P_{\text{sat}} \\ \rho = 0.99 &\leftrightarrow P_{\text{absolute}} = P_{\text{vap}}(T) \end{aligned}$$

Then, the density and the viscosity of the homogeneous mixture can be determined from the vapour volume fraction.

$$\rho(P, T) = (1 - \alpha)\rho_l + \alpha\rho_v \quad (2.15)$$

$$\mu(P, T) = (1 - \alpha)\mu_l + \alpha\mu_v \quad (2.16)$$

Where the liquid viscosity is calculated according to the ASTM D341 equation[4]:

$$\mu_l : \log_{10}(\log_{10}(\mu_l + 0.7)) = A - B\log_{10}(T(K)) \quad (2.17)$$

In this equation, A and B are constants obtained from curve fitting to the IsoVG 100 viscosity curve. Therefore, the density of the lubricant is a function of temperature:

$$\rho_l(T) = \frac{\rho_{\text{ref}}(T)}{1 + \beta_1(T(\text{K}) - T_{\text{ref}})} \quad (2.18)$$

Where the reference temperature is 40°C, β_l is the thermal expansion coefficient and can be found in table 2.1. According to those equations, α value rises, the lubricant mixture's viscosity and density decreases accordingly.

2.2.4 Forces

The Radial Load

During the reciprocating motion of the piston on the cylinder liner, the external force is the sum of the chamber pressure and the pretension of the ring. It occurs on the interface of the compression ring. As the piston moves close to the dead center, this load should be balanced by the hydrodynamic force and the load carried by the interacting asperities on the surface of the compression ring. Whilst, the asperity contact make a major role in balancing this external load. The compression ring and cylinder liner contact works at the mixed lubrication regime. In most processes of a four-stroke engine cycle, this external load is balanced by the pressure generated from the lubricant, and this balance is under the hydrodynamic lubrication regime. At each crank angle, the balance is formed for a unique value of the minimum film thickness which depends on the engine geometry, lubricant properties and operating conditions. Generally, the inertial effect of the piston rings should also be considered. However, Roman et al.[17] showed that it has very small effect on the average friction force. Therefore, the inertial force is not included in this expression. The normal load equilibrium is expressed as below and this equation is satisfied especially when there is the surface contact, and this expression is used in the mixed lubrication regime[7].

$$F_{\text{hydrodynamic}} + F_{\text{asperities}} = F_{\text{ring}} + F_{\text{compression}} \quad (2.19)$$

For the situation that there is not the surface contact, the load is balanced by the hydrodynamic force from the lubricant, and the equation is shown as follows:

$$F_{\text{hydrodynamic}} = F_{\text{ring}} + F_{\text{compression}} \quad (2.20)$$

To calculate the hydrodynamic force, the pressure is integrated along the ring's sliding direction x . Each force per unit length in θ direction is derived from[7]

$$F_{\text{hydrodynamic}} = \int_{-\frac{b}{2}}^{\frac{b}{2}} p(x, \theta) dx \quad [N/m] \quad (2.21)$$

$$F_{\text{ring}} = \frac{16l_{\text{gap,f}}E_r I}{3\pi b D^4} b \quad [N/m] \quad (2.22)$$

$$F_{\text{compression}} = (p_{\text{comb}}(\psi) - p_a) b \quad [N/m] \quad (2.23)$$

Where b is the height of the compression ring, D is the diameter of the cylinder bore, $l_{\text{gap,f}}$ is the free gap size of ring, E_r is the young's modulus of the ring. All of those value

can be found in table 2.2. As mentioned before, there are two different lubricant regimes during the piston motion, i.e. the mixed lubrication regime and hydrodynamic regime. To distinguish them, the dimensionless film thickness λ is considered. It is the ratio of the minimum film thickness (clearance) h_o and the square root of two surface roughness numbers. [10][7]

$$\Lambda = \frac{h_o}{\sqrt{\sigma_c^2 + \sigma_r^2}} \quad (2.24)$$

Where σ_c is the cylinder liner surface roughness and σ_r is the surface roughness of compression ring. The dimensionless film thickness determines $F_{\text{asperities}}$ and the mixed lubrication regime occurs in this model when:

$$\Lambda = \frac{h_o}{\sqrt{\sigma_c^2 + \sigma_r^2}} \leq \Lambda_{\text{mixed}} \quad (2.25)$$

Where Λ_{mixed} represents the transition value between the mixed lubrication regime and the hydrodynamic regime.

Asperity Contact Model And The Friction Force

At dead centers, the piston has to change direction, its velocity fades briefly down to zero. At those processes, the dimensionless film thickness goes below Λ_{mixed} . The lubricated surfaces contact each other and the mixed-lubricant regime occurs. Hence, the force carried by asperities should be considered. The contact model of Greenwood and Tripp[8] is used in this study to account for the contact of the asperities. Its model takes into account the probabilistic distribution of contact points in the mixed and boundary lubrication regime. It represents the share of load carried by the interacting surfaces and it is based on the Gaussian distribution of the surface roughness. Hence, the asperity force is calculated as follows[7]:

$$F_{\text{asperities}} = \frac{16}{15} \sqrt{2\pi} (\zeta k \sigma)^2 \sqrt{\frac{\sigma}{k}} F_{5/2}(\Lambda) b \quad [N/m] \quad (2.26)$$

Where the dimensionless group $(\zeta k \sigma) \approx 0.04$ is a roughness parameter while $\frac{\sigma}{k} \approx 0.001$ is a measure of typical asperity slope. The statistical function $F_{5/2}(\Lambda)$, which represents the Gaussian distribution of asperities as function of the dimensionless film thickness Λ , is approximated as

$$F_{5/2}(\Lambda) = -0.0046 \left(\frac{\Lambda}{2}\right)^5 + 0.0574 \left(\frac{\Lambda}{2}\right)^4 - 0.2958 \left(\frac{\Lambda}{2}\right)^3 + 0.7844 \left(\frac{\Lambda}{2}\right)^2 - 1.0776 \left(\frac{\Lambda}{2}\right) + 0.6167 \quad (2.27)$$

In the PRCL contact, an equivalent Young's modulus should be considered in the surface contact between the compression ring and the cylinder liner:

$$\frac{1}{E_{\text{eq}}} = \frac{1 - \nu_c^2}{E_c} + \frac{1 - \nu_r^2}{E_r} \quad (2.28)$$

where ν_c and E_c are the Poisson ration and Young's modulus of the cylinder liner, while ν_r and E_r are the Poisson ratio and Young's modulus of the compression ring. The asperity force plays an important role in the calculation of the friction force at the mixed lubrication regime. The friction force generated at entire engine cycle is determined by different processes. at the

hydrodynamic lubrication regime which takes place at the mid-stroke, the viscous friction force is generated. Whilst, when the piston speed decreases, and surface contact occurs, the boundary friction force should also be considered as well. Thus, the friction force at two lubrication regimes can be calculated using the following equations[7]:

$$F_{\text{friction}} = \begin{cases} F_{\text{boundary}} + F_{\text{viscous}} & \Lambda \leq \Lambda_{\text{mixed}} \\ F_{\text{viscous}} & \Lambda > \Lambda_{\text{mixed}} \end{cases} \quad (2.29)$$

$$F_{\text{viscous}} = \int_0^{2\pi} \int_{-\frac{b}{2}}^{\frac{b}{2}} \tau(x, \theta, z = 0) dx d\theta \quad (2.30)$$

with the viscous shear stress at the surface of the cylinder liner:

$$\tau(z = 0) = \mu \left(\frac{u_2 - u_1}{h} \right) - \frac{\partial p}{\partial x} \frac{h}{2} \quad (2.31)$$

$$F_{\text{boundary}} = \tau_0 A_{\text{asperity}} + f_b F_{\text{asperities}} \quad (2.32)$$

Where u_2 is the fluid velocity at the upper surface of the fluid film and equals the piston velocity U , whereas u_1 is the velocity at the lower fluid film and equals 0 in this study. The friction coefficient of the boundary lubricated contacts is given by f_b , whereas τ_0 represents the lubricant limiting shear stress (i.e the stress at which slip between oil and wall occurs) and h is the film thickness which will be discussed later on.

For the friction force coming from the asperities, we consider a 2D-dimensional model for the asperity area A_{asperity} which is the cumulative area of contacting asperities given by;

$$A_{\text{asperity}} = \pi^2 (\zeta k \sigma)^2 \sqrt{\frac{\sigma}{k}} F_2(\Lambda) 2\pi R_{\text{cyl}} b \quad (2.33)$$

With statistical function $F_2(\Lambda)$ approximated as follows;

$$F_2(\Lambda) = -0.0018 \left(\frac{\Lambda}{2}\right)^5 + 0.0281 \left(\frac{\Lambda}{2}\right)^4 - 0.1728 \left(\frac{\Lambda}{2}\right)^3 + 0.5258 \left(\frac{\Lambda}{2}\right)^2 - 0.8043 \left(\frac{\Lambda}{2}\right) + 0.5003 \quad (2.34)$$

2.2.5 Film Thickness Equation

In the simulation, film thickness is time-dependent at each crank angle. The 2D film thickness of the textured compression ring in axial direction consists of three terms, i.e. the minimum film thickness (clearance) $h_o(t)$ at each crank angle, the film thickness based on the barrel shaped ring profile h_r and the film thickness h_d coming from different textures. The film thickness of textured ring $h(t)$ can be represented by the following functions:

$$h(t) = h_o(t) + h_r + h_d \quad (2.35)$$

$$h_r = 4 \frac{\delta x^2}{b^2} \quad (2.36)$$

Where δ represents the ring's crown height, t is time stamp of each crank angle, b is the height of the compression ring. In this work, the applied texture is chosen based on existing studies. The partial texture at two side of ring is implemented, because it has been found that the friction force is more reduced for a partially textured ring than a fully textured one[18]. Meanwhile, for a wide range of textures and operating conditions, a texture portion of 60% yields better performance[14]. Due to a reciprocating motion between the piston and the cylinder liner, it makes sense that a symmetrical and partial texture of transverse grooves is considered, which is

referenced from one research by Usman et al[24]. Before the definition of h_d , two dimensionless texture parameters are introduced. Firstly, the texture area density [15]:

$$S_p = \frac{r_p}{r_l} \quad (2.37)$$

Where r_p is the radius of the groove and r_l is the radius of the cell containing one groove. The figure below can schematically represent these two parameters of a groove-shaped texture:

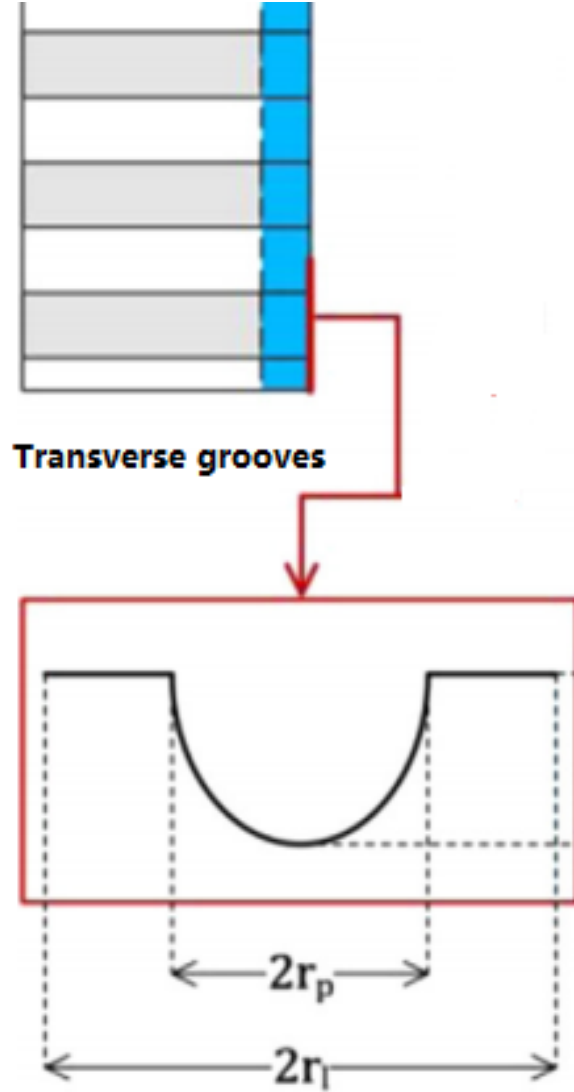


Figure 2.5: Transverse grooves on one side of ring[24]

Another important parameter is the aspect ratio ε , which is the ratio between the depth and the width of the groove.

$$\varepsilon = \frac{d_d}{w_d} \quad (2.38)$$

Where, d_d is the depth of the groove and w_d is the width of the groove.

In order to implement this transverse grooves on our ring, an arctangent function along the x direction is considered. Meanwhile, there is no geometrical variation in the circumferential

direction. The shape of the groove depends on those two texture parameters, i.e. S_p and ε . To better understand, The formula of h_d is shown:

$$h_d = d_d \left(\frac{1}{2} + \frac{1}{\pi} \left(\frac{x + L_d}{0.0005} \right) - \left[\frac{1}{2} + \frac{1}{\pi} \left(\frac{x - L_d}{0.0005} \right) \right] \right) \quad (2.39)$$

Where x is the angular domain and L_d is the radius of groove in the angular domain. They are shown as follows:

$$x = -\pi : \Delta x : \pi \quad (2.40)$$

$$\Delta x = \frac{2\pi}{N_d} \quad (2.41)$$

$$L_d = \frac{3\pi S_p}{5n_d} \quad (2.42)$$

Where the N_d is the grid number in x direction, n_d is the number of transverse grooves at one side of ring, and the depth of grooves can be shown:

$$d_d = \frac{0.3bS_p\varepsilon}{n_d} \quad (2.43)$$

To apply those grooves inside Matlab code, a 2D shape is shown in Figure 2.6. Texture parameters are chosen based on Usman's model[24]. Where the area density $S_p = 0.50$ and depth-to-width ratio $\varepsilon = 0.11$.

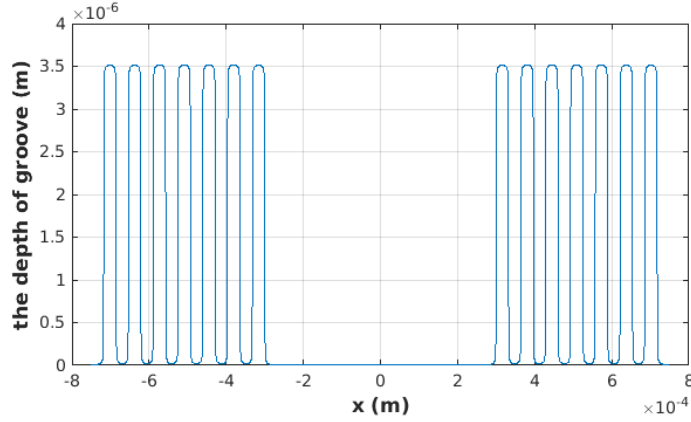
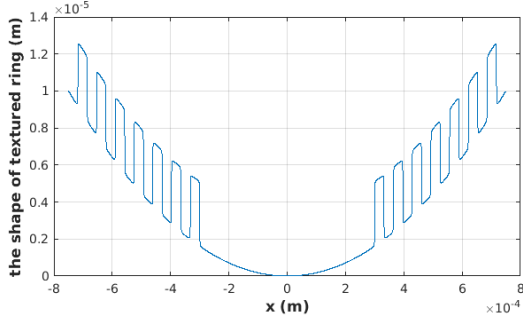
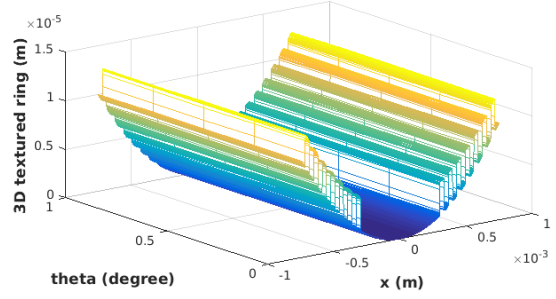


Figure 2.6: A 2D graph of transverse groove texture considering $S_p = 0.5$ and $\varepsilon \approx 0.11$ [24]

After applying the 2D texture groove of previous figure to the ring, the 2D and 3D plot of the textured ring are displayed as following:



(a) A 2D plot



(b) A 3D plot

Figure 2.7: The 2D and 3D plot of the textured ring [24], considering transverse grooves: $S_p = 0.5$ and $\varepsilon \approx 0.11$

2.2.6 Algorithm

Previous mathematical equations are solved using a computational algorithm in Matlab code, which was developed by Prof. Fauconnier. This algorithm consists of a time-dependent outer loop which is iterated over crank angles. The minimum film thickness (clearance) is determined after the end of loop. Whilst, there is an inner loop as well. The Reynolds and the temperature equations are solved at a given film thickness $h(x, \theta)$ resulting in the outer loop. The relative tolerance errors are calculated at the inside loops, which are the difference between the calculated values of two consecutive iterations[25]. For instance, clearance tolerance, temperature and pressure tolerance of the inner loop. Furthermore, after defining the film thickness an absolute tolerance is used to balance the radial load. In the Matlab code, this equilibrium has been satisfied when[19]:

$$ERR_{load} = \frac{|F_{(\psi)} - W_{(\psi)}|}{F_{(\psi)}} \leq E_{limit} \quad (2.44)$$

Where, $F_{(\psi)}$ is the sum of hydrodynamic and asperity load, $W_{(\psi)}$ is the inner ring's load coming from the combustion chamber and the pretension of the ring, and the E_{limit} is a small number which will guarantee the computational stability. Before the initialization of the outside loop, some input data are defined accordingly and shown as below:

1. Define the geometry of the compression ring, cylinder liner, engine configuration and the geometry parameters of texture.
2. Create the computational grid and discretize using Finite Difference Method.
3. Define lubricant properties, operating conditions (i.e. nominal oil temperature and engine speed).
4. Construct a State structure in the code to store variables at each crank angle (i.e. pressure, temperature, vapour volume fraction, COF, λ . etc).

The outer loop procedure goes as the flow chart below:

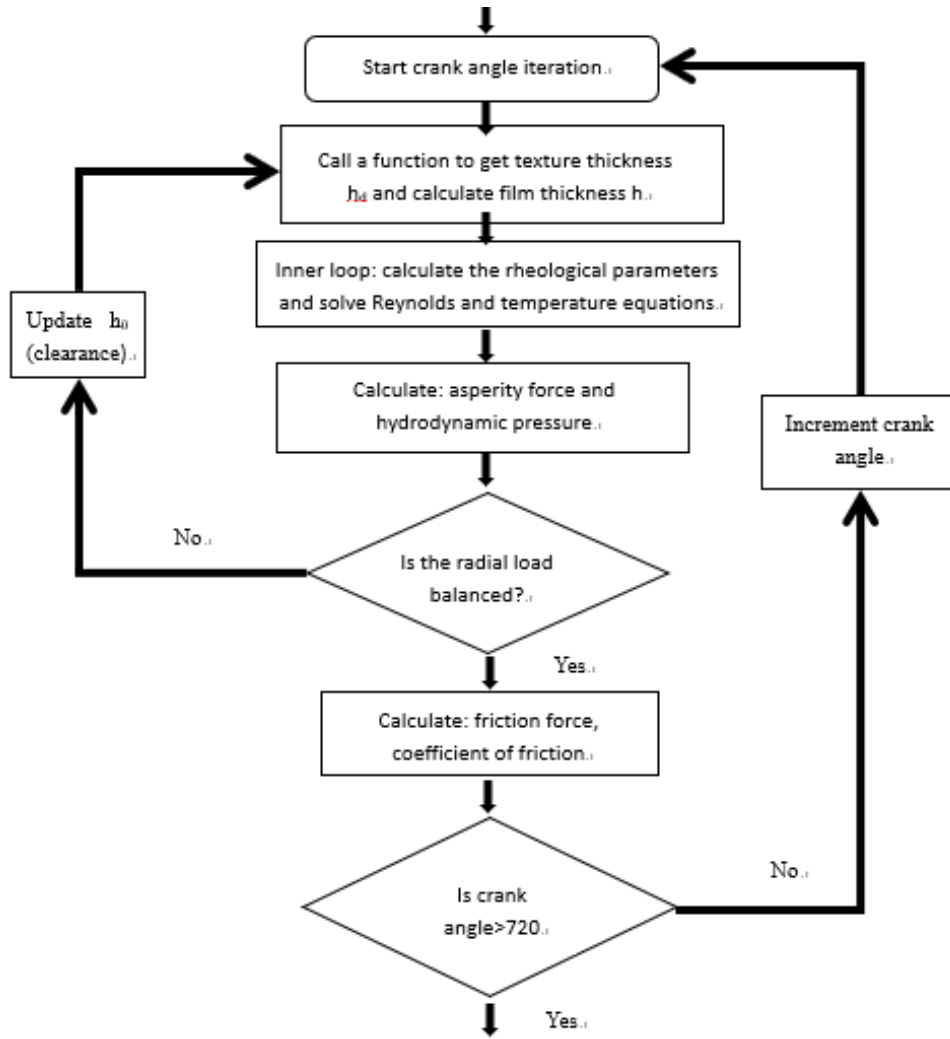


Figure 2.8: A computational flow chart for outer loop

To update the clearance h_o , the function is applied with[19]:

$$(h_o)^n = (1 + 0.05X)(h_o)^o \quad (2.45)$$

$$X = \frac{F(\psi) - W(\psi)}{F(\psi)} \quad (2.46)$$

Where the minimum film thickness is updated at each crank angle. X is an adjusting parameter. n and o denote new and old iteration numbers.

Chapter 3

Result

3.1 Stribeck Curve

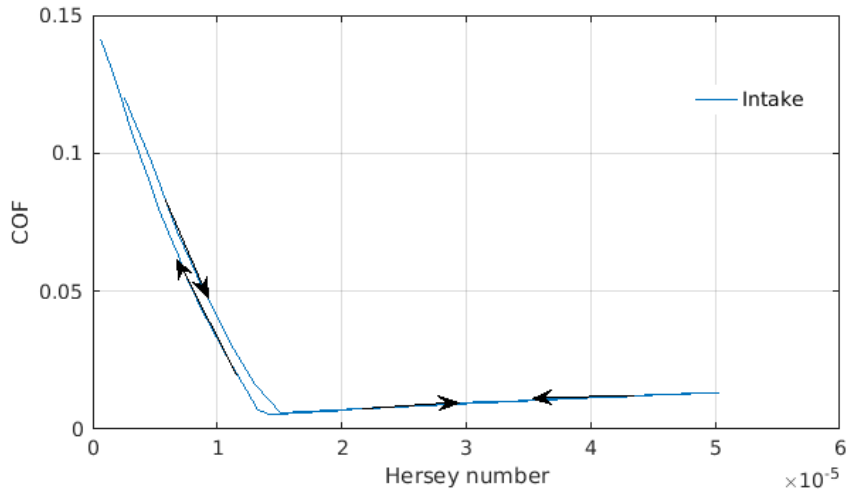
The Stribeck curve is a plot indicating the coefficient of friction over different lubrication regimes, which composes boundary, mixed and hydrodynamic lubrication regimes. Stribeck introduced this curve, for which a plot of the coefficient of friction (COF) vs Hersey number was taken into account. The dimensionless Hersey number:

$$\text{Hersey number} = \frac{\mu v}{N} \quad (3.1)$$

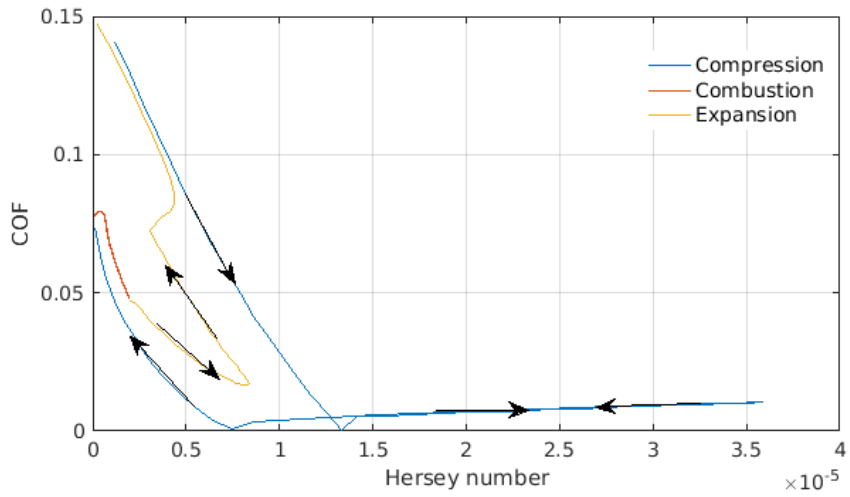
Where μ is the dynamic viscosity, v is the speed of the fluid and N is the normal load. Inside four-stroke engine cycle, Hersey number is very small at the beginning point of each stroke, because the velocity of piston decreases at the dead center. As we known, the coefficient of friction is the ratio between the friction force and the normal load. This dimensionless value, in this study, is represented:

$$\text{COF} = \frac{F_{\text{friction}}}{F_{\text{ring}} + F_{\text{compression}}} \quad (3.2)$$

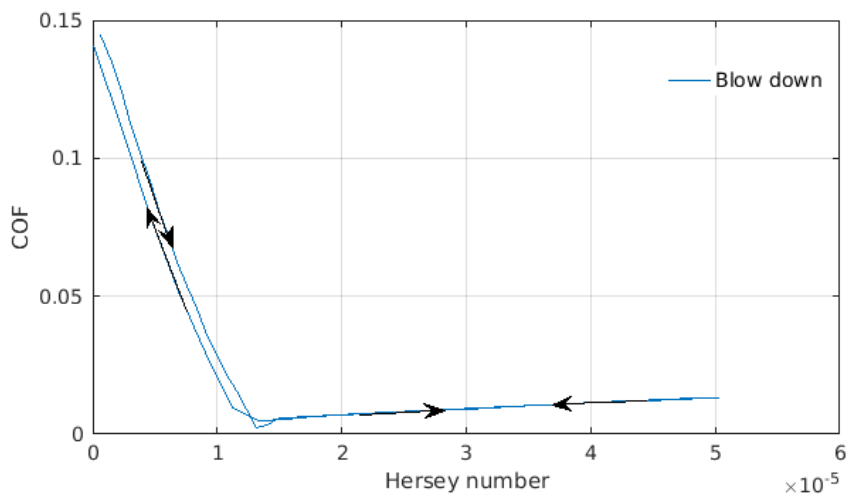
Where F_{friction} , F_{ring} and $F_{\text{compression}}$ have been defined before (see equations 2.29, 2.22, 2.23). In order to evaluate the Stribeck curve for this four-stroke engine cycle, the smooth ring reciprocating on the cylinder liner is considered. A warm engine operating condition includes the temperature equation for the lubrication. In those figures, the arrow represents the direction corresponds to the increment of the crank angle. To better observation, Stribeck curves for different processes are shown respectively:



(a) Intake process



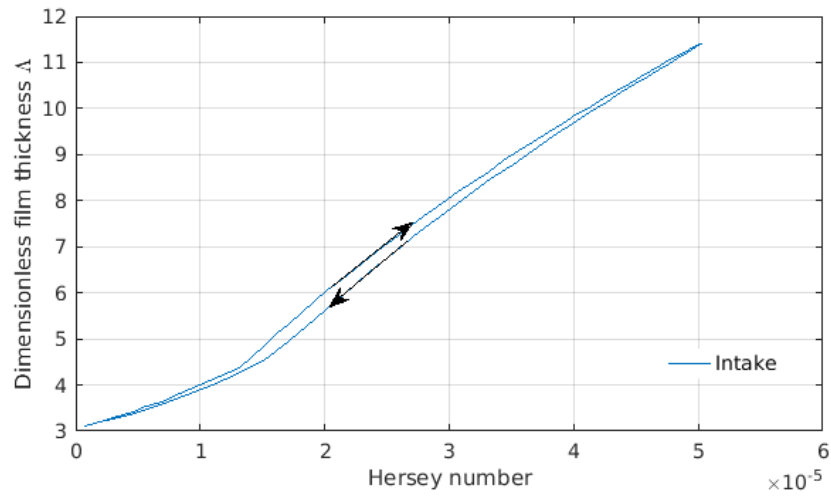
(b) The processes includes compression, combustion and expansion



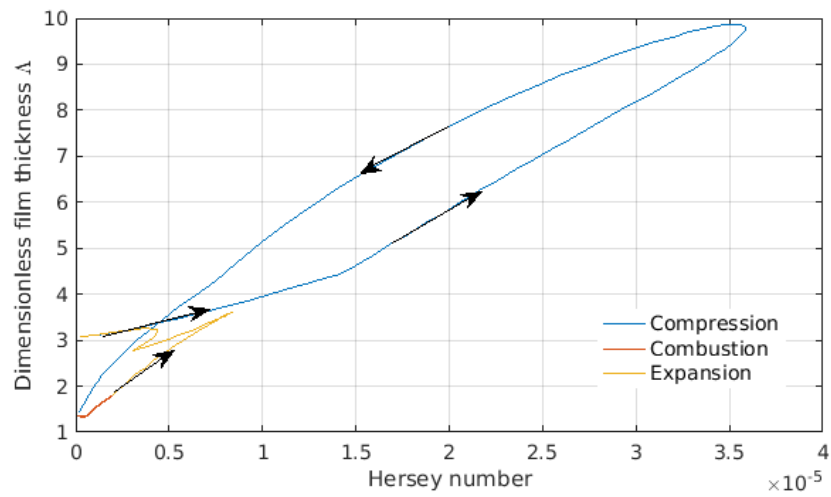
(c) The blow down process

Figure 3.1: The Stribeck curve of the Hersey number at x axis, COF at y axis

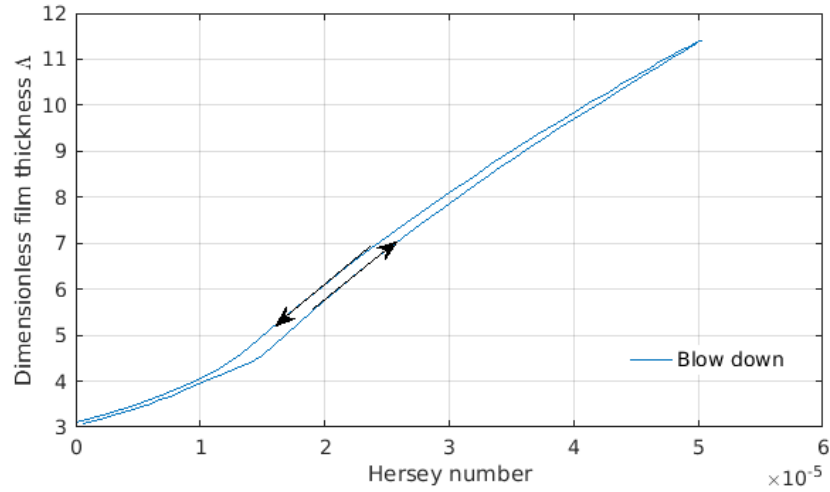
Meanwhile, the plots of the dimensionless film thickness Λ (see eq:2.24) with respect to the Hersey number are considered as well. Different processes are represented as follows:



(a) Intake process



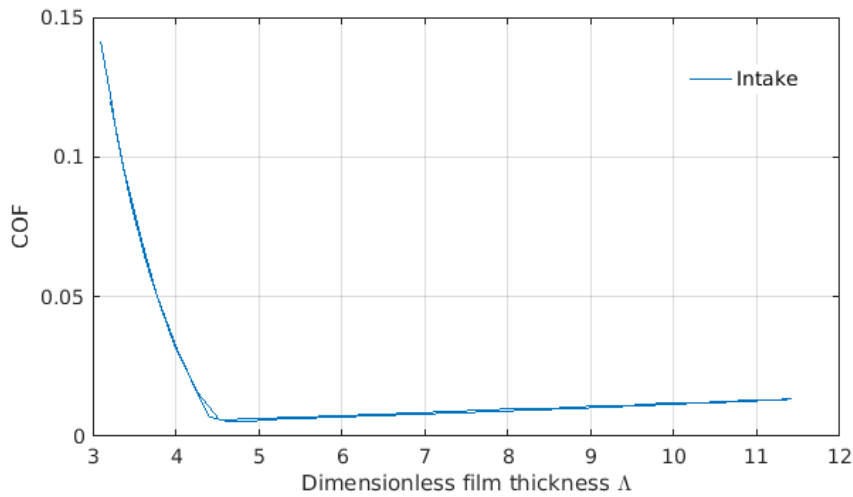
(b) The processes includes compression, combustion and expansion



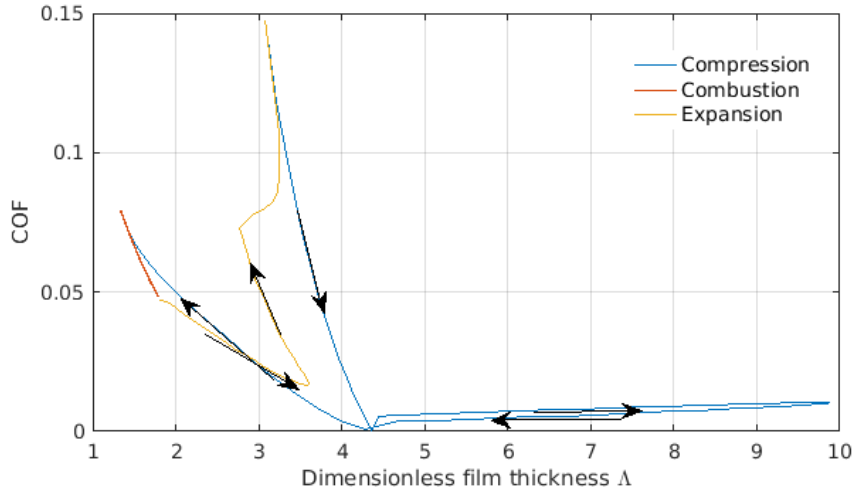
(a) The blow down process

Figure 3.3: The curves of the Hersey number at x axis, the dimensionless film thickness (Δ)

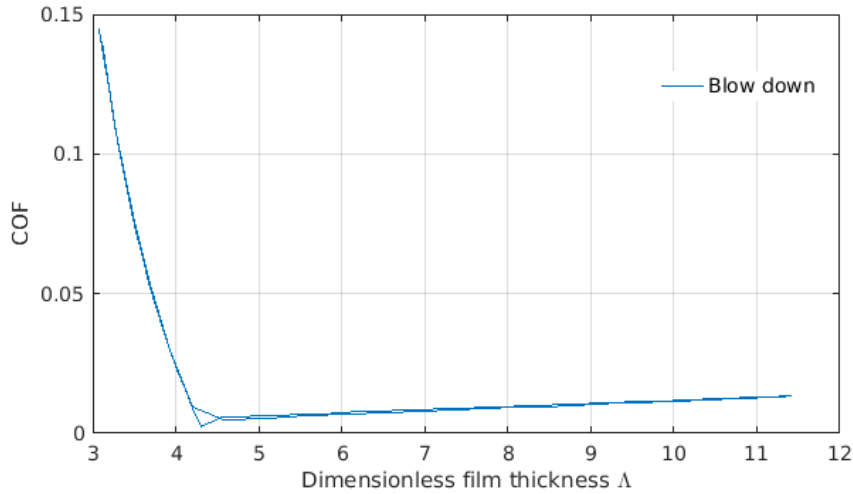
On the other hand, the dimensionless film thickness at the horizontal axis is introduced by Tallian[23]. It has been found that the Δ value can be used to determine the lubricant regimes and is able to correlate the amount of friction force at each film thickness with the reasonable accuracy[13]. In this study, the plot of the dimensionless film thickness at x axis, and the COF value at y axis are displayed for those processes:



(a) Intake process



(a) The processes includes compression, combustion and expansion



(b) The blow down process

Figure 3.5: The curves of the dimensionless film thickness (Λ) at x axis, COF at y axis

We can say that either for the Stribeck curve or the curve introduced by Tallian, in Figure 3.1 and 3.5, different engine processes have variable behaviors. Those differences are relevant for a region with higher COF value. It translates that those processes are different to each other at the mixed lubrication regime. In this study, the piston starts to move from the top dead center. Meanwhile, it can say that each process is a reciprocating motion which starts from the dead center, moves to the mid-stroke and back into another dead center. Therefore, the Stribeck curve (see eq:3.1) shows clearly that the mixed lubrication regime occurs at the dead center, and the hydrodynamic lubrication regime appears at mid-stroke. Firstly, the Hersey number corresponds to each crank angle generates different dimensionless film thickness value, even if the piston moves on the same path. The reason is that the piston moves with different accelerations at each process (see fig:2.3). This consequence can be found in Figure 3.3, and it can translate that the piston generates different film thickness, even if it passes through the same path (i.e, intake, compression and blow down processes). The combustion process should not be included. Secondly, Figure 3.5 shows that the COF corresponds to each dimensionless

film thickness. Based on those two consequences, it can prove that each Hersey number induces different COF value in Figure (3.1). It translates that curves at each processes are not superimposed. For those engine processes, combustion and expansion processes locate inside the mixed lubrication regime, because their Λ values are lower than 4 (see fig:3.3). In addition, Intake, compression and blow down processes composes the mixed and the hydrodynamic lubrication regimes. According to previous figures, the intake and blow down processes are quite similar. However, the compression process and intake process have different behaviors in the mixed lubrication regime. It means that the compression process has a lower COF compared to the intake process. To better explain it, the equation of COF is derived regarding the equation 3.2, the result of COF value includes two compositions which are related to $F_{\text{asperities}}$ (eq:2.26) and F_{viscous} (eq:2.30):

$$\text{COF} = \frac{F_{\text{asperities}}}{F_{\text{ring}} + F_{\text{compression}}} + \frac{F_{\text{viscous}}}{F_{\text{ring}} + F_{\text{compression}}} \quad (3.3)$$

The result of COF value coming from the term of $F_{\text{asperities}}$ for each processes are positioned at the mixed lubrication regime. According to previous figures, different processes have different behaviors in this regime. In order to better understand the reason behind it, the asperity friction force and the normal load ($F_{\text{ring}} + F_{\text{compression}}$) correspond to each crank angle are displayed as below:

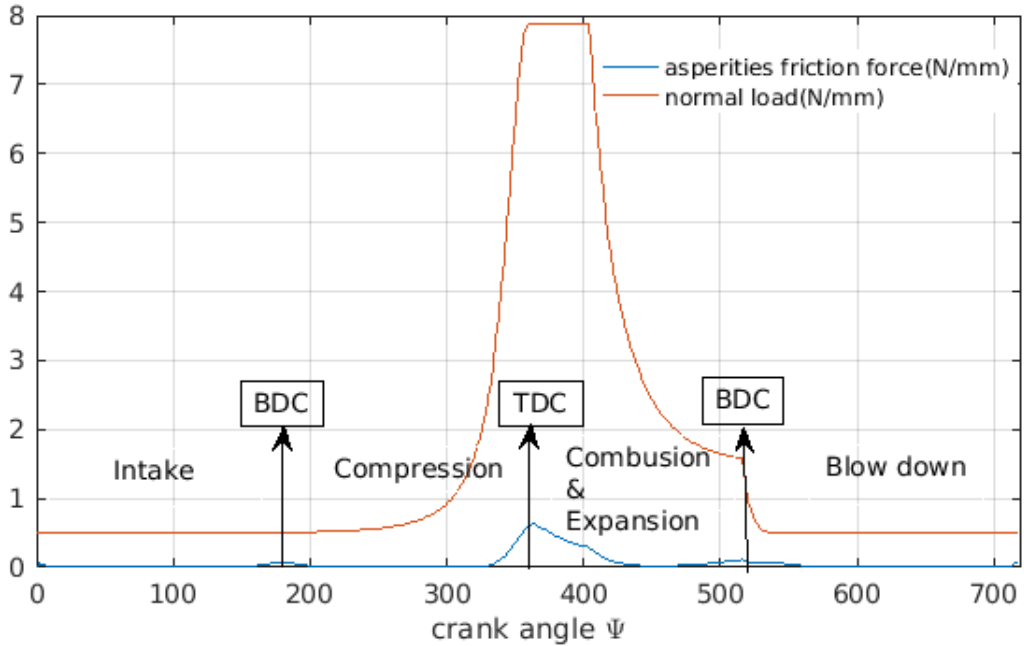


Figure 3.6: The figure of the asperity friction force and the normal load at each crank angle

As found in Stribeck curve in Figure 3.1, the result of COF value at the end of the compression process is lower than the end of intake process. The reason can be found in Figure 3.6. It can prove that the normal load increases at the end of the compression process. Even if the asperity friction force increases as well and even more effective than other processes. Meanwhile, it can also prove that the COF at combustion and expansion processes are still lower. Furthermore, the viscous friction force at each crank angle in four-stroke engine cycle goes as follows in Figure 3.7. It is easily found that the viscous friction forces are higher in the compression and

expansion processes, because these two processes have the lower dimensionless film thickness values (see fig:3.3). Regarding to equation 2.30, the lower is the film thickness (h), the larger the viscous friction force is generated. Also, as the viscous friction force depends on the film thickness, the slope of those curves is related to the slope of the Λ curves (see fig:3.3). The viscous friction force of the combustion process is neglected in Figure 3.7.

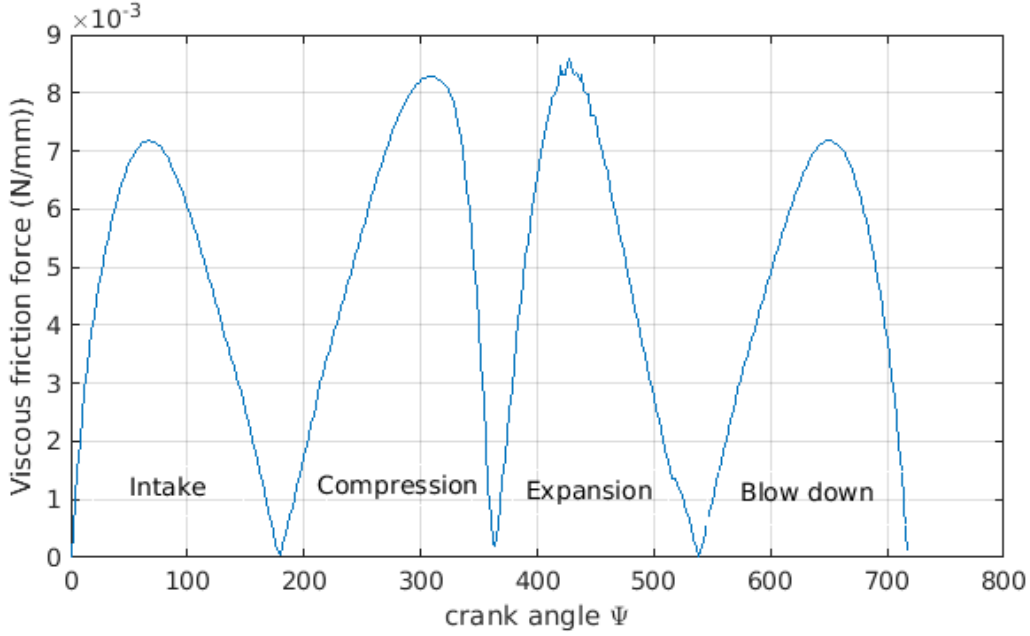


Figure 3.7: The figure of viscous friction force at each crank angle

3.2 A Comparison Study

In this section, after studying one of previous articles done by Usman et al.[24]. A comparison of their engine and operating conditions to those of this study is done. Consequently, it has been found in this study that the operating temperature has a significant influence on tribological parameters, i.e. the dimensionless film thickness and the coefficient of friction.

The texture of transverse grooves at two side of the compression ring is considered. This texture is referenced from Usman et al.[24]. Two texture parameters are chosen as: $S_p=0.5$, $\varepsilon=0.11$. This textured ring-liner model is working under the operating conditions: a nominal temperature $T_{oil}=95^\circ\text{C}$ and the engine speed $n=2400$ rpm. Also, an isothermal warm engine is considered, which means that there is not convective heat transfer inside the lubricant film. Furthermore, the dimensionless film thickness and the COF are taken into account at entire engine cycle:

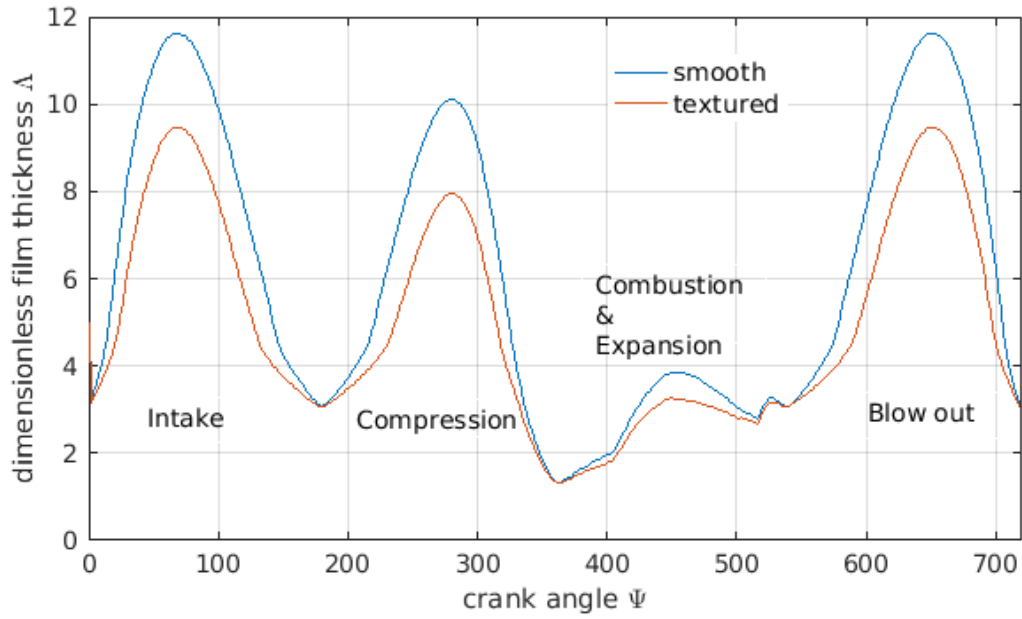


Figure 3.8: The figure of dimensionless film thickness at each crank angle under an isothermal warm condition. A comparison of a smooth ring and a textured ring is considered. Two texture parameters for the texture are assumed as: $S_p=0.5$, $\varepsilon=0.11$

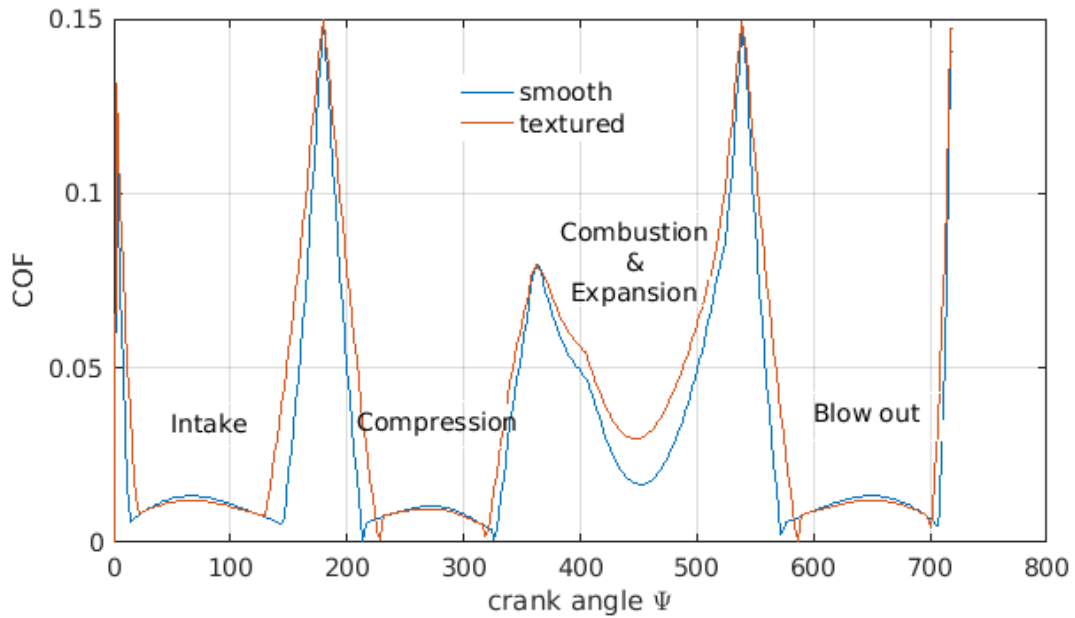


Figure 3.9: The figure of coefficient of friction (COF) at each crank angle under an isothermal warm condition. A comparison of a smooth ring and a textured ring is considered. Two texture parameters for the texture are assumed as: $S_p=0.5$, $\varepsilon=0.11$

According to figures before, the textured ring reciprocating on the cylinder liner does not improve the dimensionless film thickness. Also, it has a wider mixed lubrication region than the smooth ring. The coefficient of friction is higher at the combustion and the expansion processes. In order to better understand the reason that this texture geometry doesn't work well at this engine condition, a step-by-step simulation analysis is performed. The engine compartment from the article [24] and the cold engine operating conditions are taken into account (i.e. $n = 1600rpm$, $T_{oil} = 20^{\circ}C$). The analysis condition is executed in this order, which initiates from Usman's engine and cold conditions to the case of this study one by one:

K: The condition includes the engine compartment of Usman[24] and the cold engine operating conditions

K+w: The ring's width (w) of this study is added in this case

K+w+s: This engine stroke (s) is added in this case

K+w+s+ δ : The ring's crown height (δ) is added in this case

K+w+s+ δ + γ : This engine compression ratio (γ) is added in this case

K+w+s+ δ + γ + n : This engine speed ($n=2400$ rpm) is added in this case

K+w+s+ δ + γ + n + σ : The surface roughness (σ) is added in this case

Q: The condition includes the engine compartment and the warm engine operating conditions of this study

The textured ring is considered as well as the smooth rings for condition K and Q. The change of condition due to the engine geometry and operating conditions are concerned as well. Whilst, for further verification, only a half intake stroke (i.e. from the top dead center (mixed lubrication regime) to mid-stroke (hydrodynamic lubrication regime)) is considered, because it includes the mixed lubrication regime and the hydrodynamic lubrication regime. Firstly, the comparison between different textured rings (i.e. K and Q) is done, as well as the smooth ring corresponding to those two conditions.

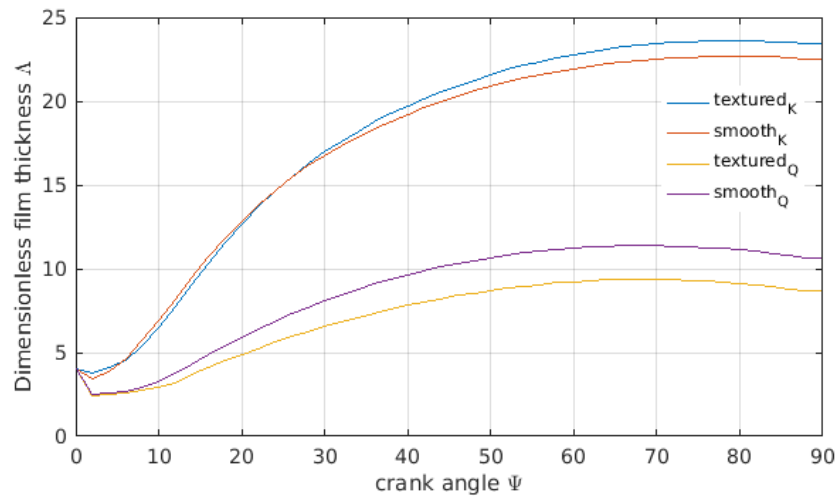


Figure 3.10: The figure of dimensionless film thickness value at each crank angle for the textured rings and smooth rings. A half intake process is concerned

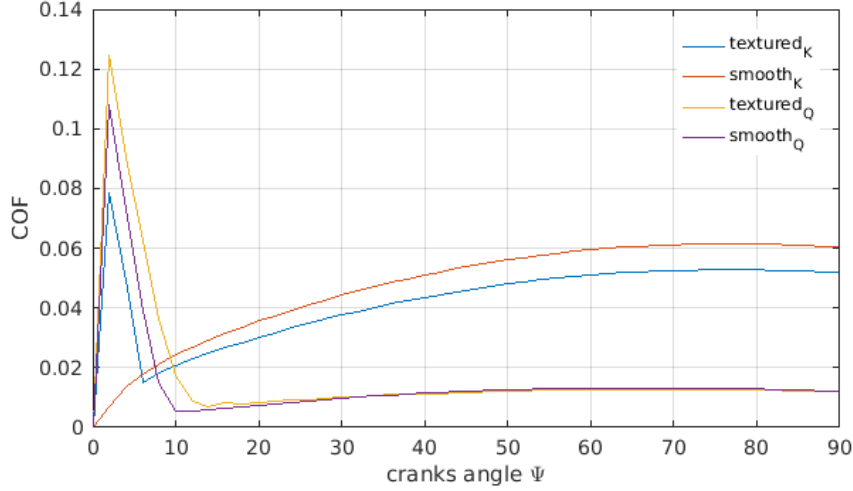


Figure 3.11: The figure of coefficient of friction (COF) at each crank angle for the textured rings and smooth rings. A half intake process is regarded

Figure 3.10 can easily show that the textured ring of condition K improves the dimensionless film thickness, which happens when the piston moves to the mid-stroke region. It means that the film thickness can increase through the texture under this condition. However, for the case of this study, the textured ring does not make positive effect on the film thickness. In Figure 3.11, it can be found that lower Λ generated by the textured ring of condition Q induces more boundary friction force at the mixed lubrication regime. Whilst, for the condition of K, the Λ improves at the hydrodynamic lubrication regime which results in the reduction of COF at this regime. But, there is significant increasing of COF at the mixed lubrication regime. Besides, to quantitatively understand the texture's influence, two parameters are introduced.

$$\Delta\Lambda = \frac{\Lambda_{\text{textured}} - \Lambda_{\text{smooth}}}{\Lambda_{\text{smooth}}} \% \quad (3.4)$$

$$\Delta\text{COF} = \frac{\text{COF}_{\text{smooth}} - \text{COF}_{\text{textured}}}{\text{COF}_{\text{smooth}}} \% \quad (3.5)$$

the positive values of $\Delta\Lambda$ and ΔCOF are expected. For those two conditions (K and Q), $\Delta\Lambda$ and ΔCOF at each crank angle are represented in Figure 3.12. Meanwhile, logarithmic scale at y axis of ΔCOF plot is used.

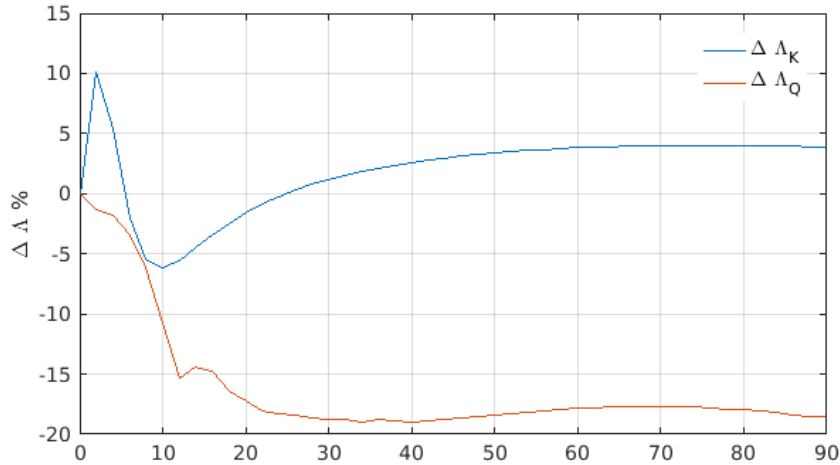


Figure 3.12: The figure of $\Delta\Lambda$ at each crank angle for the condition K and Q. A half intake process is concerned

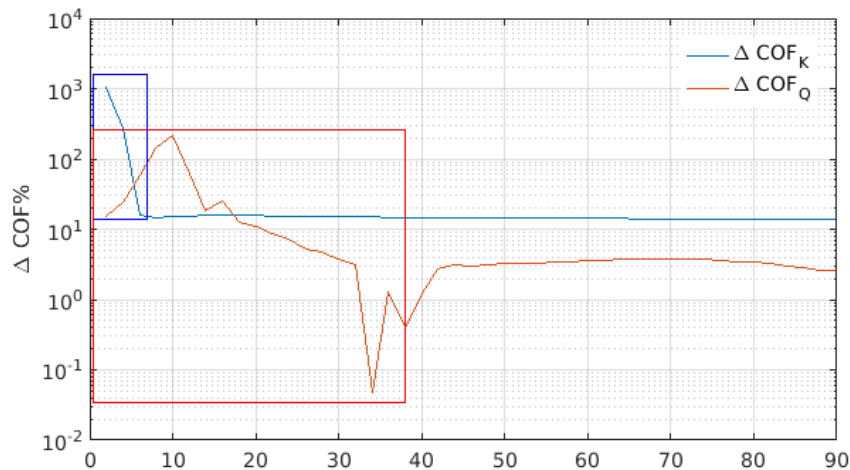


Figure 3.13: The figure of ΔCOF at each crank angle for condition K and Q. A half intake process is concerned

Based on Figure 3.12, the textured ring can approximately increase 4% Λ value at the hydrodynamic lubrication regime and 10% at the mixed lubrication regime under condition K. In addition, a logarithmic plot is used in Figure 3.13. The rectangle areas represent the negative value regions for these two conditions respectively. For the condition of this study (Q), the coefficient of friction reduces in the hydrodynamic lubrication regime compared to the case of smooth ring, which initiates when $\Psi \approx 38$ (see fig:3.13). Meanwhile, for the case K, the friction force is decreased at the whole hydrodynamic lubrication regime. On the other hand, the COF is much higher for the textured ring than the smooth at the mixed lubrication regime, which is proved by a large negative ΔCOF value. Secondly, in order to verify the reason that makes those difference, the effect of engine configuration is taken into account. The dimensionless film thickness and the COF from case 1 to case 4 are shown. Meanwhile, in the following plots, the condition K and Q are particularly marked as well.

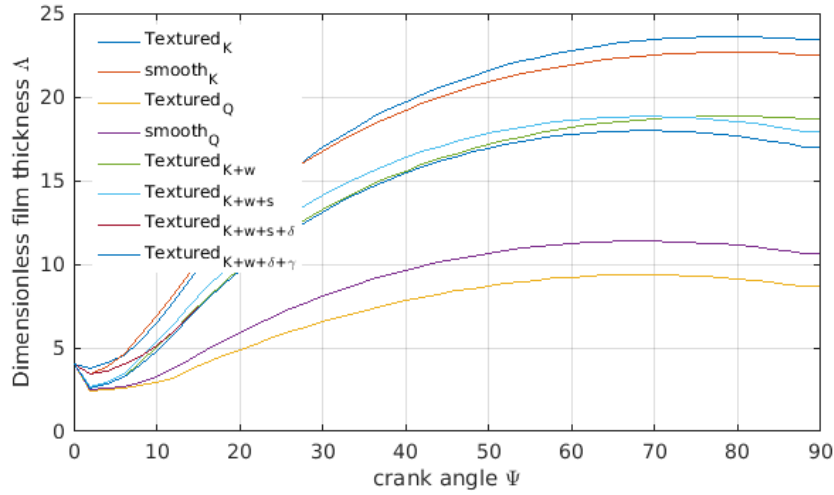


Figure 3.14: The figure of Λ value at each crank angle for the verification of the effect of engine configuration. A half intake process is concerned

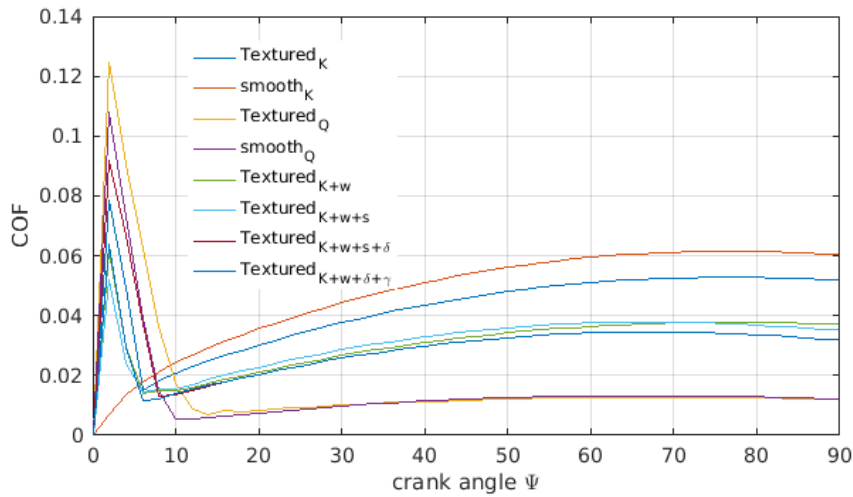


Figure 3.15: The figure of COF at each crank angle for the verification of the effect of engine configuration. A half intake process is concerned

Figure 3.14 indicates that the dimension of the engine compartment influences the Λ . Especially, the width of the ring reduces the dimensionless film thickness. Figure 3.15 shows that the coefficient of friction is reduced by applying the engine of this study at hydrodynamic lubrication regime but increases at the mixed lubrication regime. Meanwhile, the effect coming from the operating conditions and the surface roughness are shown as follows:

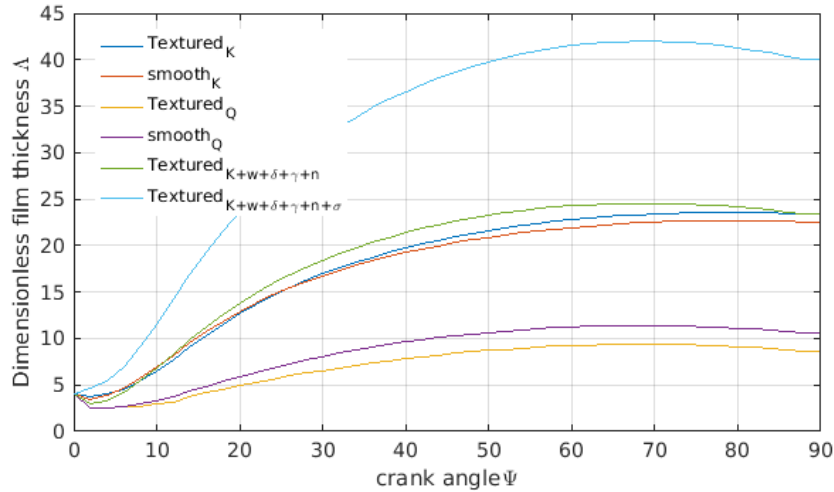


Figure 3.16: The figure of Λ value at each crank angle for the verification of the effect of operating conditions and surface roughness. A half intake process is concerned

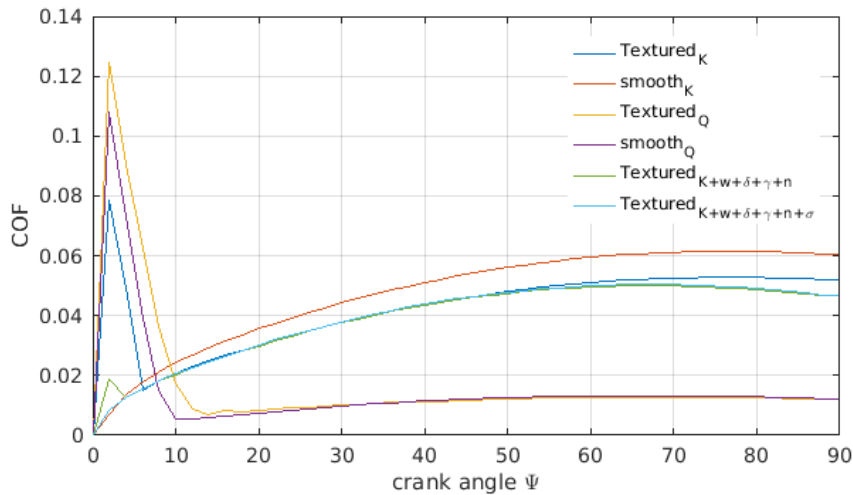


Figure 3.17: The figure of COF at each crank angle for the verification of the effect of operating conditions and surface roughness. A half intake process is concerned

Through the comparison of Figure 3.14 and 3.16, a higher engine speed of this study increases the dimensionless film thickness. In addition, the surface roughness has a larger effect compared to the engine speed, because the surface roughness is small (see table:2.2). By considering the high temperature from this study, it can be found that the temperature has the largest effect of this step-by-step study. Consequently, there are three parameters that make a significant difference in this comparison study, i.e. the width of the ring, the engine speed and the temperature. Furthermore, a higher temperature generates the lower Λ , which gets different tribological results from the condition K to condition Q. The reason is that the temperature changes the viscosity of mixture. This value is relevantly higher for a lower temperature condition than a warm one. This is proved by the following figure.

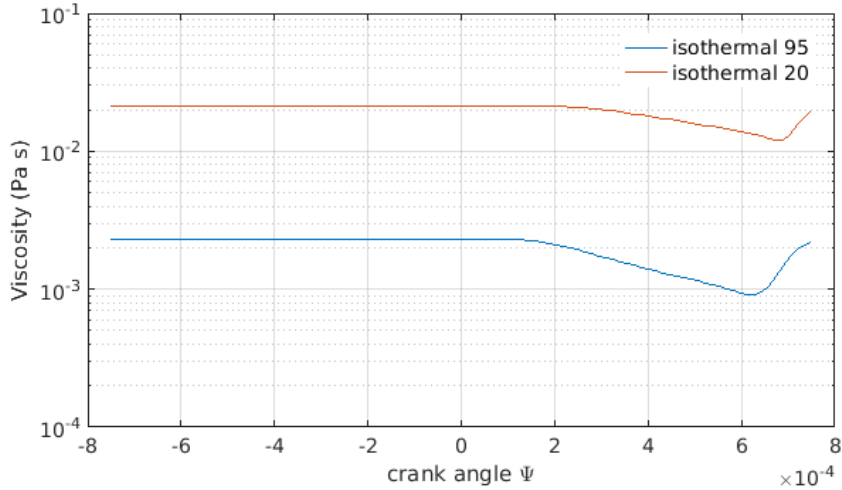


Figure 3.18: The figure of viscosity along the ring profile (x direction). Isothermal engine condition is considered for the warm and cold engines. The plot is taken at the crank angle ($\Psi=70$) when the piston reaches its maximum speed

Where two conditions with respect to different temperatures are considered. The smooth ring and the logarithmic scale in y axis are concerned as well. The profile of figure 3.18 is related to the vapour volume fraction (α) at the right part of ring ($x > 0$). The following plots display the vapour volume fraction' behavior along the ring profile (x-direction), in which two temperature cases are defined.

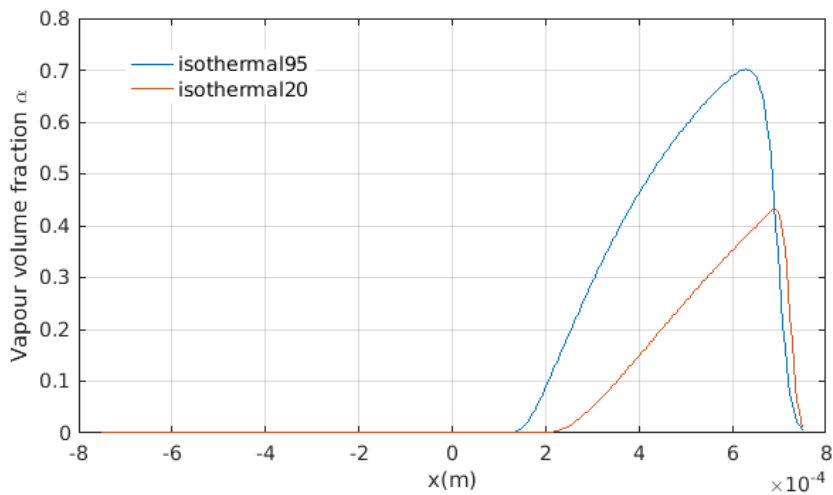


Figure 3.19: The figure of vapour volume fraction's behavior along the smooth ring profile (x direction) for two cases with respect to different temperatures. The crank angle ($\Psi=70$) is considered.

So far, it has also been found in Figure 3.19 that temperature has impact on α . Especially, high temperature case generates more α than the low temperature case at cavitation region. It can prove the profile of viscosity in Figure 3.18.

3.3 Texture Profile Analysis

At this part, two different engine operating temperatures are investigated, i.e. the cold and warm engine operating conditions. For the cold engine operating condition, the temperature equals 20 °C. The 95 ° warm engine operating conditions with or without temperature equation consideration for the lubricant film are compared each other. Regarding the table 3.1, different textured rings are taken into account as well as the smooth ring. Those different texture profiles influence the tribological parameters in the four-stroke engine cycle. They are the dimensionless film thickness, COF and $\bar{\alpha}$. Furthermore, $\bar{\alpha}$ is the measure of the total released gases from the lubricant oil and it is defined as below:

$$\bar{\alpha} = \int_{-\frac{b}{2}}^{\frac{b}{2}} \alpha dx \quad (3.6)$$

In this section, the textured ring with different texture profiles are shown. The transverse grooves on two side of ring are considered(see fig:2.7). Whilst, the texture profile depends on two parameters, i.e. the area density S_p and the depth-to-width ratio ε . 9 different kinds of textured rings have different geometries. They are shown in the following matrix.

	$0.75S_p$	S_p	$1.25S_p$
$\frac{\varepsilon}{2}$	$w_d/2, d_d/4$	$w_d, d_d/2$	$2w_d, d_d$
ε	$w_d/2, d_d/2$	w_d, d_d	$2w_d, 2d_d$
2ε	$w_d/2, d_d$	$w_d, 2d_d$	$2w_d, 4d_d$

Table 3.1: A texture geometry matrix

Where w_d and d_d represent the width and depth of grooves, which are referenced from Usman's article[24]. Also, $S_p=0.5$, $\varepsilon=0.11$ are considered. $1.25S_p$ is chosen as the greatest area density, This value is higher than the values chosen by previous articles[24][20].

3.3.1 Analysis At The Cold Engine Operating Temperature

Temperature is recognized as an important operating parameter in this study for a tribological analysis. In this section, a 20° C cold engine operating temperature is considered, which is referenced from Usman's article[24]. The convective heat transfer is not included in this case. Regarding 9 different kinds of textures in Table 3.1, a comparison between textured rings and the smooth one is taken into account to investigate their effect on parameters. Those parameters are the dimensionless film thickness, coefficient of friction and $\bar{\alpha}$. Firstly, an analysis of the dimensionless film thickness is based on $\Delta\Lambda$ (see eq:3.4). In the figures below, each three textures with the same area density S_p are considered. The difference between the textured ring and the smooth one through a full engine cycle is given by:

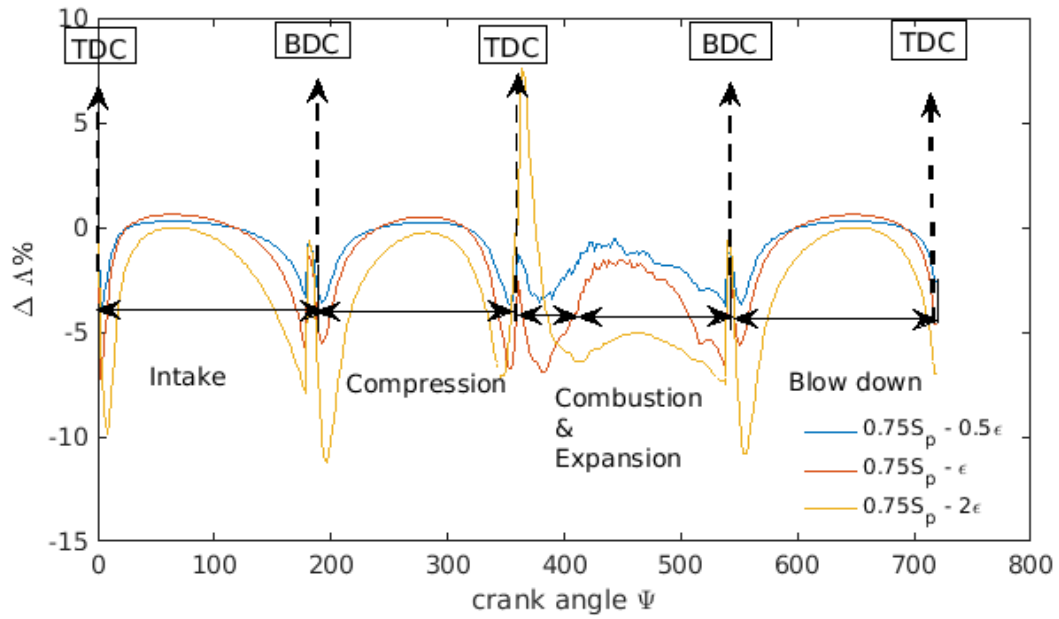


Figure 3.20: The figure of $\Delta\Lambda$ at entire engine cycle for three textures with the same area density ($0.75S_p$). An isothermal cold engine operating condition is considered

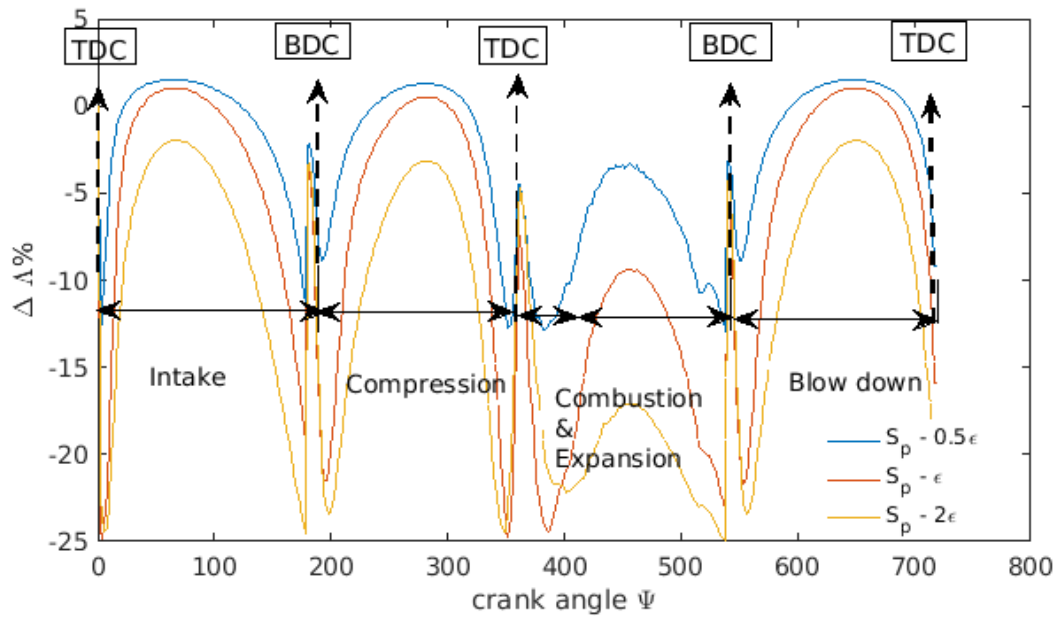


Figure 3.21: The figure of $\Delta\Lambda$ at entire engine cycle for three textures with the same area density (S_p). An isothermal cold engine operating condition is considered

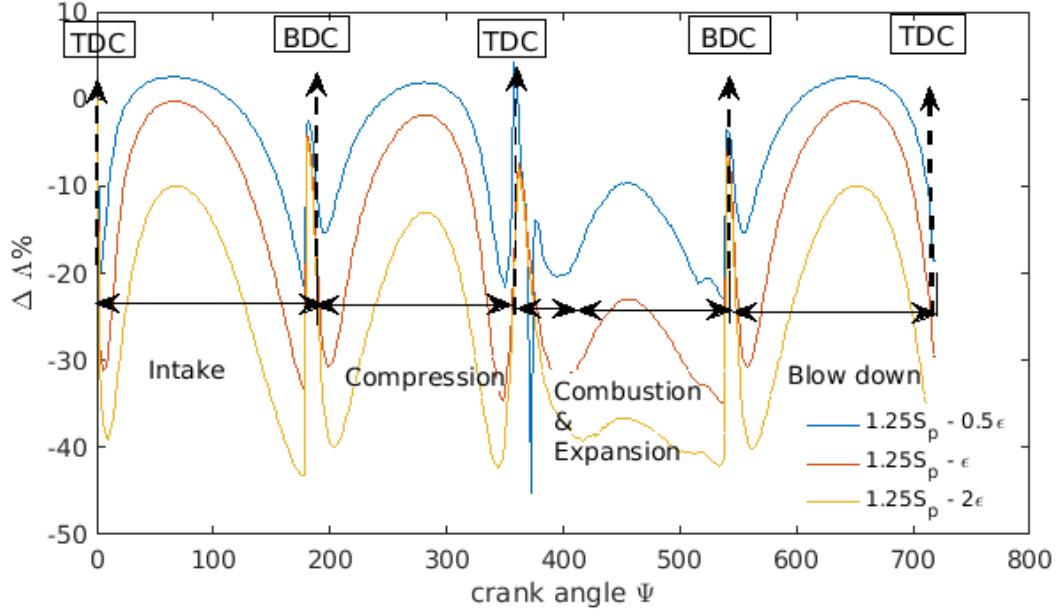


Figure 3.22: The figure of $\Delta\Lambda$ at entire engine cycle for three textures with the same area density ($1.25S_p$). An isothermal cold engine operating temperature is considered

It can be found that those two texture parameters influence the $\Delta\Lambda$ value at cold temperature. Difference in area density seems have more relevant effect on $\Delta\Lambda$ (see fig:3.20 and 3.21). Figure 3.10 shows that the textured ring generates higher Λ value than the smooth ring at lower temperature, especially at mid-stroke (the hydrodynamic lubrication regime). Whilst, based to previous figures of $\Delta\Lambda$, transverse grooves considering small depth-to-width ratio or small area density make an positive improvement at the mid-stroke of each process. Especially, the texture considering the small depth-to-width ratio (0.5ϵ) seems have better improvement. In addition, the dimensionless film thickness does not improve in the dead centers for textured ring as well as the processes of combustion and expansion. Also, large grooves do not improve Λ especially for the grooves having large depth-to-width ratio. Furthermore, to predict the best texture of those who has the most dimensionless film thickness increment at the mid-stroke, a numerical matrix is used. A $\Delta\Lambda\%$ value is taken at the mid-stroke where the piston has the maximum speed ($\Psi = 70$).

	$0.75S_p$	S_p	$1.25S_p$
$\frac{\epsilon}{2}$	0.28	1.5	2.5
ϵ	0.6	1	-0.3
2ϵ	-0.0017	-1.98	-9.96

Table 3.2: A matrix of $\Delta\Lambda\%$ at the cold engine operating condition

Table 3.2 shows that the textured ring of a small depth-to-width ratio and a large area density of the transverse grooves generates more value of $\Delta\Lambda$. In addition, for the narrow grooves, increasing the width of groove or decreasing the depth of groove induces a good result of $\Delta\Lambda$. It is can be found by looking at this table in the direction of diagonal or vertical, i.e. the textures $S_p - 0.5\epsilon$ and $0.75S_p - \epsilon$ and the textures $S_p - 0.5\epsilon$ and $S_p - \epsilon$. Due to the reason that the dimensionless film thickness is related to the hydrodynamic pressure, the pressure generated

at ring profile (x-direction) is investigated. Based on the result from the table 3.2, the textured ring who has the best improvement of $\Delta\Lambda$ is compared to the smooth ring. It devotes that the integral of pressure along ring profile is larger for this textured ring (see eq:2.21). As α is related to Λ , their pressure distribution along the x direction is shown, as well as the vapour volume fraction α . A 2D plot is used, because there is not the variation of texture profile and pressure distribution in circumferential direction.

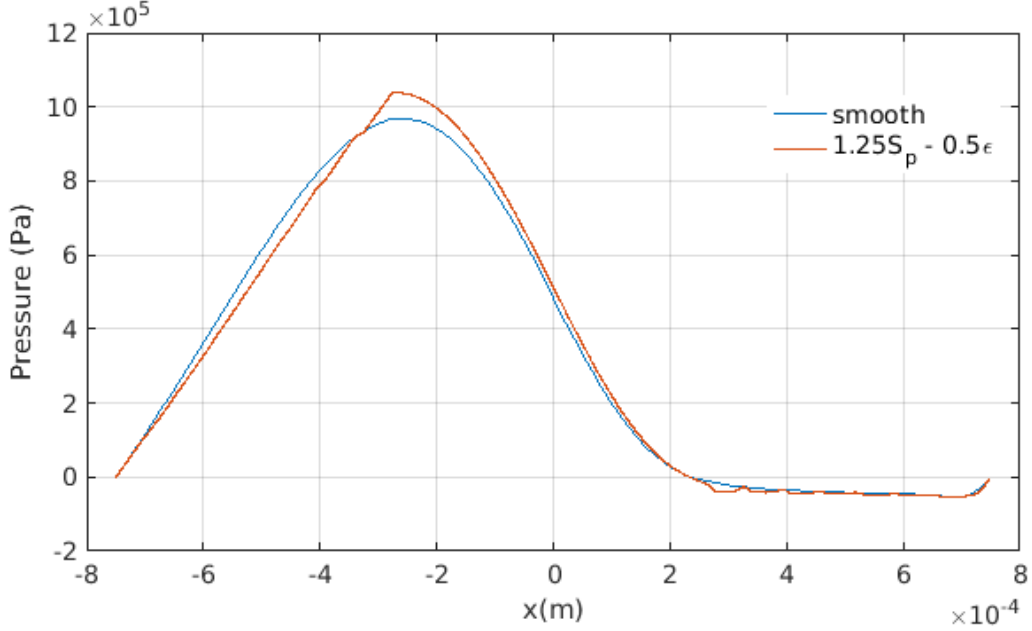


Figure 3.23: The figure of pressure comparison between a textured ring ($1.25S_p - 0.5\epsilon$) and the smooth ring. $\Psi = 70^\circ$ is considered.

Regarding the Figure 3.23, texture determine the pressure distribution. The textured ring induces more pressure at the pressurized region, at which the pressure value is positive. The pressure is decreased at the textured area. This is because that the film thickness is increased by applying the grooves, and the flow is obstructed in the groove. Also, the reason that the pressure increases at the end edge of the textured area ($x \approx -3$) is determined by the geometry wedge effect along the ring profile (x-direction). This is based on the right side of Reynolds equation (see eq:2.3).

$$\frac{\partial h}{\partial x} \left(\rho \frac{U}{2} \right) \quad (3.7)$$

This film thickness along x direction for this textured ring and this smooth ring is shown in the figure below, and it can be seen that the derivative of h along x is increased at the edge of the groove:

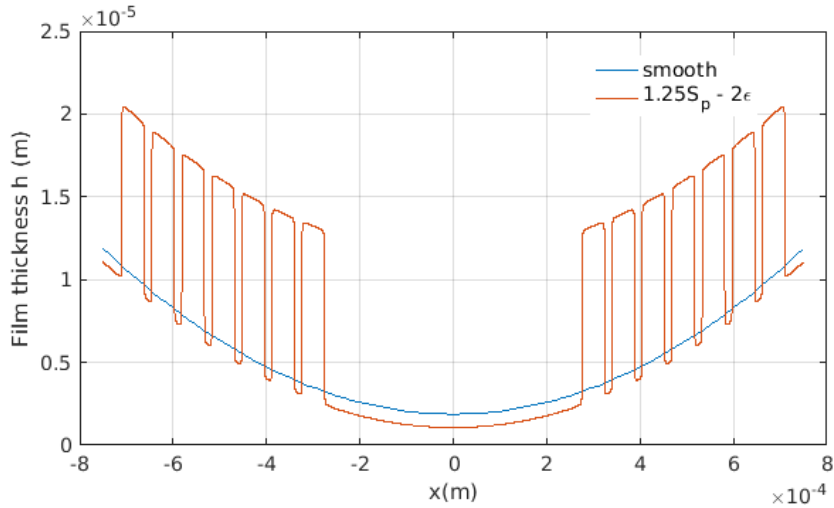


Figure 3.24: The figure of film thickness (h) along the ring profile for the textured ring ($1.25S_p - 0.5\epsilon$) and the smooth ring

In addition, Figure 3.25 shows there are more gases released from the lubricant for this textured ring, because this textured ring has a larger area of α than the smooth ring. It can translate that the pressure is reduced more at the cavitation region (see fig:3.23). Also, it can be found that the profile of vapour volume fraction depends on the film thickness based on texture geometry at the cavitation region. According to Figure 2.7a, the higher is the film thickness generated through the texture, a larger α is generated.

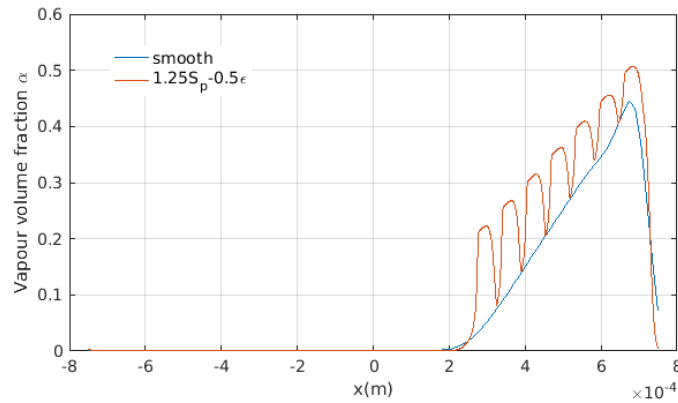


Figure 3.25: The figure of vapour volume fraction along x direction of the smooth ring and a textured ring ($1.25S_p - 0.5\epsilon$). A cold engine operating temperature is considered, and $\Psi = 70^\circ$.

Furthermore, the figures of ΔCOF at each crank angle are plot for 9 different kinds textures. A logarithmic y axis is applied. They are sorted with respect to different area densities.

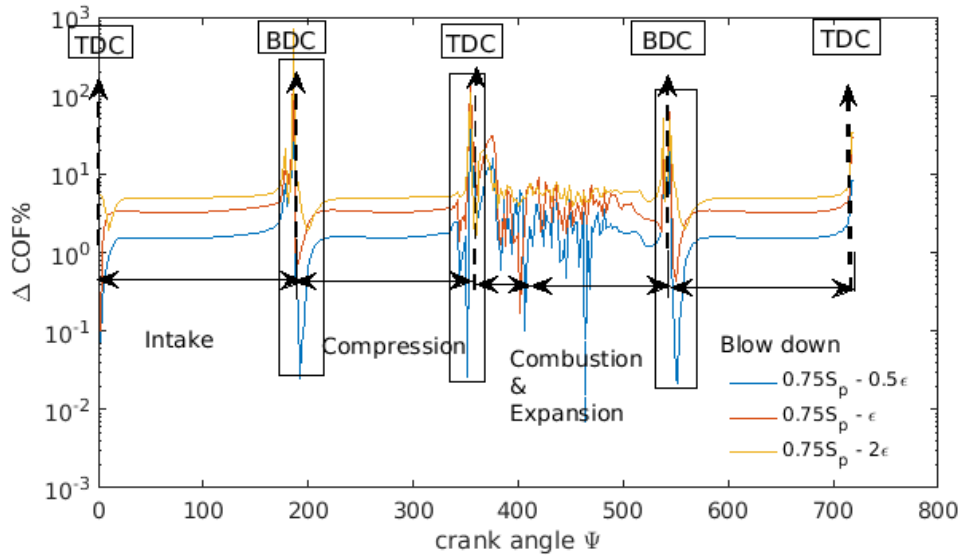


Figure 3.26: The figure of ΔCOF at entire engine cycle. The textured rings have the same area density ($0.75 S_p$). The negative value region is shown inside the rectangle

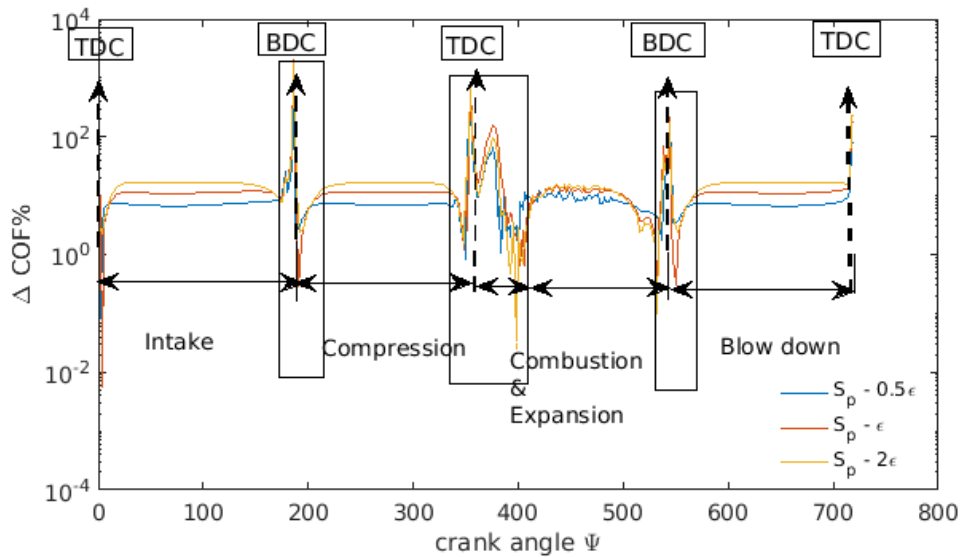


Figure 3.27: The figure of ΔCOF at entire engine cycle. The textured rings have the same area density (S_p). The negative value region is shown inside the rectangle.

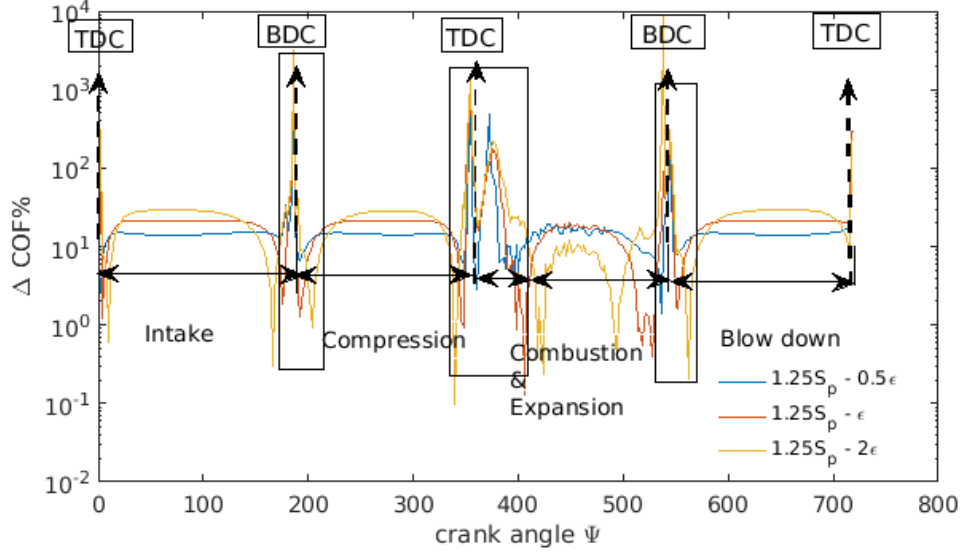


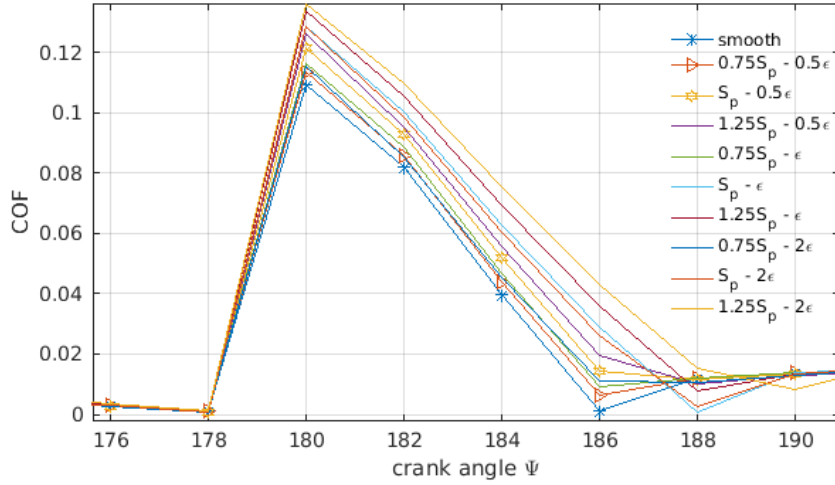
Figure 3.28: The figure of ΔCOF at entire engine cycle. The textured rings have the same area density ($1.25S_p$). The negative value region is shown inside the rectangle.

Those figures show that the grooves induce more friction force reduction at mid-stroke. When the piston moves to dead centers and combustion process, the COF is generated more for the textured rings. This can be proved by those values inside the rectangle. As the viscous friction force reduces through a thinner film thickness (see fig:3.5), it means that the viscous friction force reduction is improved through a texture profile with a larger depth-to-width ratio for those grooves having the same area density. In addition, a numerical matrix of $\Delta\text{COF}\%$ for each textures is displayed in table 3.3. Those values are taken when the piston has the maximum speed at mid-stroke ($\Psi = 70^\circ$), which means the viscous friction force plays a major effect in the result of coefficient of friction.

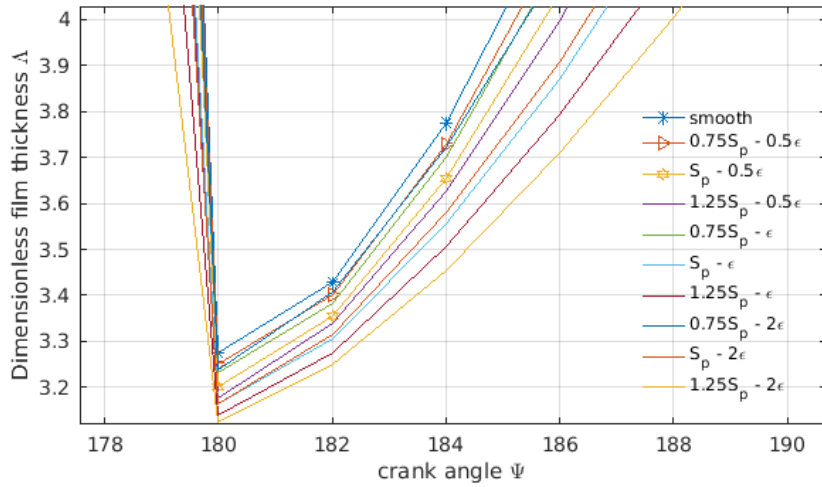
	$0.75S_p$	S_p	$1.25S_p$
$\frac{\epsilon}{2}$	0	6.68	13.9
ϵ	3.18	10.93	21.25
2ϵ	4.92	16.77	29.23

Table 3.3: A matrix of $\Delta\text{COF}\%$ at the cold engine operating condition

Regarding to this table, increasing the size of grooves makes better improvement of viscous friction force reduction. The maximum reduction comes from the texture ($1.25S_p - 2\epsilon$), who has 29.23% reduction. However, according to Figure 3.26, 3.27 and 3.28, the boundary friction force increases by applying texture on the compression ring. This is because that textured ring generates lower film thickness than the smooth ring. It is much earlier for the textured ring to across Λ_{mixed} and the mixed lubrication occurs. This can be proved by Figure 3.29. In this graph, all the textured rings induce more friction force than the smooth ring. Especially, the textured ring ($1.25S_p - 2\epsilon$) who has the greatest COF. It is because that it has the lowest film thickness compared with other textured rings.



(a) The COF at each crank angle of dead center



(b) The dimensionless film thickness at each crank angle of dead center

Figure 3.29: The figure of coefficient of friction (COF) and the dimensionless film thickness at the region of top dead center (the mixed lubrication regime), different texture profiles are considered as well as a smooth ring

Based on the equation 2.30, the reason that the textured ring has positive effect at mid-stroke can be explained by the following detailed analyses of the viscous shear stress. As shown in table 3.2, the largest grooves have the best improvement of viscous friction force reduction at mid-stroke. A comparison between a textured ring ($1.25S_p - 2\epsilon$) and a smooth one along the ring profile (x-direction) is taken into account.

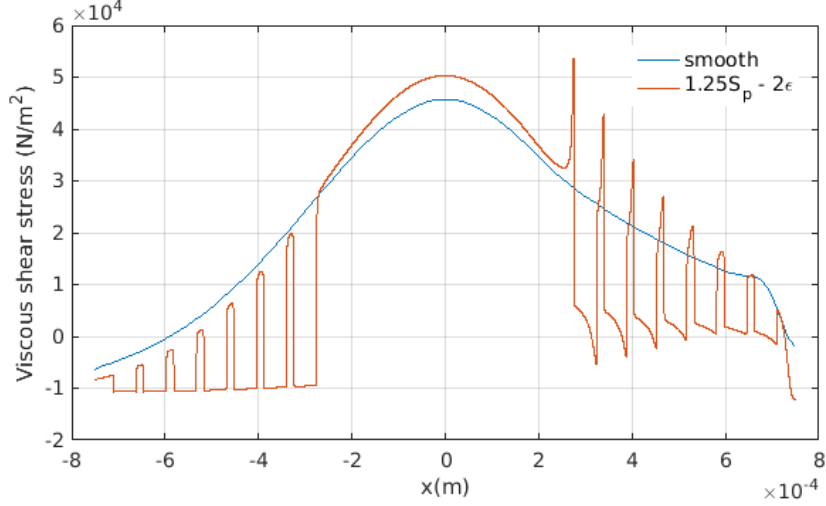
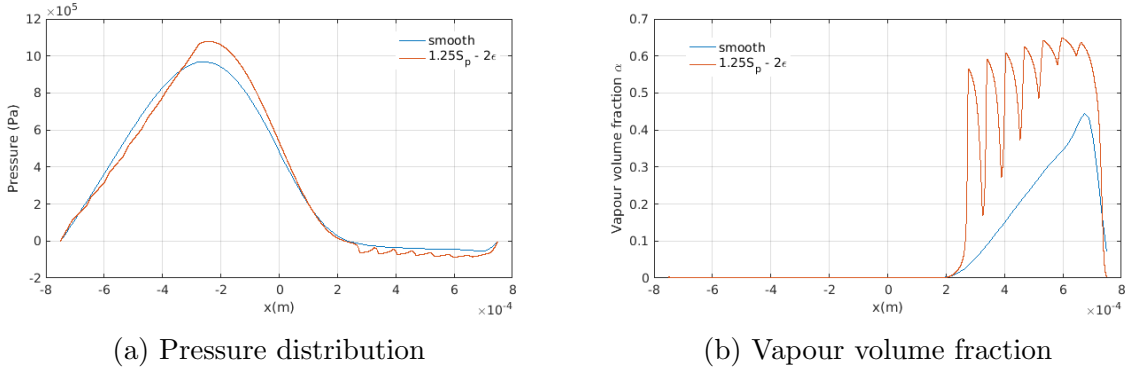


Figure 3.30: The figure of viscous shear stress along the ring profile (x-direction) of a textured ring ($1.25S_p - 2\epsilon$) and the smooth ring at mid-stroke



(a) Pressure distribution

(b) Vapour volume fraction

Figure 3.31: The figure of α and pressure distribution along the ring profile for the textured ring($1.25S_p - 2\epsilon$) and the smooth ring at mid-stroke. The cold engine operating temperature is considered.

It can be found that the viscous shear stress is reduced, especially at two sides of the ring. Regarding to equation 2.31, the reason is the increment of film thickness through grooves. There is the maximum viscous friction force at the center ($x = 0$) for two cases. It is because of the ring profile who induces the least film thickness at center. Whilst, the textured ring generates more shear stress there, because it has larger negative pressure gradient than the case of smooth ring (see fig:3.31). Based on equation 2.30, the slope of viscous shear stress at the negative regions ($x < 0$) is determined by the slope of pressure in Figure3.31. Also, there is more gases released at cavitation region ($x > 3$) for textured ring. It induces more negative pressure and negative pressure gradient as well. It results that the viscous shear stress at positive region is larger than

the negative region. Also, the profile of viscous shear stress for the textured ring at cavitation region depends on the pressure gradient. It means that at this cavitation region ($x > 3$) in Figure 3.30, the increment of film thickness reduces viscous shear stress. Furthermore, it is found that the textured ring has larger negative pressure gradient than the smooth ring, based on the plot of pressure distribution above. It generates more viscous shear stress for the textured ring than the smooth ring in general trend, Therefore, there are more gases released from the lubricant. The figure above also shows the behavior of vapour volume fraction along the ring profile (x-direction). It can found that there are larger value of vapour volume fraction for the textured ring especially at the cavitation region.

Consequently, according to the result of the coefficient of friction, the textured ring has a better improvement of friction force reduction at the mid-stroke but worse effect at the dead center, as well as the combustion process. Furthermore, the total energetic losses (E_{total}) is taken into account for an entire engine cycle. The equation is derived from:

$$E_{\text{total}} = \int_0^{720} E d\Psi \quad (3.8)$$

Where

$$E = \text{COF}(F_{\text{ring}} + F_{\text{compression}})U \quad [w] \quad (3.9)$$

Where COF and U are the coefficient of friction and the piston speed at each crank angle, E is the energetic loss at each angle. Furthermore, in other to better represent their difference with respect to the smooth ring, ΔE_{total} is applied and their relationship is shown:

$$\Delta E_{\text{total}} = \frac{E_{\text{smooth}} - E_{\text{textured}}}{E_{\text{textured}}} \% \quad (3.10)$$

A positive value is expected. It means that the textured ring have better improvement on energy losses reduction at entire engine cycle. A table of $\Delta E_{\text{total}}\%$ for 9 kinds of textures is presented as below:

	$0.75S_p$	S_p	$1.25S_p$
$\frac{\varepsilon}{2}$	1.4	11.1	10.4
ε	2.6	6.8	13.3
2ε	5.4	11.6	11.8

Table 3.4: A matrix of $\Delta E_{\text{total}}\%$ at the cold engine operating temperature

Regarding to the table above, all those textured rings have positive effect on the energy loss compared to the smooth ring. Whilst, the textured ring ($1.25S_p - \varepsilon$) has the lowest ΔE_{total} about 13.3%. To better understand, plots of energetic losses (E) for this textured ring and the smooth ring at each crank angle are taken into account in Figure 3.32.

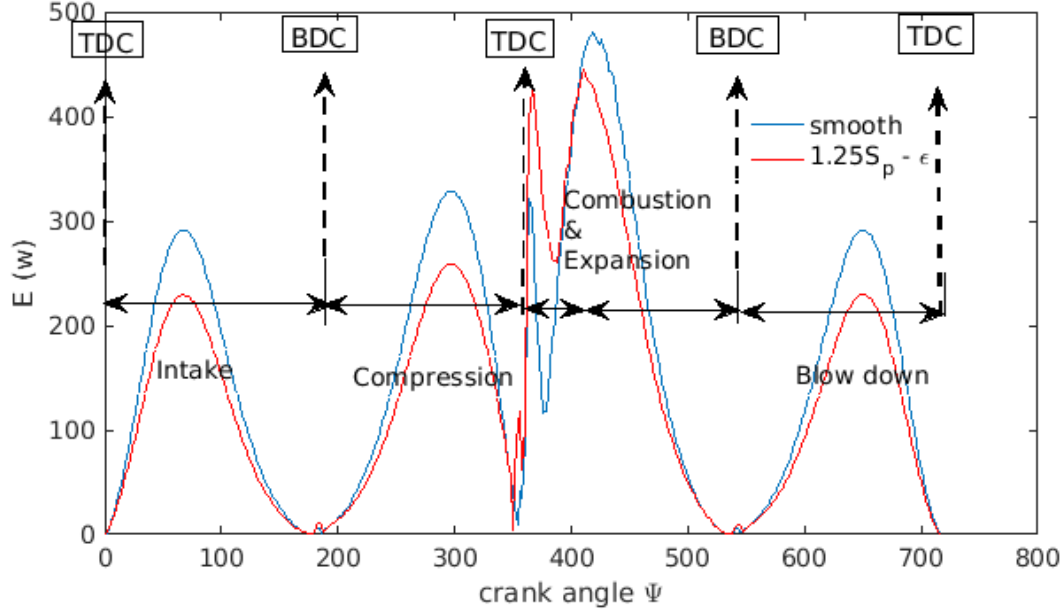


Figure 3.32: The figure of the energy loss E at entire engine cycle. Textured ring ($1.25S_p - \epsilon$) and smooth ring are considered as well as an isothermal cold engine operating temperature

This figure shows that the combustion process has different behavior in the energy loss (E) compared to other processes. The textured ring generates more energy loss than the smooth ring at this process. Based on the equation 3.8, this is because that The COF value is larger for the textured ring (see fig:(3.28)). Also, Figure 2.3 shows that the pressure from the chamber is increased by the ignition process, which increases the radial load ($F_{ring} + F_{compression}$) increases as well. Meanwhile, Figure 3.32 also shows that the energetic loss is higher at mid-stroke than at the dead center, because the maximum piston speed occurs here at the mid-stroke and minimum speed occurs at the dead center. At the mid-stroke, as the textured ring has less COF than the smooth ring (see fig: 3.28), which induces less energetic loss. Besides, The vapour volume fraction determined from the pressure distribution and results in the film thickness and coefficient of friction at entire engine cycle. It means that the higher pressure generated from the lubricant oil, larger α is got at cavitation region (see fig:3.31). Also, it is an important factor to determine the density and viscosity of the homogeneous mixture in this study (see eq:2.14). Thus, $\bar{\alpha}$ at each crank angle are taken into account. 9 different kinds of textures for the textured ring are considered. Figure 3.33 indicates that the textured ring generates more gases from the lubricant oil at mid-stroke.

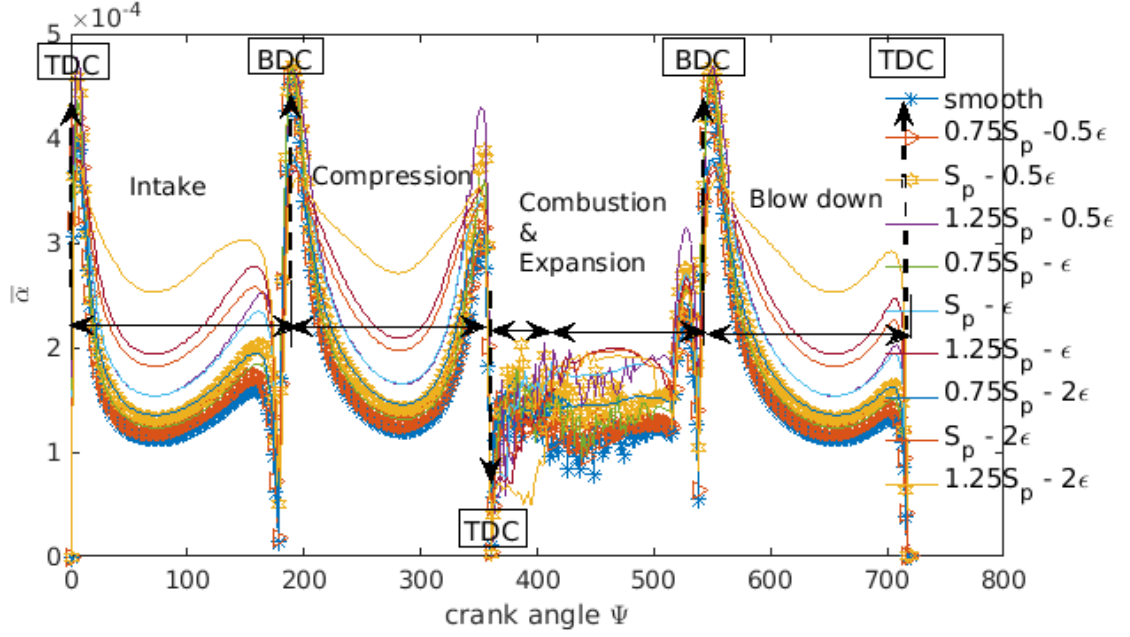
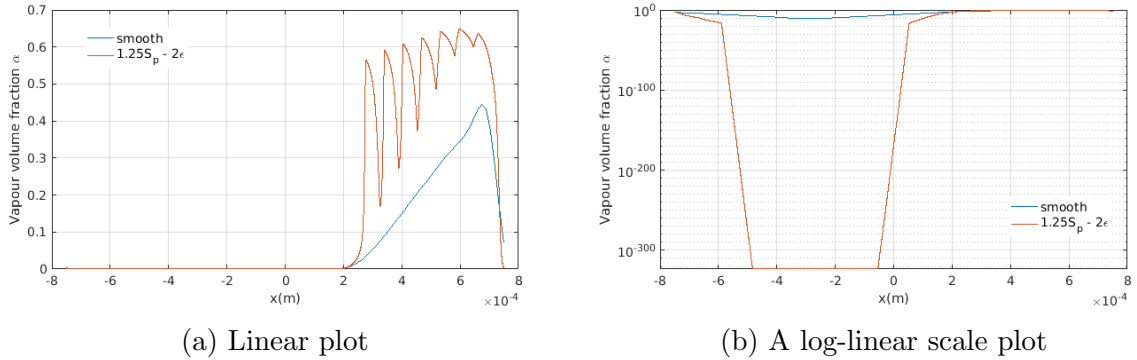


Figure 3.33: The figure of $\bar{\alpha}$, different texture profiles are considered as well as a smooth ring considering an isothermal cold engine operating condition

This can be explained by the vapour volume fraction α along the ring profile (x-direction). The texture ring ($1.25S_p - 2\epsilon$) and the smooth ring are compared each other at the condition that the piston has the maximum speed at mid-stroke ($\Psi = 70^\circ$). The graphs are shown in Figure 3.34, in which the logarithmic scale is used.



(a) Linear plot

(b) A log-linear scale plot

Figure 3.34: The figure of α value along the ring profile for the textured ring ($1.25S_p - 2\epsilon$) and the smooth ring at mid-stroke $\Psi = 70^\circ$. The cold engine operating temperature is considered.

It can be found that the α value is induced more at the cavitation region for the textured ring. Even if it is decreased at the pressurized area (see fig:3.34b). It means that there are more gases released from the lubricant oil for the textured ring. However, when the piston moves to the dead center, $\bar{\alpha}$ approaches zero at these cases. This is because the piston reduces speed and changes direction. In addition, the profile of the curve of $\bar{\alpha}$ is wave-shaped. It is determined by the time dependent term at the right side of the Reynolds equation (see eq:2.3) and its equation

is shown [26]:

$$\frac{\partial \rho h}{\partial t} = \underbrace{h(x, \theta) \frac{\partial \rho}{\partial t}}_{\text{Expansion effect}} + \underbrace{\rho \frac{\partial h(x, \theta)}{\partial t}}_{\text{Normal squeeze effect}} \quad (3.11)$$

Also, the term coming from the shear effect should be considered as well. It depends on the flow velocity and includes the effect of density wedge and geometry wedge. Its equation is derived from:

$$\frac{U}{2} \frac{\partial \rho h}{\partial x} = \underbrace{\frac{U h}{2} \frac{\partial \rho}{\partial x}}_{\text{Density wedge}} + \underbrace{\frac{U \rho}{2} \frac{\partial h}{\partial x}}_{\text{Geometry wedge}} \quad (3.12)$$

In addition, these two terms make important effect. For the smooth ring, effects at entire engine cycle are shown in Figure 3.35. The sum of those effects along x direction are given:

$$\bar{a} = \int_{-\frac{b}{2}}^{\frac{b}{2}} \frac{\partial \rho h}{\partial t} dx \quad (3.13)$$

$$\bar{b} = \int_{-\frac{b}{2}}^{\frac{b}{2}} \frac{U}{2} \frac{\partial \rho h}{\partial x} dx \quad (3.14)$$

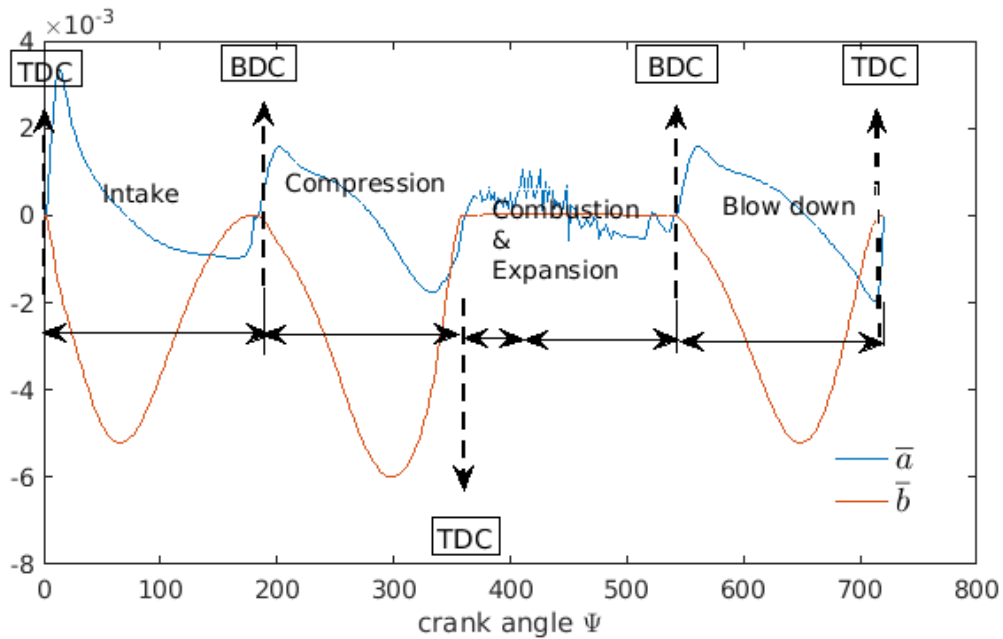


Figure 3.35: The figure of \bar{a} and \bar{b} at entire engine cycle. An isothermal cold engine operating condition is concerned

It can be found that they have an essential influence at the bottom dead center and the top dead center. As shown in Figure 3.35, the result of the time dependent term increases at one dead center and starts to decrease during the mid-stroke, which means that it mostly impacts the profile of the curve at the initial of the stroke (see fig:3.33). This is because the normal squeeze effect plays an important role in curve shape and it is related to the slope of the film thickness with respect to each crank angle. Therefore, the figure of Λ with respect to the crank angle is shown in Figure 3.36.

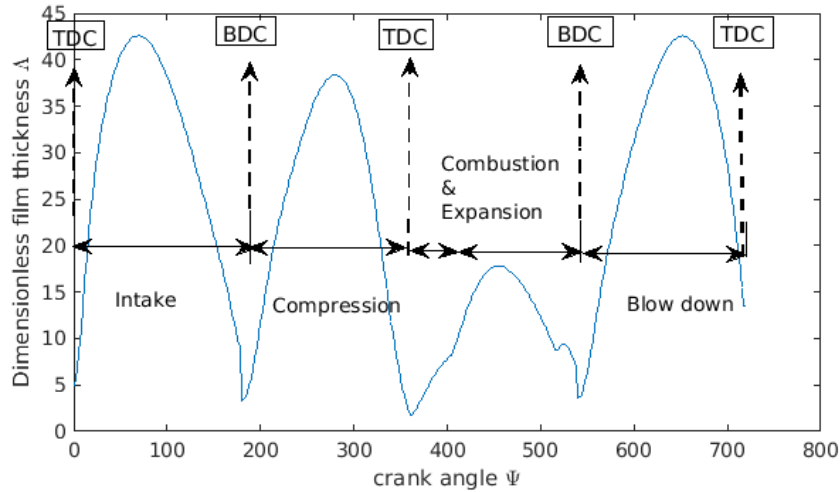


Figure 3.36: The figure of dimensionless film thickness with respect to crank angle at entire cycle. The smooth one is considered as well as the isothermal cold engine operating temperature

The smooth ring is considered. It is easily found that the slope of this curve is different for each stroke. For instance, the Λ value increases much rapidly from the top dead center to mid-stroke and decreases slowly to the bottom dead center at intake stroke. On the other hand, the result coming from the shear effect impacts the wave-shaped curve when the piston moves to another dead center, which increases the value of $\bar{\alpha}$. As shown in Figure 3.35, $\bar{\alpha}$ is more affected by the shear effect (b) at the mid-stroke. It is because that the maximum piston speed occurs there. As a result, a plot of the sum of those two at entire engine cycle is shown in Figure 3.37, in which the profile of wave shape appears.

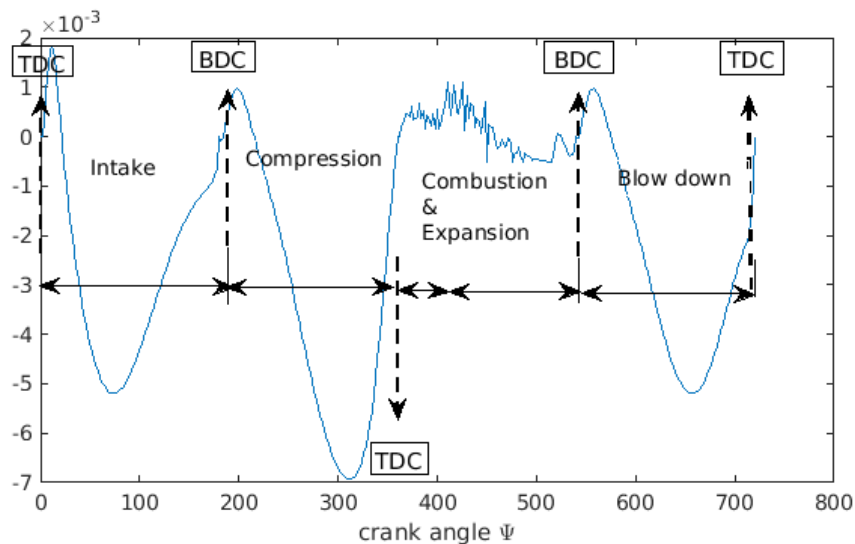


Figure 3.37: The figure of the sum of the effects coming from \bar{a} and \bar{b} at entire engine cycle. The smooth one is considered, as well as the cold engine operating temperature

3.3.2 Analysis At The Warm Engine Operating Temperature

Non-isothermal Operating Case

In this section, a non-isothermal warm engine operating condition is concerned, which means that we consider the 95°C nominal lubricant temperature. Also, there is the convective heat transfer in the lubricant. According to the texture profile matrix (see table:3.1), different texture profiles are used to analysis their influence on the dimensionless film thickness, coefficient of friction and $\bar{\alpha}$ at entire engine cycle. Firstly, the investigation of the dimensionless film thickness is determined by $\Delta\Lambda$. Each figure below contains three cases and each of them has the same area density.

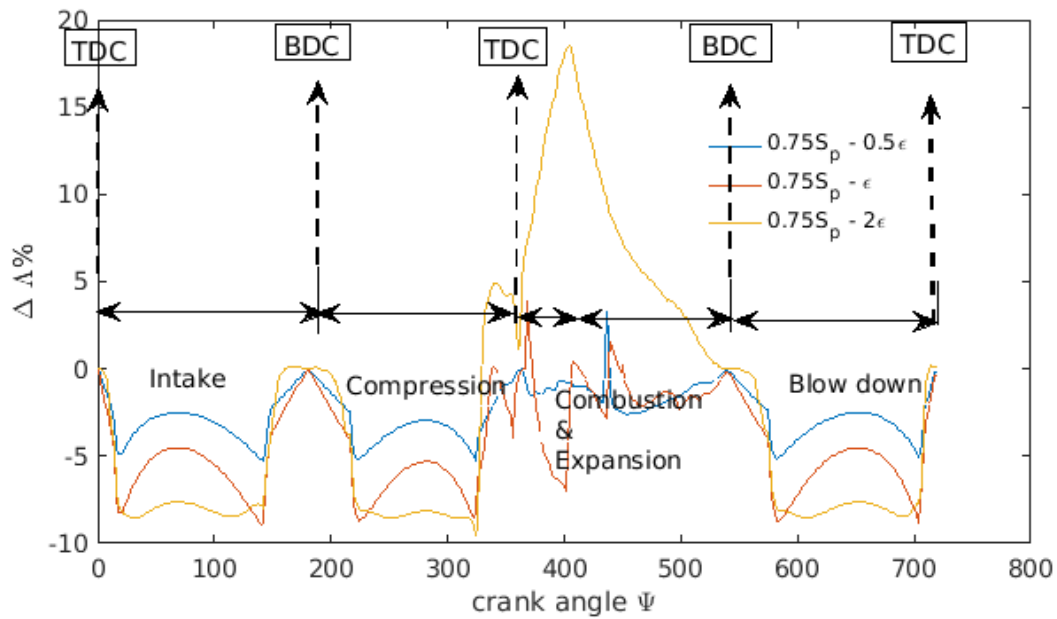


Figure 3.38: The figure of $\Delta\Lambda$ at entire engine cycle for three textured rings with the same area density ($0.75S_p$). A non-isothermal warm engine condition is investigated

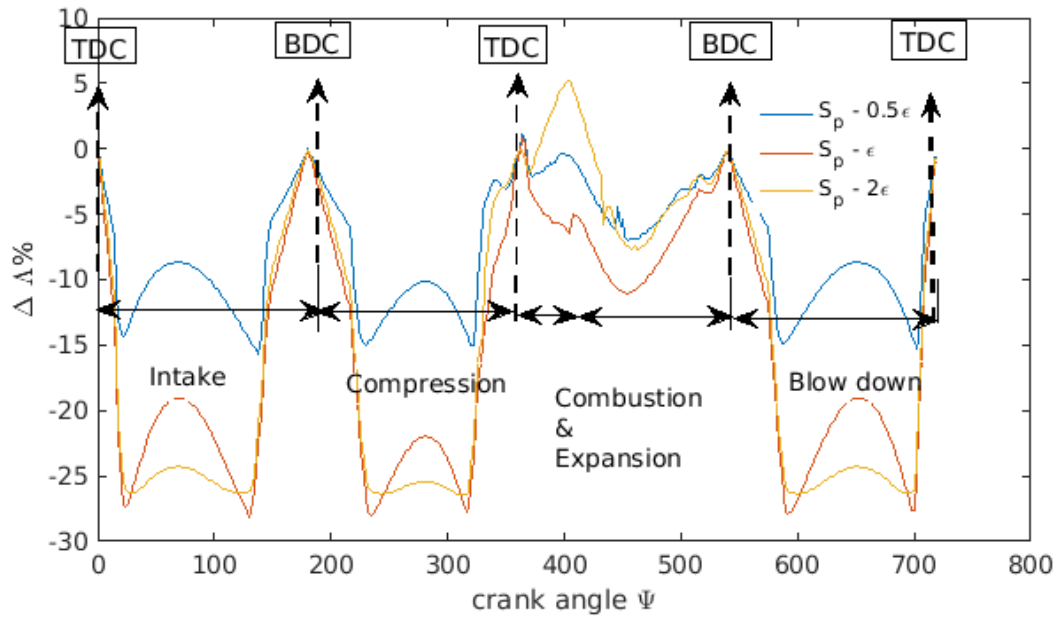


Figure 3.39: The figure of $\Delta \Lambda$ at entire engine cycle for three textured rings with the same area density (S_p). A non-isothermal warm engine condition is investigated

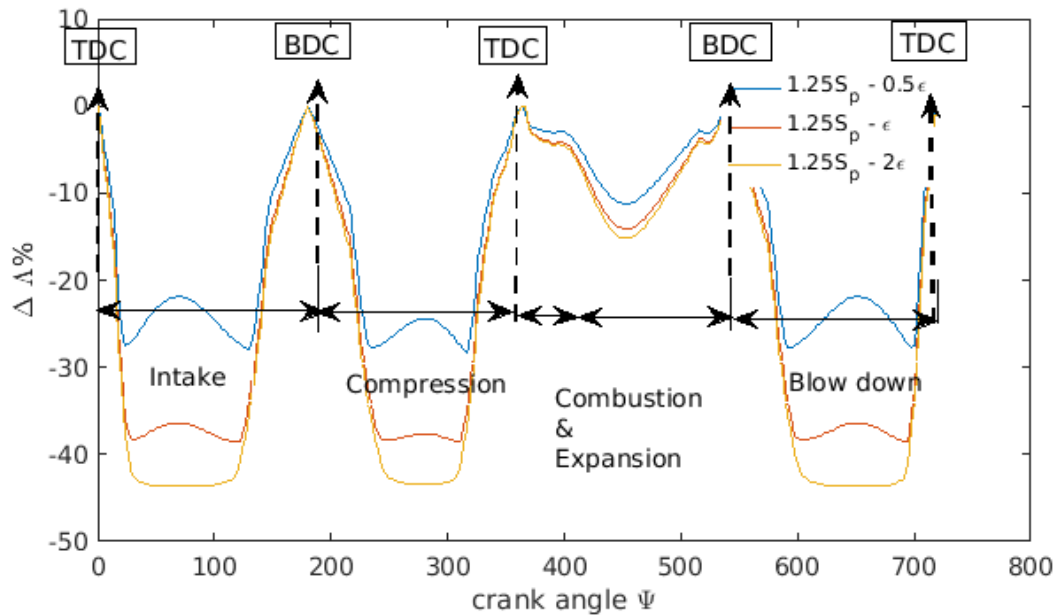


Figure 3.40: The figure of $\Delta \Lambda$ at entire engine cycle for three textured rings with the same area density ($1.25S_p$). A non-isothermal warm engine condition is investigated

Those three figures show that the textured ring has lower dimensionless film thickness than the smooth ring, especially at the mid-stroke. This result is quite different for a cold engine operating temperature. Also, regarding three textured rings having the same area density of grooves, the textured ring considering deeper grooves reduces more the Λ value. For those two texture parameters, the area density has more significant influence on $\Delta\Lambda$. By increasing the area density, there is more reduction of Λ around 50% for the grooves having the maximum area density. In order to better understand, a numerical matrix is used, which contains the $\Delta\Lambda\%$ values of 9 kinds of grooves. A condition of maximum piston speed at mid-stroke ($\Psi = 70^\circ$) is taken into account.

	$0.75S_p$	S_p	$1.25S_p$
$\frac{\varepsilon}{2}$	-4.25	-10.31	-23.3
ε	-6.23	-20.5	-37.51
2ε	-9.28	-25.65	-44.57

Table 3.5: A matrix of $\Delta\Lambda\%$ at the non-isothermal warm engine condition

It can be found that there is more dimensionless film thickness reduction by considering the grooves with a large depth-to-width ratio and area density. It means that the wider and deeper grooves reduce hydrodynamic pressure. The pressure distribution of the textured ring and the smooth ring can explain it. In Figure 3.41, the textured ring ($1.25S_p - 2\varepsilon$) and smooth ring are considered.

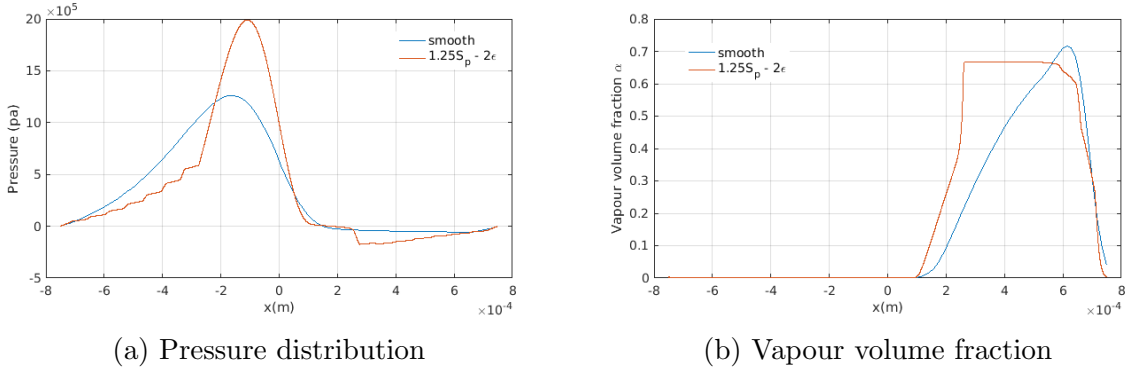


Figure 3.41: The figure of pressure distribution and vapour volume fraction along the ring profile (x-direction) between a smooth and textured ring. A non-isothermal warm engine operating condition is considered.

As stated before, the pressure is reduced by the grooves, it can be found that pressure is significantly reduced by large grooves, even if the maximum pressure is generated because of geometry wedge effect at center region ($x \approx -1$). Based on equation 2.14, α is determined by pressure. So the vapour volume fraction along the ring profile (x-direction) for this textured ring and the smooth one are shown in Figure 3.41 as well. At the cavitation region, the α area is larger for the textured ring than the smooth one. It means that there are more gases released from the lubricant oil. This is because that there is more negative pressure generated by the texture. Secondly, regarding the matrix of texture profile (see table:3.1), the coefficient of friction for these 9 kinds of textured rings are considered. ΔCOF is regarded as an important parameter to investigate at entire engine cycle. Those rings are classified by different area density values as follows:

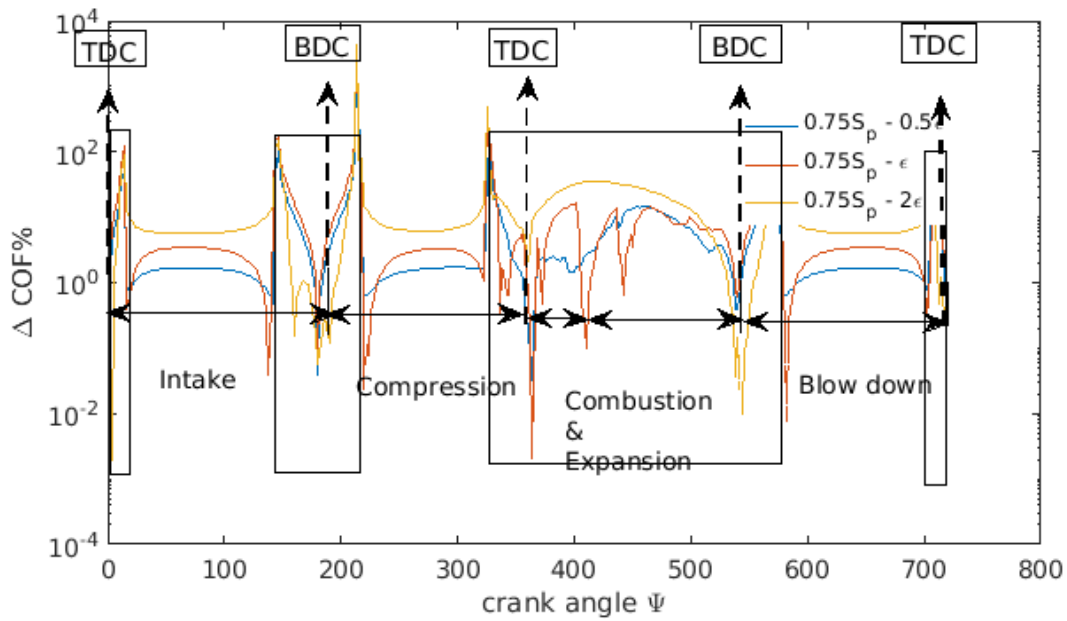


Figure 3.42: The figure of ΔCOF at entire engine cycle for three textured rings with the same area density ($0.755S_p$). An non-isothermal warm engine condition is investigated. The negative value region is represented inside the rectangle.

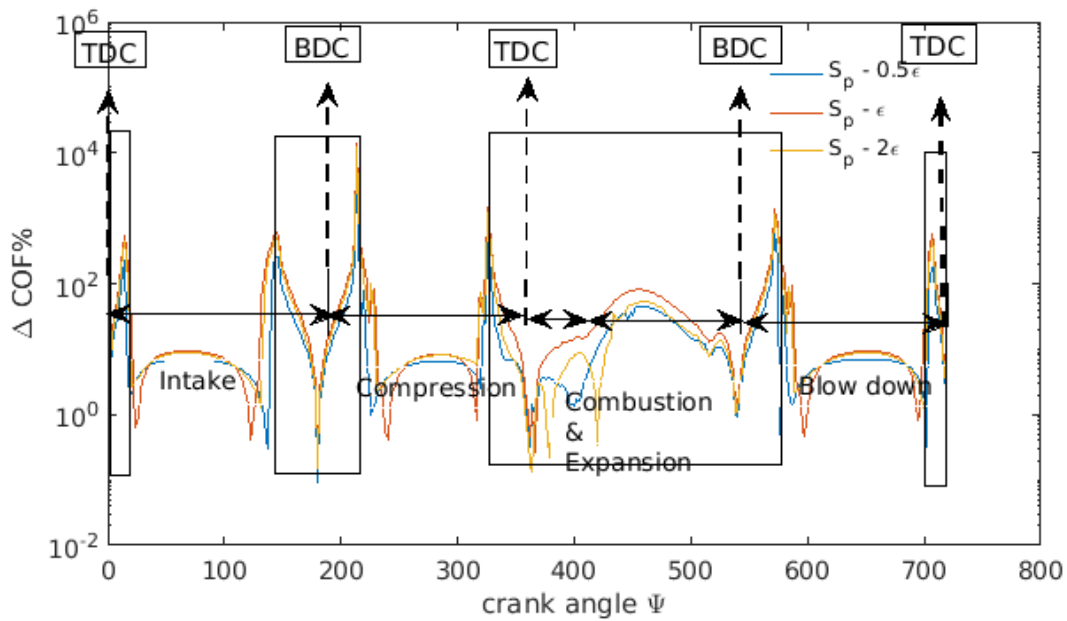


Figure 3.43: The figure of ΔCOF at entire engine cycle for three textured rings with the same area density (S_p). An non-isothermal warm engine condition is investigated. The negative value region is represented inside the rectangle

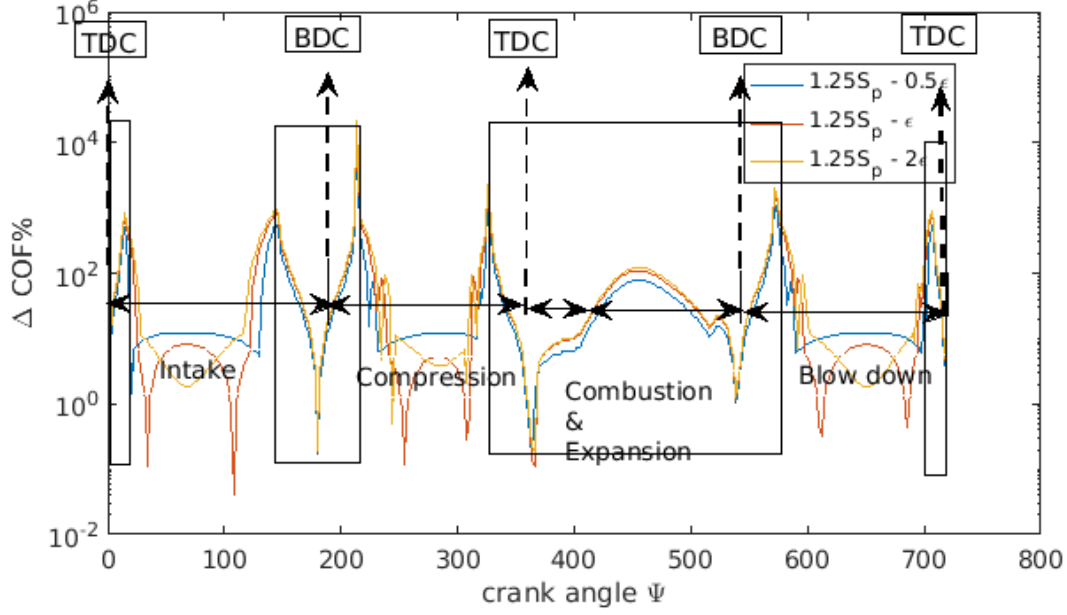


Figure 3.44: The figure of ΔCOF at entire engine cycle for three textured rings with the same area density ($1.255S_p$). An non-isothermal warm engine condition is investigated. The negative value region is represented inside the rectangle

The logarithmic scale in y axis is considered for previous figures of ΔCOF . Generally, the viscous friction force reduction is improved at mid-stroke and the narrow grooves have more positive effect. Regarding previous three figures, the grooves with lower area density or lower depth-to-width ratio seems reduce more COF. To better understand their different influence, a numerical matrix is taken into account.

	$0.75S_p$	S_p	$1.25S_p$
$\frac{\epsilon}{2}$	1.68	6.97	12.26
ϵ	3.46	9.32	8.08
2ϵ	5.60	8.9	-1.84

Table 3.6: A matrix of $\Delta\text{COF}\%$ at the non-isothermal warm engine condition

Those data are taken at the condition that the piston has the maximum speed at mid-stroke ($\Psi = 70^\circ$). It can be found that the textured ring with grooves ($1.25S_p - 0.5\epsilon$) has the best improvement around 12.26% and the grooves ($1.25S_p - 2\epsilon$) does not have COF reduction. Furthermore, a graph of viscous shear stress along ring profile (x-direction) is taken into account to better understand. In Figure 3.45, the textured ring considering grooves ($1.25S_p - 2\epsilon$ and $1.25S_p - 0.5\epsilon$) and the smooth ring are compared each other.

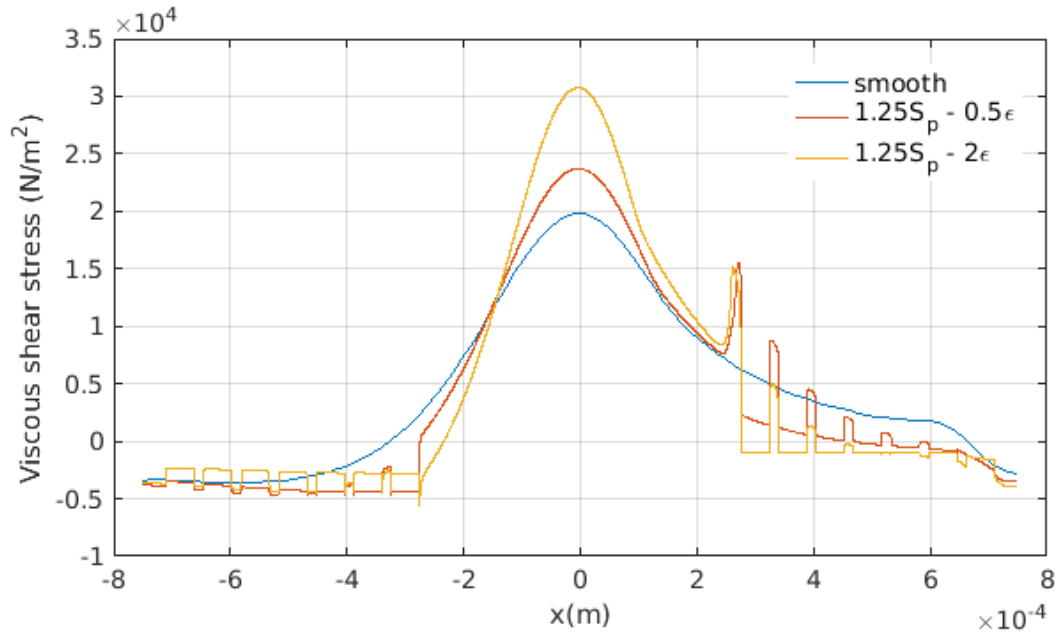


Figure 3.45: The figure of the viscous shear stress along the ring profile (x-direction) for the textured rings and the smooth ring. A non-isothermal warm engine operating temperature is considered

As stated in table 3.6, the integral of viscous shear stress along the ring profile is lower for the textured ring at mid-stroke. However, this conclusion does not include the case for the grooves ($1.25S_p - 2\epsilon$). This is because that the viscous shear stress increases at these grooves in the region ($x < -3$). Also, it has the highest viscous shear stress at the center (see fig:3.45). As stated before, the result of viscous shear stress depends on the pressure gradient along x direction and the film thickness, Regarding to Figure 3.45, textured areas, for which $x < -3$ and $x > 3$, has lower viscous shear stress. The reason is the increment of the film thickness due to the grooves (see fig:3.46). Meanwhile, the maximum viscous shear stress occurs at the center ($x=0$) for the grooves ($1.25S_p - 2\epsilon$) because of the geometry wedge effect. This film thickness of those rings are plot as below:

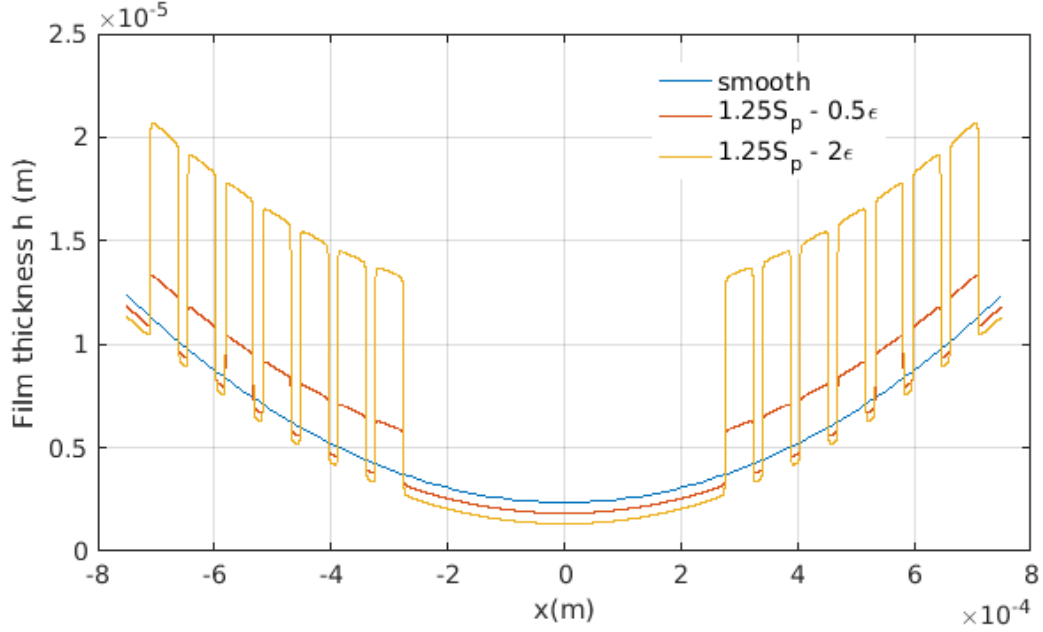


Figure 3.46: The figure of the film thickness along the ring profile (x-direction) for the textured rings and the smooth ring. A non-isothermal warm engine operating temperature is considered

On the other hand, Figure 3.42, 3.43 and 3.44 show that the textured ring generates more COF than the smooth ring when the piston moves to the region, in which the mixed lubrication happens. This is because that the textured ring reduces the film thickness, thus that those cases go to the mixed lubrication regime earlier than the case of smooth ring. Meanwhile, it can be found that the region of negative value of $\Delta\text{COF}\%$ is more wider than those cases at lower temperature (see fig: 3.26, 3.27 and 3.28). This is because that the Λ is reduced for a high temperature compared to a cold temperature in Figure 3.10. So far, from the coefficient of friction point of view, the textured ring improves the friction reduction at mid-stroke and has negative effect at dead centers, compared to the smooth ring. According to the equation 3.8, the total energy loss at entire engine cycle is investigated for textured rings of 9 different kinds of grooves. A numerical matrix is considered as follows:

	$0.75S_p$	S_p	$1.25S_p$
$\frac{\varepsilon}{2}$	-3.3	-6.8	-17.1
ε	-6.8	-21.4	-25.5
2ε	23.3	-1.5	-28.0

Table 3.7: A matrix of $\Delta E_{\text{total}}\%$ at the non-isothermal warm engine condition

It can be seen from the table above that the textured ring ($0.75S_p - 2\varepsilon$) has positive effect on the reduction of total energy losses around 23.3%. Whilst, the textured ring ($1.25S_p - 2\varepsilon$) has the highest energy losses compared to other rings. Furthermore, to better explain, a graph of the energetic loss (E) at each crank angle is considered for those two textured rings and the smooth one.

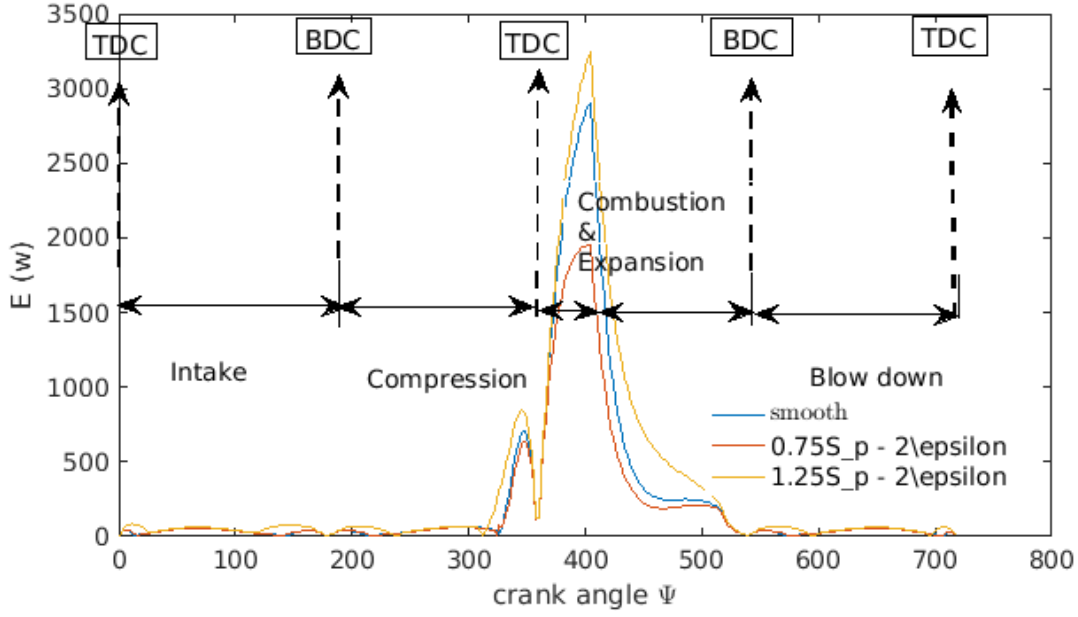


Figure 3.47: The figure of the energetic loss (E) at entire engine cycle. Textured rings ($0.75S_p - 2\epsilon$ and $1.25S_p - 2\epsilon$) are considered as well as a smooth ring under a non-isothermal warm engine condition

It can be found that there are significant energetic losses at the combustion process at warm temperature, because relevant pressure is generated. Regarding to Figure 2.3, the piston speed equals zero at the top dead center, from which the combustion process starts. Thus, at the process starts from the end of compression process until the end of expansion process, E decreases to zero and start to increases in the combustion process. Also, the textured ring ($1.25S_p - 2\epsilon$) has greater losses than the smooth ring at this process. However, The case for the textured ring ($0.75S_p - 2\epsilon$) has the lowest losses compared to other rings. The reason is that the COF at this processes take an important role. As the Λ value for the texture ($0.75S_p - 2\epsilon$) is improved, the coefficient of friction decreases, as well as energetic losses. The figures of COF and the dimensionless film thickness are plot as below:

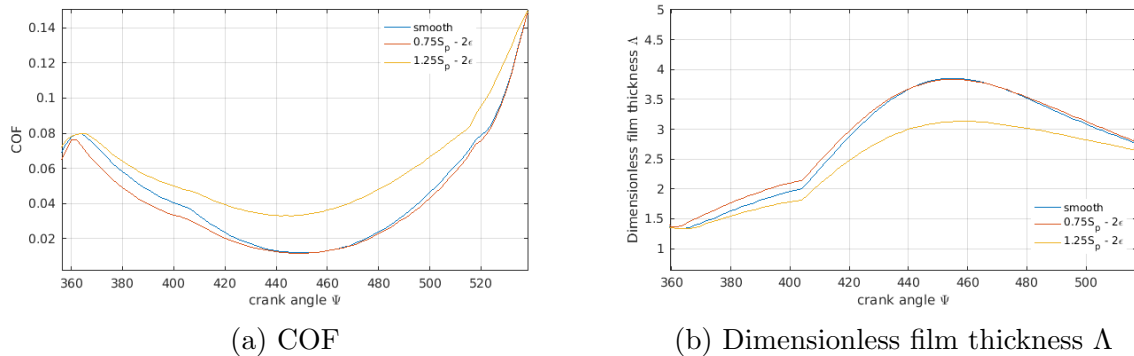


Figure 3.48: The figure of the COF and the dimensionless film thickness at combustion and expansion processes. Different texture profiles are considered as well as a smooth ring under an non-isothermal warm engine operating condition

Thirdly, the total amount of gases released from the lubricant oil is taken into account at each angle. $\bar{\alpha}$ is used to investigate the different behaviors between those 9 different kinds of grooves, with respect to the smooth ring. The figure is shown as below:

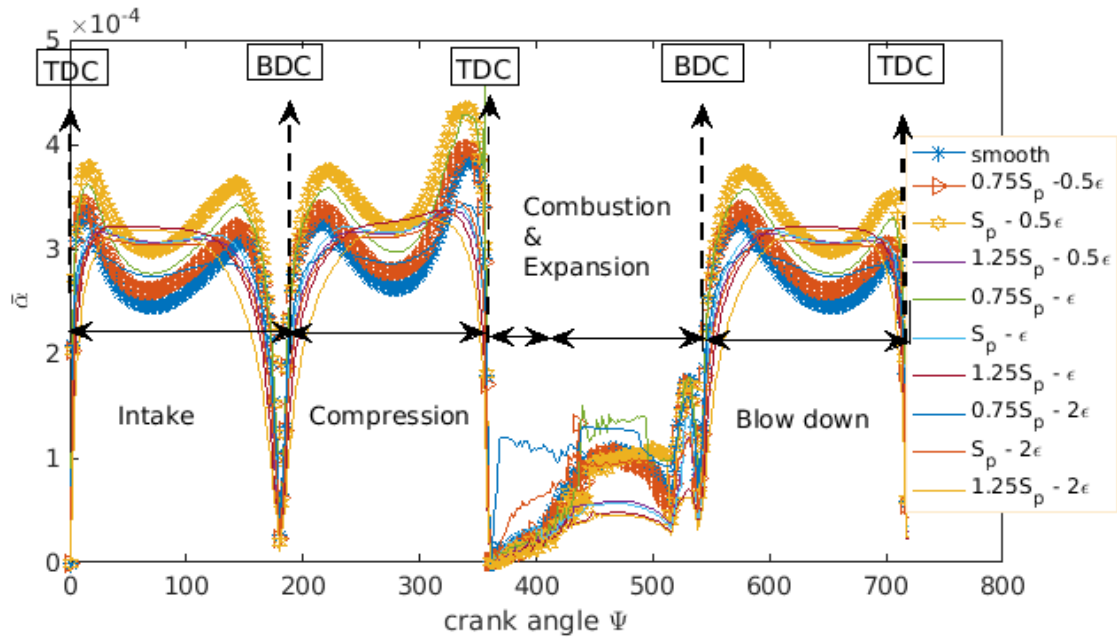


Figure 3.49: The figure of vapour volume fraction value at entire engine cycle. Different texture profiles are considered as well as a smooth ring under a non-isothermal warm engine operating condition

It is evidently found that all the textured rings generate larger vapour volume fraction than the smooth one. Whilst, the textured ring has larger vapour volume fraction than a smooth ring, which is easily to be observed at the mid-stroke. In addition, those textures with the narrow grooves (i.e. $0.75S_p - 0.5\varepsilon$, $S_p - 0.5\varepsilon$ and $0.75S_p - \varepsilon$) have different type of curve shape compared to others. They are more asymmetrical and similar to the case of the smooth ring. Furthermore, a comparison is made for the vapour volume fraction along the ring profile (x-direction) between the textured rings ($1.25S_p - 2\varepsilon$ and $0.75S_p - \varepsilon$) and the smooth ring. The plot is shown as below:

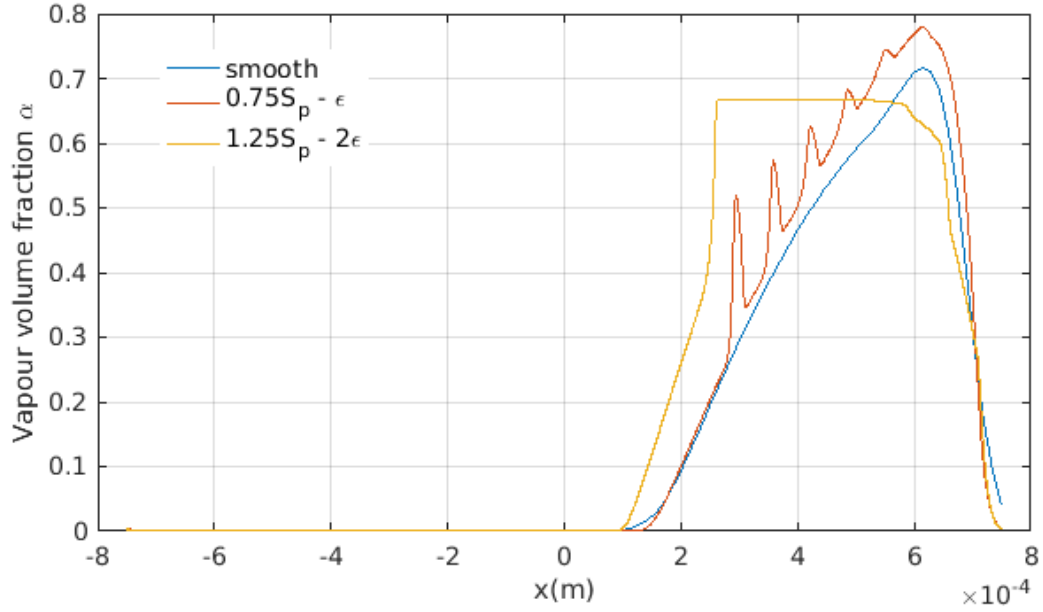


Figure 3.50: The figure of the vapour volume fraction along the ring profile (x-direction) between a smooth and the textured rings. A non-isothermal warm engine operating condition is considered.

A detailed analysis of the vapour volume fraction's behavior at the mid-stroke (i.e. $\Psi = 70$) is considered in Figure 3.50. Also this figure can indicate that different textured rings generate different profiles of α . It is easy to find that the total area of vapour volume fraction is larger for the textured ring than the case of smooth ring. Whilst, as the profile of α at cavitation region ($x > 1$) is shaped based on the texture profile, the grooves impact the profile of vapour volume fraction. This can be proved for the grooves ($0.75S_p - \epsilon$). However, the case for the large grooves ($1.25S_p - 2\epsilon$) has more gentle curve at the cavitation region. As proved before, the asymmetrical profile is resulted from the geometry wedge effect. The plot of the dimensionless film thickness in Figure 3.51 can show that the large grooves has less derivative of updated film thickness (h) along crank angle than other cases which induces a more smooth profile of $\bar{\alpha}$.

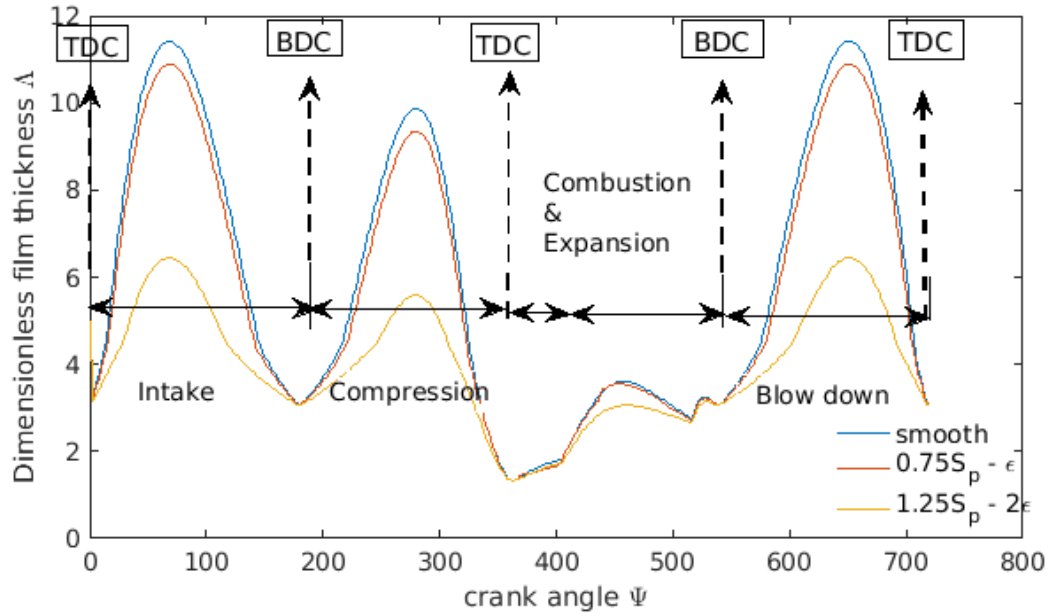


Figure 3.51: The figure of the dimensionless film thickness at entire engine cycle between the smooth ring and the textured rings. A non-isothermal warm engine operating condition is considered

Isothermal Operating Case

An isothermal operation condition is taken into account. The dimensionless film thickness, coefficient of friction and $\bar{\alpha}$ with respect to 9 different kinds of grooves are investigated at entire engine cycle. Firstly, the plot of $\Delta\Lambda$ of there cases with the same area density is shown as below:

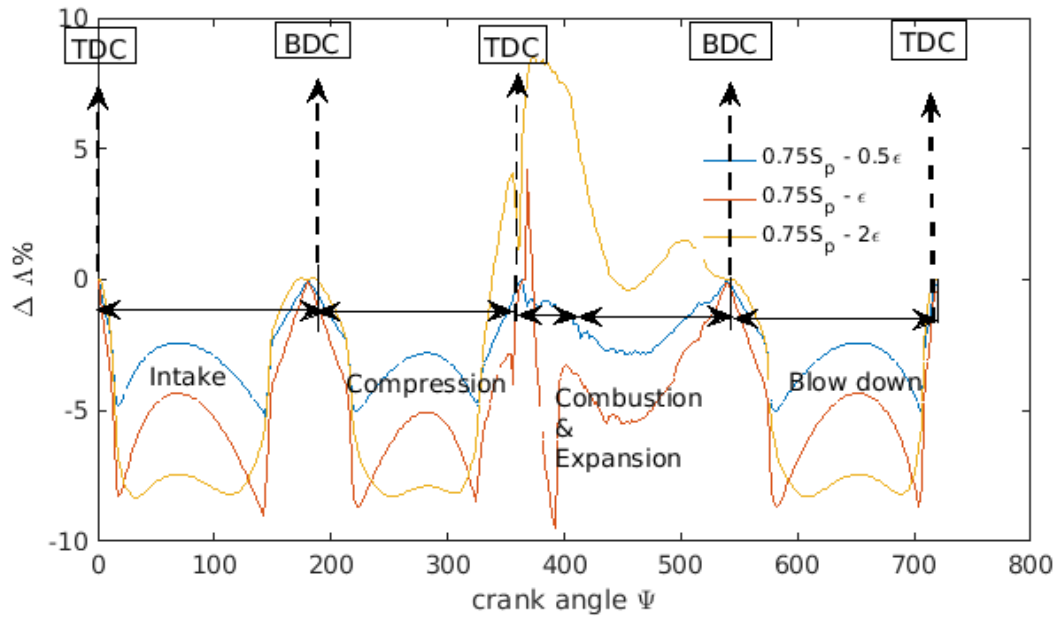


Figure 3.52: The figure of $\Delta\Lambda$ at entire engine cycle for three textured rings with the same area density ($0.75S_p$). An isothermal engine condition is investigated

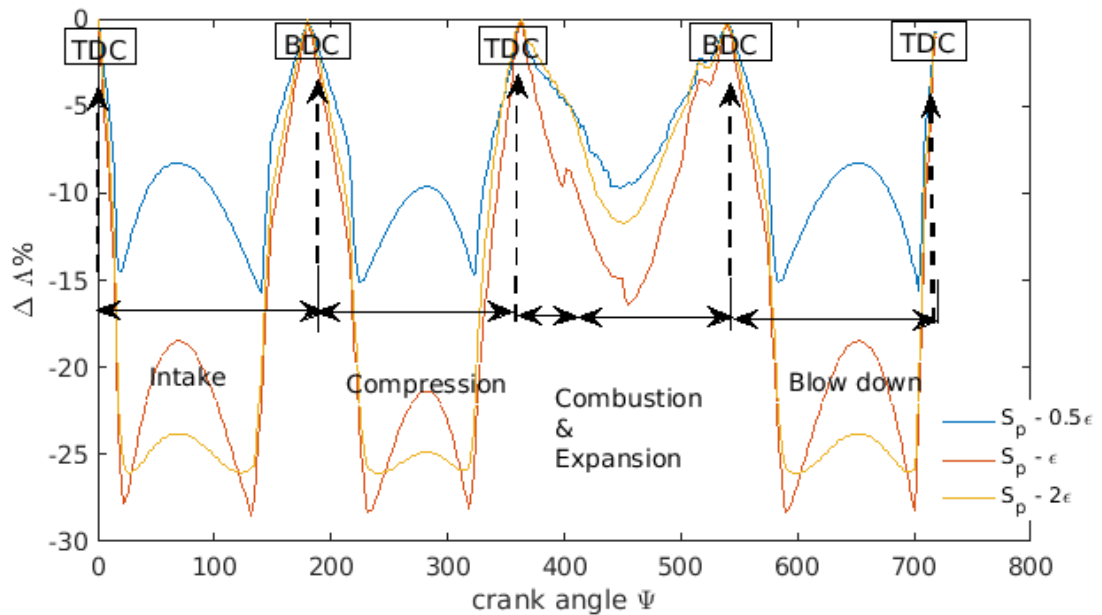


Figure 3.53: The figure of $\Delta\Lambda$ at entire engine cycle for three textured rings with the same area density (S_p). An isothermal engine condition is investigated

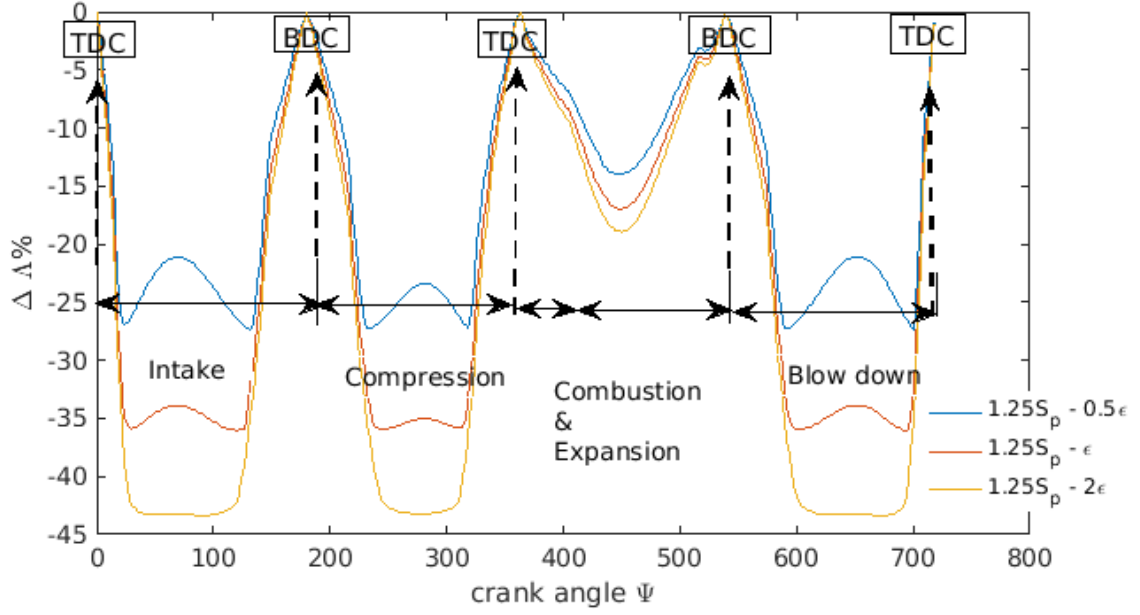


Figure 3.54: The figure of $\Delta\Lambda$ at entire engine cycle for three textured rings with the same area density ($1.25S_p$). An isothermal engine condition is investigated

In those figures, it can be found that the textured ring has lower dimensionless film thickness than the smooth ring at entire cycle. Especially at mid-stroke, the grooves with higher depth-to-width ratio have more reduction of the film thickness. Those conclusion under this isothermal engine condition is similar the non-isothermal one (see fig:3.38,3.39 and 3.40). Furthermore, a numerical matrix of the $\Delta\Lambda\%$ value at the mid-stroke ($\Psi = 70^\circ$) is shown.

	$0.75S_p$	S_p	$1.25S_p$
$\frac{\epsilon}{2}$	-2.41	-8.3	-21.12
ϵ	-4.35	-18.5	-33.87
2ϵ	-7.45	-23.81	-43.26

Table 3.8: A matrix of $\Delta\Lambda\%$ at the isothermal engine condition

According to results in this table, the grooves ($0.75S_p - \epsilon$) has the lowest $\Delta\Lambda$. Furthermore, at this condition, It also means that the grooves with large area density or large depth-to-width ratio get more thinner film thickness the conclusion of previous non-isothermal condition is also agreed in this condition. Secondly, ΔCOF is implemented to investigate different grooves' effect on the coefficient of friction with respect to the smooth ring. A logarithmic scale in y axis is taken into account.

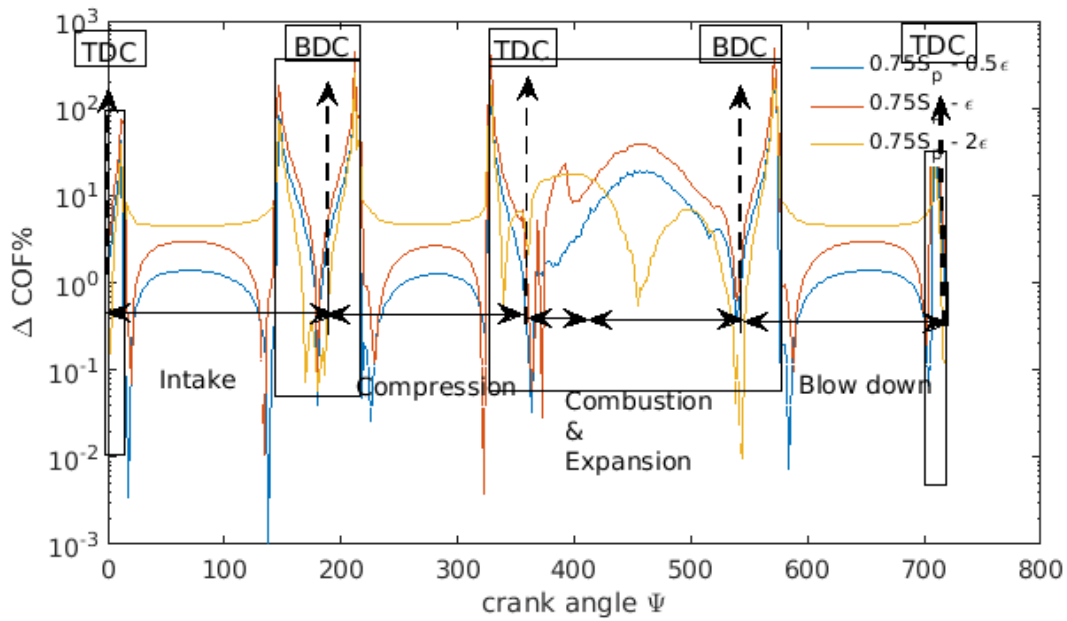


Figure 3.55: The figure of ΔCOF at entire engine cycle for three textured rings with the same area density ($0.75S_p$). An isothermal engine temperature is investigated. The negative value region is represented inside the rectangle.

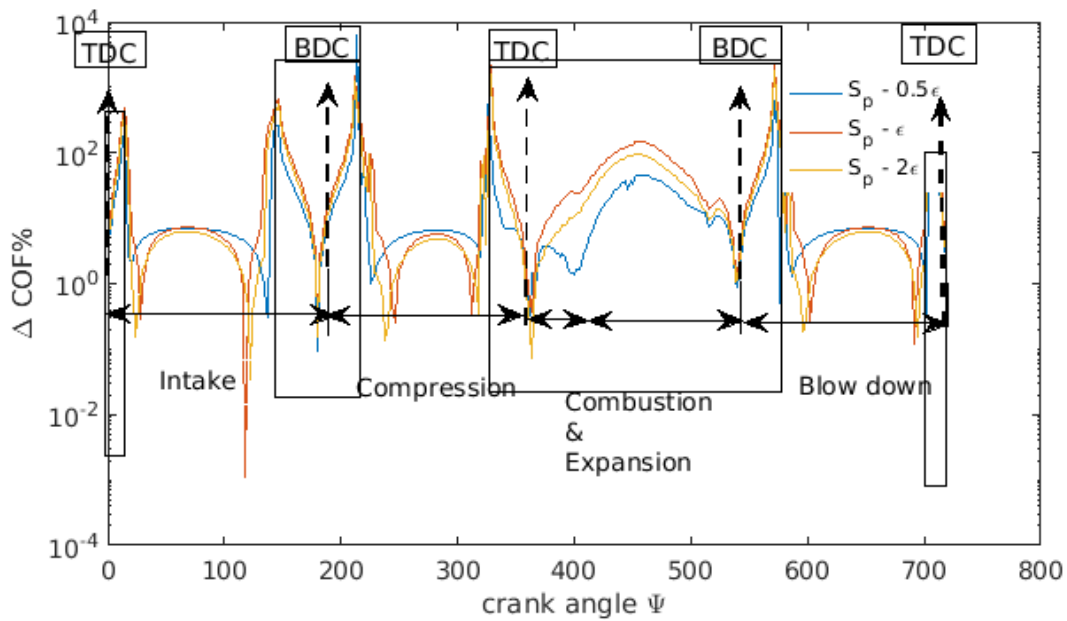


Figure 3.56: The figure of ΔCOF at entire engine cycle for three textured rings with the same area density (S_p). An isothermal engine temperature is investigated. The negative value region is represented inside the rectangle.

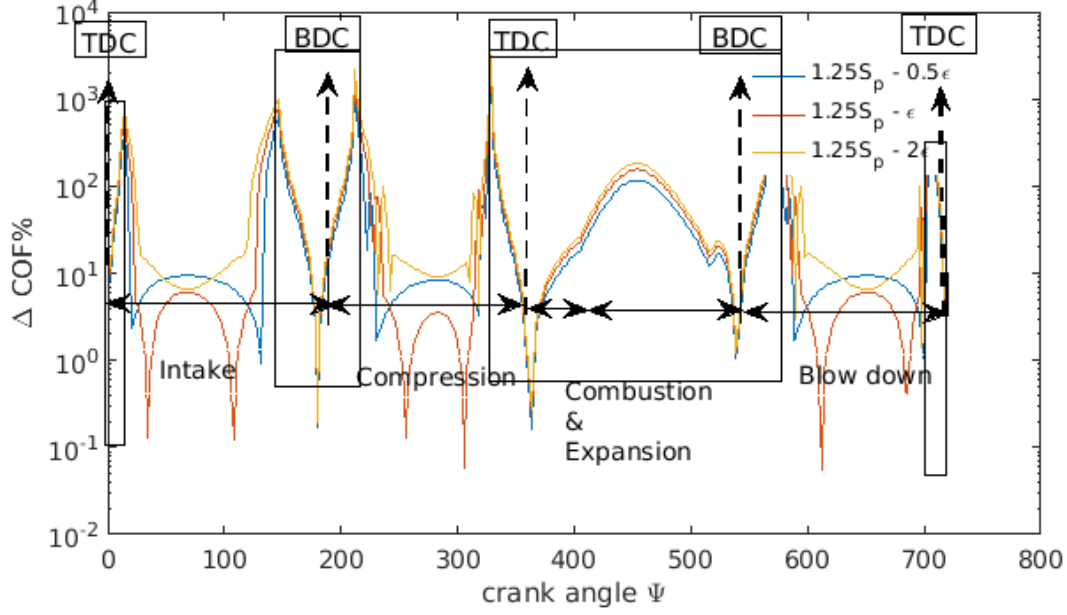


Figure 3.57: The figure of ΔCOF at entire engine cycle for three textured rings with the same area density ($1.25S_p$). An isothermal warm engine temperature is investigated. The negative value region is represented inside the rectangle

Based on results of ΔCOF for a non-isothermal warm temperature, those figures show that the coefficient of friction for an isothermal warm temperature is also reduced for the textured ring, especially the textured ring with narrow grooves at mid-stroke. As lower film thickness generated by the texture, the result shows that the combustion process and expansion process have more friction losses for the textured ring. Whilst, the coefficient of friction is reduced for all kinds of grooves at dead centers. In Figure 3.56, the difference between those three cases are relevantly small compared to other cases of different area density value. Thus, the area density is more effective than the depth-to-width ratio. A numerical matrix of $\Delta\text{COF}\%$ is listed.

	$0.75S_p$	S_p	$1.25S_p$
$\frac{\varepsilon}{2}$	1.37	6.01	9.38
ε	2.96	7.20	6.05
2ε	4.55	6.26	-6.52

Table 3.9: A matrix of $\Delta\text{COF}\%$ at the isothermal engine condition

The maximum piston speed at mid-stroke ($\Psi = 70$) is taken into account to get those data. It states that the grooves ($1.25S_p - 0.5\varepsilon$) have the best result in viscous friction reduction about 9.38%. The same texture for a non-isothermal warm temperature. But this improvement is less in this case without the consideration of temperature equation. Also, the largest grooves ($1.25S_p - 2\varepsilon$) do not have improvement at this engine condition, which is the same for the non-isothermal condition. In addition, the total energy losses ($\Delta E_{\text{total}}\%$) at entire cycle for 9 different kinds of textures are listed inside the matrix as below:

	$0.75S_p$	S_p	$1.25S_p$
$\frac{\varepsilon}{2}$	-4.5	-16.3	-24.4
ε	-12.4	-32.4	-32.8
2ε	11.6	-19.1	-40.1

Table 3.10: A matrix of $\Delta E_{\text{total}}\%$ at the isothermal engine condition

Regarding to the table above, the case of grooves ($0.75S_p - 2\varepsilon$) reduces the energy losses at entire cycle about 11.6%. This best texture is same as the case of non-isothermal warm engine condition, but the reduction percentage is less. In addition, the grooves with large area density and depth-to-width ratio generate more energy losses. This result is same for the non-isothermal condition. Thirdly, the total gases released from the lubricant at each crank angle is considered as well. Those textures have the similar behaviors for the non-isothermal warm engine operating condition. This graph is shown as below:

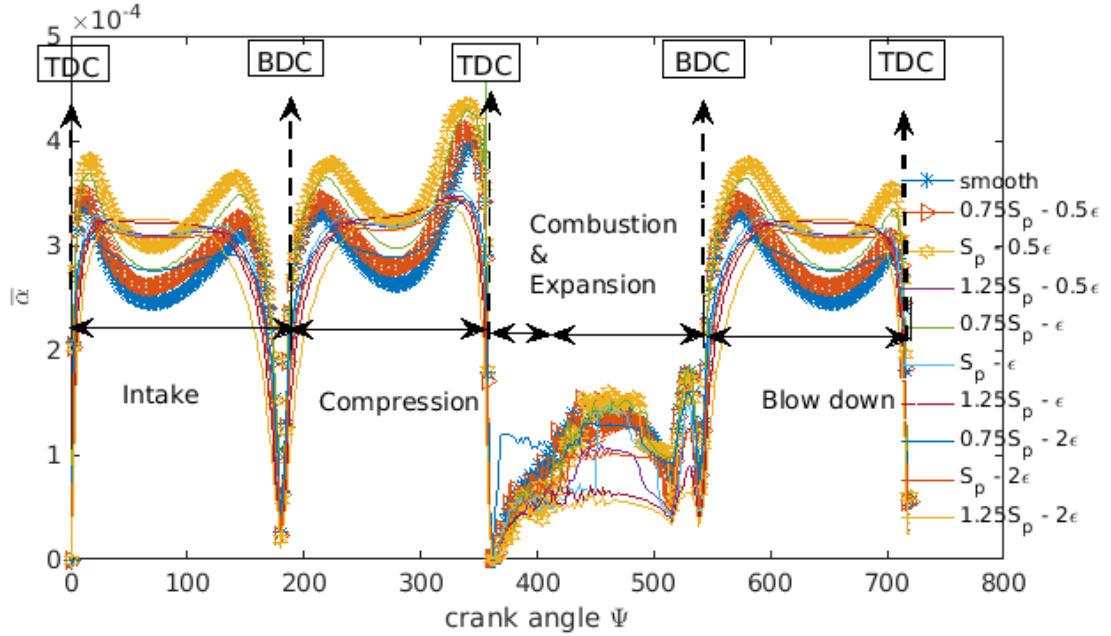


Figure 3.58: The figure of $\bar{\alpha}$ value at each each crank angle. Different textures are considered as well as a smooth ring under an isothermal warm engine

3.3.3 Discussion

For this section, a comparison study between those three engine operating conditions is made. It includes an investigation of the effect of the temperature equation for the lubricant at the warm engine operating temperature condition. Also, a comparison of the cold and the warm engine conditions is analyzed by comparing their difference in parameters, i.e. the dimensionless film thickness, the coefficient of friction and $\bar{\alpha}$, as well as the total energy losses at entire engine cycle.

The Warm Engine Operating Condition

Under the warm engine operating condition, a comparison between the non-isothermal case and the isothermal one can find that taking into account the convective heat transfer in the lubricant film doesn't have significant influence on tribological parameters. Regarding to the warm engine operating condition, different parameters' behavior at entire cycle are indicated before. Firstly, the dimensionless film thickness is lower for all cases of the textured rings than the smooth ring. Especially, the largest grooves who induces the least film thickness. Therefore, those textured rings reach the mixed lubrication regime more earlier than the smooth ring. On the other hand, the viscous friction force is reduced through the texture when the piston moves to mid-stroke, and narrow grooves generate more friction reduction. The grooves having the lowest depth-to-width ratio and highest area density generates the maximum ΔCOF about 12.26% for the non-isothermal condition. From the coefficient of friction point of view, as textured ring has good improvement at mid-stroke but worse behavior at mixed lubrication regime (i.e. dead centers and combustion process). Total energetic losses at entire engine cycle shows that the combustion process plays an important role in generating energetic losses at warm engine operating condition. However, There is only one textured ring has lower E_{total} than the smooth ring, i.e. the texture $0.75S_p - 2\varepsilon$ has maximum around 23.3% less total energy losses by considering the convective heat transfer. This is because this texture has better improvement of friction reduction at the combustion and expansion processes. Generally speaking, the textured ring could not improve the film thickness and minimize the surface contact at dead centers compared to the smooth ring. On the other hand, the viscous friction force can be reduced, especially for the texture considering the lowest depth-to-width ratio and highest area density. Last but not least, the total gases released from the lubricant at entire cycle is considered. It is a significant parameter determined by the hydrodynamic pressure and plays an important role in the behavior of film thickness and coefficient of friction. In addition, textured rings have better improvement of vapour volume fraction, especially at mid-stroke.

The Cold Engine Operating Condition

As stated before, the dynamic viscosity is the main reason that different temperatures have different results of the dimensionless film thickness and coefficient of friction. Under the cold engine operating condition, the dimensionless film thickness is improved through textured rings having narrow grooves at two sides at mid-stroke. The maximum value of $\Delta\Lambda = 2.5\%$ for grooves considering the maximum area density and the lowest depth-to-width ratio. But this improvement of dimensionless film thickness is not agreed for combustion and expansion processes as well as dead centers. As the reason of this difference compared to warm engine operating condition, the coefficient of friction reduction has better performance for the texture considering larger area density and depth-to-width ratio at mid-stroke. Whilst, the viscous friction reduction is more relevant than the warm engine operating condition (see fig:3.6 3.9 3.3). For the energetic losses at entire engine cycle, the textured ring has improvement on the reduction of energy losses, especially the grooves considering large area density or depth-to-width ratio. Comparing to the warm engine operating condition, four strokes have effect on energy loss not just the combustion and expansion processes. Furthermore, the behavior of $\bar{\alpha}$ at entire cycle is wave-shaped for all kinds of textures. The textured ring generates more gasses from the lubricant than the smooth ring, which is same for the warm engine operating condition.

3.4 Ring Profile Study

In this section, the ring profile is another topic from the tribology point of view. In this case, a warm engine operating condition is considered as well as the temperature equation. A comparison between the half crown height ring, double crown height ring and our model is investigated. A full engine cycle of $\Delta\Lambda$ and ΔCOF are plot in figures as below:

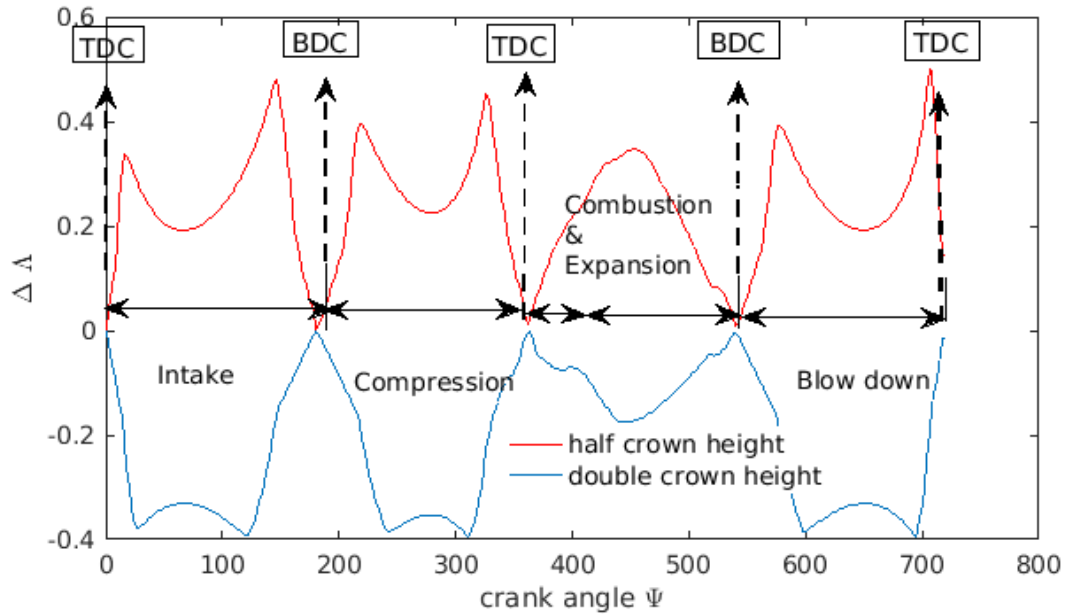


Figure 3.59: The figure of $\Delta\Lambda$ at each crank angle. Different ring profiles are considered under a non-isothermal warm engine operating condition

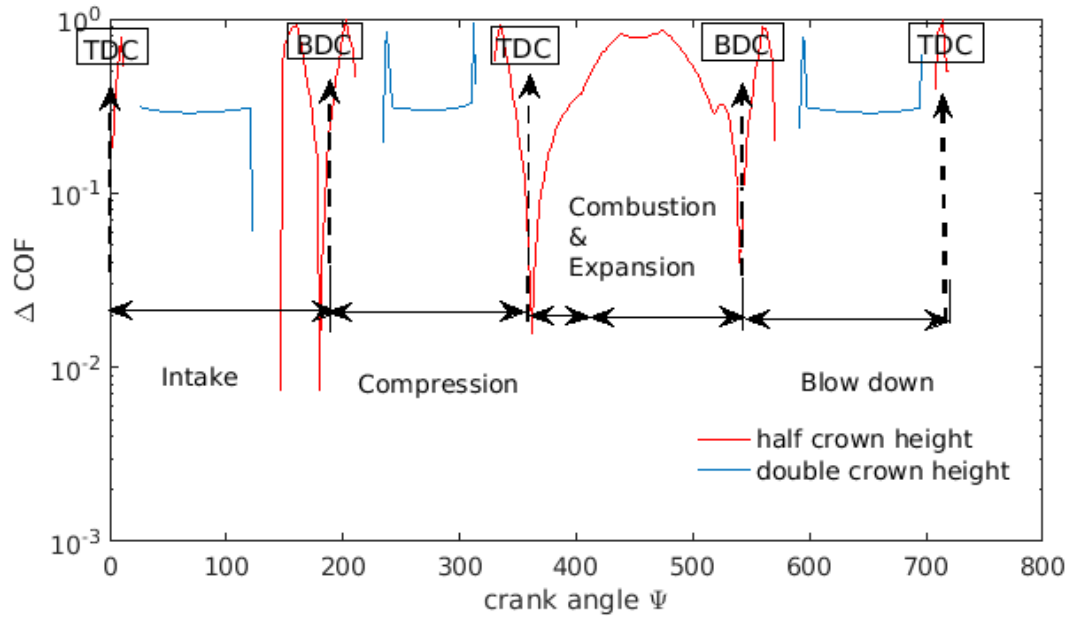


Figure 3.60: The figure of ΔCOF at each crank angle. Different ring profiles are considered under a non-isothermal warm engine operating condition

It can be found that the crown height of ring determine different results of dimensionless film thickness and coefficient of friction at entire engine cycle. Figure 3.59 shows that considering half crown height for this compression ring, the dimensionless film thickness increases at entire engine cycle. The maximum value of $\Delta\Lambda$ equals 0.5 at the dead center. But the dimensionless film thickness decreases for a ring considering a higher crown height. Also, a ring having a lower crown height generates less friction force especially at the mixed lubrication regime (i.e. dead centers, combustion and expansion processes) in Figure 3.60. On the other hand, the ring having a larger crown height improves the viscous friction force reduction. So far, it specifies that the ring with a smaller arc has better friction reduction at the mixed lubrication region and improves the film thickness. The energetic losses (E) of those two cases with respect to the smooth ring is shown as figure below:

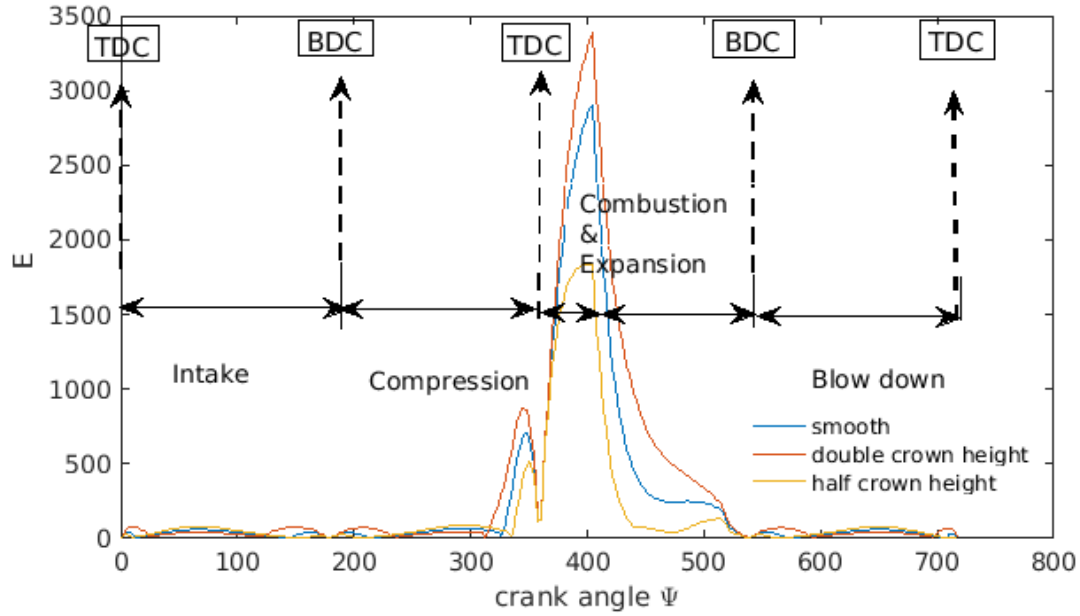


Figure 3.61: The figure of the energy loss $E[w]$ at entire engine cycle. Different ring profiles are considered under a non-isothermal warm engine operating condition

As stated before, under the warm engine operating condition the combustion and expansion processes play an important role in the energetic losses. Figure 3.61 indicates that the case of half crown height has relevant reduction of E at those processes. E_{total} for those two cases and the smooth ring are listed in table as below:

	smooth	half crown height	double crown height
$E_{total}[kw]$	93.74	61.03	123.43

Table 3.11: A matrix of E_{total} under a non-isothermal warm engine operating condition

There is approximately 34.89% reduction of total energy loss for the case of half crown height with respect to the smooth ring.

Chapter 4

Conclusion and future work

In this chapter, the result of this thesis presented above is summarized. The future work to continuously develop a suitable texture on the compression ring and the cylinder liner system is predicted.

4.1 Conclusion

In this study, there are four objectives mentioned before. i.e. The construction of a transverse groove-shaped texture on the compression ring, a tribological study of the surface texturing's influence on the friction force and the film thickness by considering different engine operating conditions, the numerical study of texture parameters to predict and make better grooves on two side of the compression ring. Also, different ring profiles are investigated. In this numerical simulation, a mixed-lubrication model, combines the Reynolds equation as well as the temperature equation for the lubricant film for a four-stroke diesel engine. The transverse grooves are located at two side of ring which reciprocating on the cylinder liner. As showed before, different operating temperatures generate variable results of the dimensionless film thickness, coefficient of friction, $\bar{\alpha}$ and total energy loss E_{total} .

1. Surface texturing can improve the reduction of viscous friction force as well as total energy losses at entire cycle. However, this groove-shaped textured ring does not minimize surface contact when the piston moves to dead center and ignition process unless by changing the curvature of the ring.
2. As stated the comparison between those three temperature conditions before, The implementation of the temperature equation for the lubricant film has less effect on tripological results. But the dynamic viscosity due to different operating temperatures plays an important role in the improvement of film thickness, especially at mid-stroke.
3. By the consideration of convective heat transfer between the lubricant film, the reduction of dimensionless film thickness is approximated 3% more than the isothermal warm engine operating condition. 23.5% more COF reduction at mid-stroke (hydrodynamic lubrication regime) for the best texture.
4. Regarding the cold engine operating temperature, those results are significantly different with respect to the warm condition, because of the increment of dynamic viscosity. The dimensionless film thickness and the total energy loss are improved for the textured ring. There are 2.5% and 13.35% respectively for the best case of texture. On the other hand, the warm engine operating temperature could not improve the film thickness through the surface texturing, but textured ring reduces viscous friction force and the total energy loss only for one specific shape of grooves $(0.75S_p - 2\varepsilon)$.

5. $\bar{\alpha}$ is improved for the textured ring at entire engine cycle, especially at mid-stroke. The profile of this curve is determined by the time dependent term and the term coming from the Couette contribution of the Reynolds equation.
6. The energy loss depends mainly on the combustion and expansion processes for a warm engine operating condition. For the reduction of total energy losses, the ring profile is more relevant than surface texturing.
7. The Stribeck curve indicates that this four-stroke engine cycle includes the mixed lubrication regime and the hydrodynamic lubrication regime. Also, as the piston reciprocating on the cylinder liner, the curves of Stribeck curve for one stroke is not superimposed. This is the reason that the piston's speed is different for the same location of piston. Thus, the updated film thickness is different, even if the piston moves at the same location. On the other hand, the curve investigated by Tallian shows a one-to-one-correspondence between the coefficient of friction and the dimensionless film thickness.

4.2 Future Work

The surface texturing has been recognized as an promising way to reduce the friction force for the lubricated piston ring-cylinder liner system and improve the dimensionless film thickness (Λ). For a future study, an optimization method can be applied to find the best texture profile. Also, different shapes of texture (i.e. mini-dimples) can be implemented on this model for further investigating. On the other hand, a texture on the cylinder liner is also interesting to devise and try to find an optimum texture for a better improvement from the tribology point of view.

Bibliography

- [1] Mohamed Kamal Ahmed Ali, Hou Xianjun, Richard Fiifi Turkson, and Muhammad Ezzat. An analytical study of tribological parameters between piston ring and cylinder liner in internal combustion engines. *Proceedings of the Institution of Mechanical Engineers, Part K: Journal of Multi-body Dynamics*, 230(4):329–349, 2016.
- [2] N Biboulet and AA Lubrecht. Analytical solution for textured piston ring–cylinder liner contacts (1d analysis). *Tribology International*, 96:269–278, 2016.
- [3] Hugo M Checo, Roberto F Ausas, Mohammed Jai, Jean-Paul Cadalen, Franck Choukroun, and Gustavo C Buscaglia. Moving textures: Simulation of a ring sliding on a textured liner. *Tribology International*, 72:131–142, 2014.
- [4] Pavol Daučík, Jozef Višňovský, Jozef Ambro, and Elena Hájeková. Temperature dependence of the viscosity of hydrocarbon fractions. *Acta Chimica Slovaca*, 1(1):43–57, 2008.
- [5] I Etsion and E Sher. Improving fuel efficiency with laser surface textured piston rings. *Tribology International*, 42(4):542–547, 2009.
- [6] Izhak Etsion. State of the art in laser surface texturing. *Journal of tribology*, 127(1):248–253, 2005.
- [7] Prof. Dieter Fauconnier[EA08]. Numerical analysis of the lubrication of piston’s compression ring in a diesel engine, machine design practical lecture. 1(1):14, 2018-2019.
- [8] JA Greengood and JH Tripp. The contact of two nominally flat rough surfaces. *Proc. Instn. Mech. Engrs*, 185:1970–1971, 1970.
- [9] Chunxing Gu, Xianghui Meng, and Di Zhang. Analysis of the coated and textured ring/liner conjunction based on a thermal mixed lubrication model. *Friction*, 6(4):420–431, 2018.
- [10] Bernard J Hamrock, Steven R Schmid, and Bo O Jacobson. *Fundamentals of fluid film lubrication*. CRC press, 2004.
- [11] P Ilanthirayan, S Mohanraj, and M Kalayarasan. Wear analysis of top piston ring to reduce top ring reversal bore wear. *Tribology in Industry*, 39(4), 2017.
- [12] Yeau-Ren Jeng. Theoretical analysis of piston-ring lubrication part i—fully flooded lubrication. *Tribology Transactions*, 35(4):696–706, 1992.
- [13] Mitjan Kalin, Igor Velkavrh, and Jože Vižintin. The stribeck curve and lubrication design for non-fully wetted surfaces. *Wear*, 267(5-8):1232–1240, 2009.

- [14] Yuri Kligerman, Isaac Etsion, and A Shinkarenko. Improving tribological performance of piston rings by partial surface texturing. *Journal of Tribology*, 127(3):632–638, 2005.
- [15] Kangmei Li, Zhenqiang Yao, Yongxiang Hu, and Weibin Gu. Friction and wear performance of laser peen textured surface under starved lubrication. *Tribology international*, 77:97–105, 2014.
- [16] Cheng Liu, Yan-Jun Lu, Yong-Fang Zhang, Sha Li, and Norbert Müller. Numerical study on the lubrication performance of compression ring-cylinder liner system with spherical dimples. *PloS one*, 12(7):e0181574, 2017.
- [17] Aviram Ronen, Izhak Etsion, and Yuri Kligerman. Friction-reducing surface-texturing in reciprocating automotive components. *Tribology Transactions*, 44(3):359–366, 2001.
- [18] G Ryk, Y Kligerman, I Etsion, and A Shinkarenko. Experimental investigation of partial laser surface texturing for piston-ring friction reduction. *Tribology Transactions*, 48(4):583–588, 2005.
- [19] Hamed Shahmohamadi, Ramin Rahmani, Homer Rahnejat, Colin P Garner, and PD King. Thermo-mixed hydrodynamics of piston compression ring conjunction. *Tribology Letters*, 51(3):323–340, 2013.
- [20] Cong Shen. Design of surface texture for the enhancement of tribological performance. 2016.
- [21] A Sonthalia and CR Kumar. The effect of compression ring profile on the friction force in an internal combustion engine. *Tribology in Industry*, 35(1):74–83, 2013.
- [22] Andrew Spencer. *Optimizing surface texture for combustion engine cylinder liners*. PhD thesis, Luleå tekniska universitet, 2010.
- [23] TE Tallian. On competing failure modes in rolling contact. *ASLE transactions*, 10(4):418–439, 1967.
- [24] Ali Usman and Cheol Woo Park. Optimizing the tribological performance of textured piston ring–liner contact for reduced frictional losses in si engine: warm operating conditions. *Tribology International*, 99:224–236, 2016.
- [25] Ali Usman and Cheol Woo Park. Numerical investigation of tribological performance in mixed lubrication of textured piston ring–liner conjunction with a non-circular cylinder bore. *Tribology International*, 105:148–157, 2017.
- [26] Anton Van Beek. Advanced engineering design. *TU Delft, Delft, The Netherlands*, 2015.
- [27] DEA Van Odyck and Cornelis H Venner. Compressible stokes flow in thin films. *Journal of tribology*, 125(3):543–551, 2003.
- [28] Bifeng Yin, Xiaodong Li, Yonghong Fu, and Wang Yun. Effect of laser textured dimples on the lubrication performance of cylinder liner in diesel engine. *Lubrication Science*, 24(7):293–312, 2012.
- [29] Anastasios Zavos and Pantelis G Nikolakopoulos. A tribological study of piston rings lubricated by power law oils. *Proceedings of the Institution of Mechanical Engineers, Part J: Journal of Engineering Tribology*, 230(5):506–524, 2016.

- [30] Zhinan Zhang, Jun Liu, and Youbai Xie. Design approach for optimization of a piston ring profile considering mixed lubrication. *Friction*, 4(4):335–346, 2016.